UNIVERSITÀ DEGLI STUDI DI PALERMO

Dottorato di ricerca in Medicina Molecolare e Clinica

Dipartimento Promozione della Salute, Materno-Infantile, di Medicina Interna e Specialistica di Eccellenza "G. D'Alessandro" (PROMISE)

Next-Generation NK Cell Immunotherapy: CAR Engineering and ADAM17-Guided Immune Regulation Across Cancer and Viral Disease

Doctoral Dissertation of:

Anna Gallina

Tutor:

Prof. Antonino Tuttolomondo

Co-tutor:

Prof. Pier Giulio Conaldi

2022–2025 Cycle XXXVIII

Contents

1. ABSTRACT

Natural Killer (NK) cells represent a pivotal component of innate immunity, positioned at the interface between early antiviral defence and tumour immunosurveillance. Their ability to integrate activating and inhibitory signals, mediate MHC-independent cytotoxicity, and dynamically adapt to environmental cues renders them uniquely suited for translational exploitation in both oncology and infectious diseases. This doctoral work explores NK-cell biology along two complementary axes: (i) the development of NK-based immunotherapeutic strategies for hepatocellular carcinoma (HCC), and (ii) the investigation of NK-cell regulation during viral infections, with particular emphasis on the sheddase ADAM17 as a biomarker and functional modulator of immune activation.

The first part of the thesis focused on optimizing NK-cell–based immunotherapy for solid tumours, using HCC as a model of immune-resistant malignancy within a tolerogenic hepatic microenvironment. Primary NK cells were isolated from liver perfusate obtained from deceased brain-dead donors, a highly enriched and biologically distinctive source of intrahepatic immune cells. Following *ex vivo* expansion, longitudinal flow cytometric analyses were performed to characterize activation, inhibitory, and maturation markers, providing a dynamic portrait of NK-cell phenotypic remodelling under cytokine stimulation.

The antitumor potential of cytokine-activated NK cells was subsequently evaluated in a preclinical orthotopic xenograft model of HCC. Luciferase-expressing HepG2 cells were implanted in immunodeficient NOG mice, allowing longitudinal monitoring of tumour burden through *in vivo* bioluminescence imaging and serum alpha-fetoprotein (AFP) quantification. *Ex vivo*–activated NK cells demonstrated measurable antitumor activity without overt toxicity, supporting the feasibility and safety of adoptive NK-cell therapy in a solid tumour setting characterized by complex immune evasion mechanisms.

Building upon these findings, a third experimental phase addressed the genetic engineering of NK cells through the generation of fourth-generation self-inactivating lentiviral vectors encoding an anti-GPC3 chimeric antigen receptor (CAR). Construct variants were designed to enhance persistence and functional fitness through cytokine armouring strategies. CAR-NK products were systematically characterized in terms of transduction efficiency, cytokine secretion profiles, and cytotoxic potency. This work contributes to the growing body of evidence supporting CAR-NK cells as a potentially safer, allogeneic, and metabolically adaptable alternative to CAR-T platforms, particularly in the context of solid tumours such as HCC.

The second major axis of the thesis investigated NK-cell regulation during viral infections, focusing on ADAM17 (A Disintegrin And Metalloprotease 17), a membrane-bound sheddase that modulates surface expression of key immune receptors, including CD16, TIM-3, and cytokine receptors, thereby fine-tuning NK-cell activation thresholds. ADAM17 expression was analysed *ex vivo* in whole blood samples from HHV-8–positive transplant recipients, revealing virus-associated modulation patterns consistent with immune tuning in chronic infection. In parallel, an *in vitro* stimulation model was established using peripheral blood mononuclear cells from healthy donors exposed to viral peptide pools derived from SARS-CoV-2, HHV-8, CMV, and EBV. Longitudinal assessment of ADAM17 expression across NK-cell subsets, together with cytokine quantification in culture supernatants, enabled dissection of virus-specific immune signatures.

Collectively, these findings suggest the possibility that ADAM17 may function as a dynamic regulator of NK-cell functional plasticity, potentially linking cytokine-driven activation, particularly TNF-α and IL-6 signalling, to receptor shedding and subsequent immune recalibration. The modulation of ADAM17 observed across distinct viral contexts raises the hypothesis that this sheddase could represent not only a surrogate marker of immune activation, but also a candidate therapeutic node through which NK-cell responsiveness might be fine-tuned in chronic infection and cancer.

By integrating translational development of NK-based immunotherapies with the investigation of NK-cell regulation in viral settings, this thesis provides a cohesive view of NK-cell functional plasticity across disease contexts. The findings inform the rational optimization of next-generation NK-based cellular therapies in oncology, particularly for solid tumours such as HCC, and suggest a role for ADAM17 as a potential regulatory node linking activation, receptor shedding, and immune adaptation in infectious contexts.

2. ABREVIATION

ACT	Adoptive Cell Therapy
ADAM	Disintegrin And Metalloprotease
ADCC	Antibody-Dependent Cellular Cytotoxicity
ADCP	Antibody-Dependent Cellular Phagocytosis
AFP	Alpha-Fetoprotein
AI	Artificial Intelligence
AAV	Adeno-Associated Virus
BLI	Bioluminescence Imaging
CAR	Chimeric Antigen Receptor
CAR-M	CAR-Macrophages
CIML	Cytokine-Induced Memory-Like
CLL	Chronic Lymphocytic Leukemia
CRS	Cytokine Release Syndrome
DC	Dendritic Cells
DLBCL	Diffuse Large B-Cell Lymphoma
EBV	Epstein–Barr Virus
GMP	Good Manufacturing Practice
HBV	Hepatitis B Virus
HCC	Hepatocellular Carcinoma
HCMV	Human Cytomegalovirus

HDR Homology-Directed Repair

HIV Human Immunodeficiency Virus

HCV Hepatitis C Virus

HHV8 Human Herpesvirus 8

ICANS Immune Effector Cell-Associated Neurotoxicity Syndrome

IVIS In Vivo Bioluminescence Imaging

KICS Kaposi Sarcoma Inflammatory Cytokine Syndrome

KIR Killer-Cell Immunoglobulin-Like Receptor

KSHV Kaposi's Sarcoma–Associated Herpesvirus

LBCL Non Definita Esplicitamente Nel Testo

LDLR Low-Density Lipoprotein Receptor

LP Liver Perfusate

LV Lentiviral Vectors

MDSC Myeloid-Derived Suppressor Cells

MFI Mean Fluorescence Intensity

ML Machine Learning

MOI Non Definita Esplicitamente Nel Testo

MTOC Microtubule-Organizing Center

NK Natural Killer

NKT Natural Killer T Cells

NHL Non-Hodgkin Lymphoma

NSCLC Non-Small Cell Lung Cancer

PAMP Pathogen-Associated Molecular Patterns

PBMC	Peripheral Blood Mononuclear Cells
PRR	Pattern Recognition Receptors
RCL	Replication-Competent Lentivirus
RNP	Ribonucleoprotein
ROS	Reactive Oxygen Species
SB	Sleeping Beauty
SIN	Self-Inactivating
TAA	Tumour-Associated Antigen
TACE	TNF-Alpha–Converting Enzyme
TCR	T-Cell Receptor
TIL	Tumour-Infiltrating Lymphocytes
TINK	Tumour-Infiltrating NK Cells
TLR	Toll-Like Receptors
TRAIL	Tumor Necrosis Factor-Related Apoptosis-Inducing Ligand
TME	Tumour Microenvironment
UCB	Umbilical Cord Blood
VSV-G	Vesicular Stomatitis Virus Glycoprotein
WBC	White Blood Cells

3. INTRODUCTION

3.1The immune system

In mammals, immune defense is classically divided into two interconnected arms: innate and adaptive immunity. Innate immunity provides rapid, broadly reactive protection, whereas adaptive immunity generates antigen-specific responses and long-term immunological memory [1]. The innate system constitutes the first line of defense and includes epithelial barriers and effector cells such as neutrophils, monocytes/macrophages, dendritic cells (DCs), and natural killer (NK) cells. Activation occurs through pattern recognition receptors (PRRs) that detect conserved pathogen-associated molecular patterns (PAMPs), enabling responses within minutes to hours and limiting early pathogen spread while shaping inflammation [2]. In contrast, adaptive immunity relies on clonally distributed antigen receptors, allowing highly specific recognition and memory formation, but typically requires several days to develop as naïve lymphocytes undergo clonal expansion and differentiation [1,3].

Among innate effectors, NK cells are cytotoxic lymphocytes that provide early control of virus-infected and transformed cells and influence broader immune responses. Importantly, certain NK-cell subsets can acquire adaptive-like features, expanding after defined stimuli and responding more efficiently upon re-exposure, a phenomenon referred to as NK-cell memory or trained immunity [4–7].

Adaptive immunity comprises humoral and cell-mediated responses. B lymphocytes mediate humoral immunity by differentiating into antibody-secreting plasma cells and memory B cells. Immunoglobulins (IgM, IgG, IgA, IgE, IgD) perform functions including neutralization, opsonization, and complement activation, often following T-cell–dependent activation within germinal centers where affinity maturation and class switching occur [2,8,9]. T lymphocytes mediate cellular immunity by recognizing peptide antigens presented by MHC molecules. $CD4^+$ T cells recognize MHC class II and differentiate into specialized helper subsets, whereas $CD8^+$ cytotoxic T lymphocytes recognize MHC class I and directly eliminate infected or transformed cells. After antigen clearance, memory T cells persist and enable faster secondary responses [10,11].

Innate and adaptive immunity operate as an integrated system. PRR-driven activation of innate cells shapes adaptive responses through antigen presentation, costimulation, and cytokine production. DCs are central to this process, as pathogen sensing induces their maturation and migration to lymphoid tissues where they prime T cells [1]. NK cells also participate in this

crosstalk by modulating DC function and influencing B- and T-cell responses during infection and cancer [5,7]. In addition, bridge populations such as γδ T cells and NKT cells combine rapid responses with antigen receptor–based recognition and contribute to both arms of immunity [12]. Together, these principles provide the immunological framework for this thesis, which focuses on NK cells in viral infections and NK-based immunotherapeutic strategies.

3.2 Natural Killer cells

3.2.1 Sources

NK cells can be obtained from several sources, each associated with specific biological properties and manufacturing advantages. The NK-92 cell line provides a highly standardized "off-the-shelf" product due to its unlimited *in vitro* expansion and robustness to cryopreservation; however, because of its lymphoma origin, it requires irradiation prior to infusion (thereby limiting *in vivo* persistence) and shows intrinsic receptor repertoire limitations, including the lack of CD16 [13,14]. Peripheral blood mononuclear cells (PBMCs) remain the most widely used source of primary NK cells, enabling donor-derived isolation followed by cytokine-based activation/expansion under GMP-compatible conditions; nevertheless, PBMC-derived NK products are often heterogeneous and enriched for mature $CD56^{dim}CD16^{+}$ subsets, which display strong cytotoxicity but relatively limited proliferative capacity [15]. Umbilical cord blood (UCB) represents an attractive allogeneic source thanks to unit banking and favourable logistics, although UCB-derived NK cells are typically less mature and less cytotoxic, with lower expression of CD16/KIRs/perforin/granzyme B and higher inhibitory features (e.g., NKG2A), moreover starting cell numbers are constrained by unit volume [16]. Beyond direct NK isolation, NK cells can be generated *ex vivo* from $CD34^{+}$ hematopoietic progenitor cells (HPCs) (from bone marrow, mobilized peripheral blood, or UCB) and differentiated into $CD56^{+}CD3^{-}$ NK cells using cytokine-driven protocols, offering scalability but requiring complex and time-consuming differentiation workflows [17]. Finally, induced pluripotent stem cells (iPSCs) represent a renewable platform for highly uniform "off-the-shelf" NK products that can be engineered at the stem cell stage to enable stable CAR integration and large-scale manufacturing; however, iPSC-derived NK cells may retain relatively immature traits, including reduced KIR/CD16 and increased NKG2A compared with peripheral blood NK cells [18].

In addition to these conventional sources, hepatic liver perfusate (LP) obtained from deceased brain donors has emerged as a particularly rich and biologically informative reservoir of liver-associated immune cells. Pagano et al. specifically analysed the "ex situ back-table" LP fraction, defined as the perfusion fluid recovered from the liver graft on the surgical bench during pre-transplant preparation outside the donor body [19]. In this cohort, the mean collected LP volume was approximately 1.2 L, yielding a mean of $316X10^6$ total cells, highlighting the high cellular recovery of LP compared with standard PBMC isolation. Importantly, matched LP–PBMC comparisons revealed a markedly distinct leukocyte composition. LP samples were strongly enriched in $CD45^+$ cells and, within the lymphocytic compartment, displayed a prominent representation of NK cells, with a median frequency of approximately 30%. Moreover, LP-derived NK cells displayed expression of key activating receptors, including NKp30, NKp44, NKp46, and NKG2D, supporting the concept that liver-derived NK cells exhibit a distinct activation-related phenotype compared with circulating PBMC-derived NK populations [19]. Collectively, these observations identify liver perfusate as a strategic alternative source of NK cells for high-yield, with translational relevance for NK-based immunotherapeutic development.

3.2.2 Human NK cell subsets

Human NK cells are innate lymphocytes that detect infected, stressed, or transformed cells by integrating activating and inhibitory signals and responding to "missing-self" and "induced-self" cues [4,5]. In peripheral blood, they are classically divided by CD56 and CD16 expression into $CD56^{bright}CD16^-$ and $CD56^{dim}$ $CD16^+$ subsets, which differ in frequency, distribution, receptor repertoire, and effector function [20,21]. $CD56^{bright}CD16^-$ NK cells account for ~5–15% of circulating NK cells but are enriched in secondary lymphoid organs due to expression of homing receptors such as CD62L, CCR7, and CXCR3. They are highly responsive to cytokines, including IL-2, IL-12, IL-15, and IL-18, through receptors such as the high-affinity IL-2 receptor (CD25), producing IFN-γ, TNF-α, and GM-CSF and thus exerting immunoregulatory roles that shape adaptive immunity. In contrast, $CD56^{dim}$ $CD16^+$ NK cells represent ~85–95% of blood NK cells and constitute the main cytotoxic population, characterized by high perforin and granzyme content, broad expression of Killer-cell immunoglobulin-like receptors (KIR), and efficient antibody-dependent cellular cytotoxicity (ADCC) mediated by CD16 (FcγRIII). Although they produce less IFN-γ per cell than $CD56^{bright}$ NK cells, their numerical dominance makes them major contributors to overall

cytokine production during immune responses. The developmental relationship between these subsets remains debated: evidence supports differentiation of $CD56^{bright}$ into $CD56^{dim}$ cells under certain conditions, but single-cell analyses also reveal parallel developmental trajectories [22–26].

Beyond this dichotomy, NK cells can acquire adaptive or memory-like features. In humans, the best-characterized example occurs during human cytomegalovirus (HCMV) infection, where $NKG2C^{+}$ NK cells expand and persist, often with reduced or absent FcRγ expression and epigenetic remodeling that enhances effector responses, particularly IFN-γ production, upon restimulation. These HCMV-associated adaptive NK cells frequently express high CD57, display strong ADCC activity, and can persist long after primary infection, supporting the concept of sustained NK "recall-like" immunity [17,25,27,28].

Another clinically relevant adaptive state is represented by cytokine-induced memory-like (CIML) NK cells, generated *ex vivo* by short priming with IL-12, IL-15, and IL-18. These cells retain enhanced IFN-γ production and antitumor activity over time and have shown promise in early clinical studies [6]. Conversely, chronic stimulation in persistent viral infection or within the tumour microenvironment can induce NK dysfunction, including exhausted and senescent-like states. Exhausted NK cells typically upregulate inhibitory or checkpoint receptors such as PD-1, TIM-3, LAG-3, and TIGIT and show reduced degranulation, cytokine production, and proliferative capacity. Senescent or terminally differentiated NK cells, often marked by CD57 and KLRG1, display limited proliferation despite sometimes preserved cytotoxicity and accumulate with aging and chronic inflammation, potentially limiting sustained immunotherapeutic responses. Notably, some features of NK exhaustion appear partially reversible, supporting therapeutic strategies that combine NK-based approaches with checkpoint blockade or microenvironmental modulation [15,22–24,29].

Finally, NK cells must be distinguished from NKT cells, which share some surface markers but belong to a different lineage. NK cells are innate lymphoid cells that lack a T-cell receptor (TCR) and recognize altered self through germline-encoded receptors. In contrast, NKT cells are T lymphocytes expressing a TCR together with NK-associated markers (e.g., CD56, CD161) and recognize lipid antigens presented by CD1d. They develop in the thymus and rapidly produce cytokines upon activation, linking innate and adaptive immunity. Experimentally, these populations are reliably distinguished by CD3 expression, which is present on NKT cells but absent on NK cells [4,5,21].

3.2.3 NK-Cell Activation and Cytotoxic Mechanisms

NK cells originate from hematopoietic progenitors in the bone marrow and undergo progressive maturation that confers cytotoxic competence and a diversified receptor repertoire. A hallmark of NK biology is the ability to detect abnormal cells without prior antigen sensitization through germline-encoded receptors sensing loss of self (missing-self) and stress-induced ligands. NK responsiveness is calibrated through NK cell education (licensing), in which inhibitory receptor interactions with self–MHC class I molecules tune functional activity. NK cells expressing inhibitory receptors recognizing self-HLA (e.g., KIRs or CD94/NKG2A) become "educated" and respond efficiently to cells with reduced MHC-I, whereas uneducated NK cells remain hyporesponsive, ensuring self-tolerance [20,21,30,31].

NK activation results from the integration of signals from multiple activating receptors. NKG2D recognizes stress-induced ligands such as MICA, MICB, and ULBPs and signals via DAP10 to activate PI3K pathways promoting cytotoxicity and cytokine production. DNAM-1 (CD226) binds CD155 (PVR) and CD112 (Nectin-2), enhancing adhesion and immune synapse stability. Natural cytotoxicity receptors (NKp30, NKp44, NKp46) further mediate tumor and antiviral recognition through ITAM-associated adaptors (CD3ζ, FcRγ), triggering degranulation and IFN-γ release; NKp30 binds B7-H6, while NKp46 recognizes viral hemagglutinins [20,27,28]. Additional receptors such as 2B4 (CD244) and co-stimulatory molecules including CD137 (4-1BB) modulate NK activation, survival, and proliferation, and are exploited in immunotherapeutic strategies including CAR-NK approaches [32].

NK responses are restrained by inhibitory receptors and immune checkpoints to prevent autoreactivity. KIRs recognize HLA-A/B/C molecules and inhibit activation through ITIM-mediated recruitment of SHP phosphatases, while CD94/NKG2A recognizes HLA-E and mediates potent inhibition. Under chronic stimulation, such as persistent infection or cancer, NK cells may upregulate checkpoint receptors including PD-1, TIM-3, LAG-3, and TIGIT, resulting in reduced cytotoxicity and cytokine production. Importantly, TIGIT competes with DNAM-1 for CD155/CD112 binding, suppressing DNAM-1–mediated activation and providing a rationale for combinatorial checkpoint blockade strategies [15,27,28,31].

NK-cell killing ultimately depends on the balance between activating and inhibitory signals at the immune synapse (Table 1). According to the "missing-self" model, NK cells are activated when target cells downregulate MHC-I, removing inhibitory signals from receptors such as

KIRs or NKG2A. In the "induced-self" model, stressed or transformed cells upregulate ligands for activating receptors such as NKG2D or DNAM-1, shifting signaling toward activation even if MHC-I is partially retained. NK activation therefore reflects a dynamic integration of opposing signals, often described as an "integrated signal balance model" [24,31,31].

NK cytotoxicity occurs through both granule-dependent and death-receptor pathways. The dominant mechanism involves polarized release of cytolytic granules at the immune synapse following cytoskeletal reorganization and Microtubule-Organizing Center (MTOC) polarization. This leads to secretion of perforin and granzymes, particularly granzyme B, which induce apoptosis through caspase activation and mitochondrial damage via BID cleavage and cytochrome c release. In parallel, NK cells can trigger extrinsic apoptosis through FasL/Fas (CD95) interactions and TRAIL engagement of death receptors DR4 and DR5, providing complementary cytotoxic mechanisms [20,27,28,30].

Category	Receptor	Representative ligands	Dominant functional outcome
Activating receptors	**NKG2D**	MICA, MICB, ULBPs	Promotes strong NK-cell activation, inducing cytotoxic granule polarization, degranulation, and cytokine production.
	DNAM-1 (CD226)	CD155 (PVR), CD112 (Nectin-2)	Enhances adhesion and cooperates with other activating receptors, strengthening NK-cell cytotoxic responses.
	NKp30 (NCR)	B7-H6	Triggers activating signaling through ITAM-associated adaptors, promoting degranulation and IFN-γ release.
	NKp44 (NCR)	Tumor- and virus-associated ligands (not specified in the text)	Activates NK-cell effector functions through ITAM-associated adaptors, supporting cytotoxicity and cytokine secretion.
	NKp46 (NCR)	Viral hemagglutinins (and other pathogen-associated molecules)	Induces rapid activation through ITAM-associated adaptors, leading to degranulation and IFN-γ secretion.

	2B4 (CD244)	CD48	Exerts context-dependent regulation of NK-cell activity, providing activation in the presence of SLAM-associated protein (SAP) but potentially mediating inhibition in settings where alternative adaptors predominate.
	CD137 (4-1BB)	4-1BBL	Provides co-stimulatory signals that support NK-cell survival, proliferation, and enhanced cytotoxic activity.
Inhibitory receptors (MHC-I dependent)	**KIRs (inhibitory KIRs)**	HLA-A, HLA-B, HLA-C epitopes	Deliver inhibitory signals through ITIM motifs, limiting NK-cell activation and contributing to NK-cell education and missing-self recognition.
	CD94/NKG2A	HLA-E	Provides potent inhibitory signaling through ITIM-mediated pathways, suppressing NK-cell activation and effector functions.
Immune checkpoints / exhaustion-associated inhibitory receptors	**PD-1**	PD-L1, PD-L2	Suppresses NK-cell activity and It is associated with functional exhaustion, including reduced cytotoxicity, cytokine production, and proliferative capacity.
	TIM-3	Galectin-9 (and other ligands)	Contributes to NK-cell dysfunction in cancer and chronic infection, being linked to exhaustion-like inhibitory signaling.
	LAG-3	MHC class II	Promotes inhibitory signaling and may reduce NK-cell activation in specific immunological contexts.
	TIGIT	CD155 (PVR), CD112 (Nectin-2)	Competes with DNAM-1 for ligand binding and delivers inhibitory signals that reduce NK-cell activation and effector responses.
Death receptor pathways (NK effector ligands)	**FasL**	Fas (CD95)	Induces target cell apoptosis through activation of the extrinsic apoptotic pathway involving Death-inducing signalling complex (DISC) formation and caspase activation.
	TRAIL	DR4 (TRAIL-R1), DR5 (TRAIL-R2)	Promotes apoptosis of susceptible target cells via death receptor engagement and activation of the extrinsic apoptotic pathway.

Table 1: Summary of NK cell receptors involved in target recognition and immune regulation. Receptors cited in the text are grouped by functional category (activating receptors, inhibitory MHC class I–dependent receptors, immune checkpoint and death receptor pathways). For each receptor, representative ligands and the dominant functional outcome are reported.

3.2.4 Tissue distribution

Although NK cells have traditionally been studied in peripheral blood, evidence shows that distinct NK populations reside in tissues, where local microenvironments shape their phenotype and function. Tissue-resident NK (trNK) cells have been identified in organs such as liver, lung, uterus, lymph nodes, skin, and adipose tissue, and differ from circulating NK (cNK) cells in surface markers, transcriptional programs, and effector functions [20,25,28]. Tissue residency is characterized by expression of retention markers such as CD69 and ITGA1 (CD49a) and reduced trafficking receptors including S1PR5 and CX3CR1, favouring long-term tissue localization. Functionally, trNK cells often display a CD56^bright^ phenotype and are biased toward cytokine production rather than cytotoxicity, although this varies by tissue. Their persistence relies on local proliferation and survival signals, supporting long-term immune surveillance within tissue niches [25,27,28].

The liver is one of the most NK-enriched organs, with NK cells comprising ~30–50% of intrahepatic lymphocytes, higher than in blood. In this environment, characterized by constant exposure to gut-derived antigens, tolerogenic signals, and physiological hypoxia, hepatic NK cells balance immune defense with tissue tolerance [33,34]. Liver-resident NK cells commonly express CD69, CXCR6, and CD49a, supporting localization within hepatic sinusoids and interactions with hepatocytes and liver sinusoidal endothelial cells (LSECs). $CXCR6^{+}$ NK cells are largely educated through NKG2A and display reduced cytokine production, highlighting liver-imprinted regulation [34]. Hepatic NK cells also express high levels of TRAIL, enabling killing of virus-infected hepatocytes and hepatocellular carcinoma cells. Additionally, NKp46-dependent cytotoxicity against hepatic stellate cells can limit fibrosis, linking NK activity to liver tissue remodeling [27,28,35].

The hepatic microenvironment tightly regulates NK-cell activity through inhibitory and immunomodulatory signals. LSECs express checkpoint ligands such as HLA-E and PD-L1, engaging receptors including NKG2A and PD-1 to restrain NK activation. Kupffer cells and hepatic stellate cells produce suppressive cytokines such as IL-10 and TGF-β, promoting resident phenotypes and reducing cytotoxicity. During inflammation or viral infection, however, this balance can shift toward activation through cytokines such as IL-12, IL-18, and

type I interferons and increased expression of activating ligands on stressed hepatocytes. These dynamics highlight the need for therapeutic strategies targeting liver NK cells, such as checkpoint blockade or adoptive transfer, to enhance antitumor activity while avoiding excessive inflammation and tissue damage [25,28].

3.2.5 NK cytokine-based activation

Ex vivo cytokine stimulation is widely employed to enhance NK effector activity and generate more potent cell products. Notably, IFN-α activation induces a distinct NK functional program (IFNα-NKs) compared with conventional IL-2/IL-15 stimulation (IL2/IL15-NKs), promoting enhanced antiviral effects *in vitro* against HCV-infected hepatoma targets. Importantly, IFNα-NKs show a characteristic secretory profile with robust release of IFN-γ and galectin-9, two mediators implicated in antiviral immune control [7]. IFN-γ contributes to suppression of infection by inducing antiviral pathways in target cells. Galectin-9, a soluble immunomodulatory lectin that can also be conveyed through extracellular vesicles, further contributes to antiviral effects and to shaping immune responses during chronic infection [36,37].

These observations have important implications in the broader context of NK exhaustion and dysfunction, phenomena described not only in chronic infections but also in cancer. Exhaustion-like states in NK cells involve reduced effector function and increased inhibitory signaling, often linked to checkpoints such as TIM-3 and other exhaustion-related pathways. Notably, TIM-3 blockade has been shown to restore NK function in advanced malignancies, supporting the concept that NK dysfunction can be therapeutically reversible [38]. Moreover, galectin-9 expression has been associated with NK cell subsets exhibiting reduced cytotoxic molecule expression but preserved IFN-γ production, consistent with functional rewiring typical of chronic stimulation settings [39–41]. Overall, cytokine-driven activation strategies, particularly IFN-α stimulation, may represent a rational approach to enhance NK antiviral potency and promote resistance to chronic infection–associated functional impairment, with potential relevance also for NK-based immunotherapeutic approaches in cancer [7].

3.2.6 NK cells in cancer: surveillance and tumour evasion

NK cells are pivotal mediators of early anticancer immune surveillance, yet established solid tumours frequently escape NK control through immunoediting and progressive functional suppression of NK effector programs. Tumour cells can downregulate classical MHC class I

molecules to avoid cytotoxic T lymphocytes; although this should increase susceptibility to NK "missing-self" recognition, cancers often counterbalance this vulnerability by activating strong inhibitory circuits within the tumour microenvironment (TME). A central axis is the HLA-E/NKG2A checkpoint, widely exploited across malignancies and particularly relevant in hepatocellular carcinoma (HCC), where increased NKG2A signalling contributes to NK exhaustion and reduced antitumor activity [42–44].

In parallel, tumours disrupt activating pathways such as NKG2D-mediated recognition by modulating stress ligands (e.g., MICA/B) and/or inducing chronic ligand exposure that drives NKG2D downregulation and impaired cytotoxic responses. Immunosuppressive cytokines, especially TGF-β, further dampen NK function by downregulating key activating receptors (NKp30, NKp44, NKp46, NKG2D), promoting a dysfunctional phenotype that favours immune escape. In HCC, these mechanisms converge in tumour-infiltrating NK cells (TINK), which show reduced NK frequency, enrichment of a $CD56^{bright}CD16^{-}$ "superbright" subset, decreased NKG2D, and increased NKG2A expression, consistent with a shift toward a regulatory/non-cytotoxic program. Moreover, although NKp30/NKp44 may appear upregulated, HCC is characterized by altered NCR3 splice variants and defective NKp30-mediated signalling, reinforcing the concept of "apparent activation" coupled to functional paralysis [45–48].

HCC lesions also perturb liver-resident NK identity by reducing $CXCR6^{+}$ subsets and enriching $CD49a^{+}Eomes^{+}$ NK cells, a population associated with impaired cytotoxic competence, pro-angiogenic mediator production, and poorer prognosis [49,50]. Collectively, these data highlight how NK cells are progressively reprogrammed in cancer, and in HCC in particular, by checkpoint engagement, ligand modulation, and TME-derived suppressive signals, providing a strong rationale for NK-targeted immunotherapeutic strategies such as NKG2A blockade and microenvironmental modulation.

3.3 Adoptative cell therapy in cancer

Adoptive cell therapy (ACT) represents a major advance in cancer immunotherapy, using immune cells to target and eliminate tumours. Unlike checkpoint inhibitors, which rely on endogenous antitumor immunity, ACT involves *ex vivo* manipulation of autologous or allogeneic immune cells to enhance specificity and function before reinfusion. The clinical success of CAR-T therapies in B-cell malignancies has accelerated the development of multiple

cellular platforms, including TCR-engineered T cells, tumour-infiltrating lymphocytes (TILs), dendritic cell (DC) vaccines, and emerging innate immune approaches such as CAR-NK cells, CAR-γδ T cells, and CAR-macrophages (CAR-M).

TIL therapy expands tumour-resident T cells *ex vivo* and reinfuses them without genetic modification, while DC vaccines use antigen-loaded autologous dendritic cells to stimulate endogenous T-cell responses. NK cells have attracted strong translational interest due to their MHC-independent cytotoxicity, low risk of graft-versus-host disease (GvHD), suitability for allogeneic manufacturing, and relative resistance to exhaustion, making them a promising alternative or complement to CAR-T therapies for hematologic and solid tumours [51–55]. Genetically engineered T-cell therapies within ACT include TCR-T and CAR-T cells, which differ mainly in antigen recognition: MHC-restricted for TCR-T cells and MHC-independent for CAR-T cells [56–58].

ACT (summarized in Table 2) is based on three core principles: (1) isolation of immune cells from peripheral blood or tumour tissue; (2) ex vivo expansion and/or genetic engineering to enhance antitumor specificity and function; and (3) reinfusion of the modified cells to generate durable, patient-specific antitumor immunity. Compared with passive immunotherapies such as checkpoint blockade, ACT provides sufficient effector cells independent of endogenous antitumor lymphocyte repertoires in immunosuppressed patients and enables engineering strategies, such as dual targeting, cytokine armouring, and checkpoint inhibition, to enhance therapeutic activity [59].

Platform	Antigen Recognition	CRS/GvHD Risk	Manufacturing Time	Stage
CAR-T	MHC-independent	High CRS and GvHD	3–4 weeks	FDA-approved (7 products)
TCR-T	MHC-restricted	Moderate (cross-reactivity risk)	2–3 weeks	Phase 1–2 trials; 1 FDA approval (Tecelra)
TIL	MHC-restricted	Low	4–6 weeks	FDA-approved (Amtagvi, Feb 2024)
CAR-M	MHC-independent	Very low	3–4 weeks (limited expansion)	Early Phase 1
CAR-γδ T	MHC-independent	Very low	2–3 weeks	Phase 1 trials

DC Vaccine	Patient-derived MHC presentation	Very low	1–2 weeks	Phase 1–2 trials

Table 2: Comparative overview of major adoptive cell therapy (ACT) platforms

3.3.1 CAR-Engineered Immune Cells

CARs are synthetic receptors composed of an extracellular antigen-binding domain (typically a single-chain variable fragment, scFv, derived from a monoclonal antibody), a transmembrane region, and an intracellular signalling module that includes CD3ζ as the primary activation domain together with one or more costimulatory domains (most commonly CD28 or 4-1BB/CD137). They mediate MHC-independent recognition of surface tumour antigens, allowing activity against MHC-loss, tumour variants and enabling function across HLA barriers, including in allogeneic settings. Upon antigen engagement, CAR signalling delivers a strong engineered activation signal that is independent of endogenous TCR–CD3 signalling and promotes robust activation and sustained proliferation [60,61].

First-generation CARs containing CD3ζ alone showed limited persistence and modest efficacy, whereas second-generation CARs incorporating CD28 or 4-1BB substantially improved expansion and survival. CD28-based constructs are often associated with faster proliferation but may increase susceptibility to exhaustion, while 4-1BB-based CARs tend to support more durable, central memory-like phenotypes. Building on these advances, third-generation and next-generation CARs explore dual costimulation, inducible signalling strategies, and additional immune-enhancing functions such as cytokine secretion or checkpoint modulation [62]. Clinically, CD19-directed CAR-T cells induce high initial complete remission rates in B-cell acute lymphoblastic leukemia (80–92%) and achieve meaningful responses in relapsed/refractory diffuse large B-cell lymphoma (40–60%). In multiple myeloma, BCMA-directed CAR-T therapies produce overall response rates of 71–73%, with a median progression-free survival of 13.3 months compared with 4.4 months in standard-of-care comparators [53,63]. Multiple autologous CAR-T products have obtained FDA approval (Table 3), primarily targeting CD19 in B-cell malignancies and BCMA in multiple myeloma [51,51,53].

CAR-T product	Target antigen	Costimulatory domain	Approved indications
Kymriah (tisagenlecleucel)	CD19	4-1BB	B-ALL (≤25 years), R/R LBCL, R/R FL
Yescarta (axicabtagene ciloleucel)	CD19	CD28	R/R LBCL, R/R FL (refractory/relapsed within 12 months)
Tecartus (brexucabtagene autoleucel)	CD19	CD28	R/R MCL, R/R B-ALL (adults)
Abecma (idecabtagene vicleucel)	BCMA	4-1BB	R/R MM (≥4 prior lines)
Breyanzi (lisocabtagene maraleucel)	CD19	4-1BB	R/R LBCL variants; newly approved MZL (Dec 2025)
Carvykti (ciltacabtagene autoleucel)	BCMA	4-1BB	R/R MM (≥4 prior lines)
Tecartus (label update)	CD19	CD28	Updated label approval (June 2025), reduced REMS burden

Table 3: Summary of commercially available autologous CAR-T products with regulatory approvals (FDA/EMA), stratified by antigen target and key clinical efficacy benchmarks.

Among emerging CAR-engineered platforms, CAR-macrophages (CAR-M) exploit key myeloid properties such as tissue infiltration, extracellular matrix remodeling, and phagocytic clearance of tumour cells, together with the ability to modulate local immune responses. Through CAR-mediated antigen recognition, these cells can induce antibody-dependent cellular phagocytosis (ADCP) while also presenting antigens and secreting cytokines, potentially reshaping the tumour microenvironment (TME) toward a pro-inflammatory state [53,64,65]. Despite this promise, CAR-M approaches remain largely at preclinical or early clinical stages, with translation limited by manufacturing challenges including poor proliferative capacity, modest gene-engineering efficiency, and low final yields, typically using monocyte-derived or $CD34^+$ stem cell–derived macrophages with lentiviral delivery systems [64,65].

Another emerging strategy involves CAR-engineered γδ T cells, which combine CAR specificity with the intrinsic MHC-independent tumour recognition of γδ T lymphocytes. These

cells recognize stress signals and phosphoantigens through their γδTCR, enabling rapid responses to transformed cells without classical HLA restriction. CAR engineering therefore creates a dual-recognition system that integrates CAR targeting with endogenous stress sensing [66]. From a translational perspective, CAR-γδ T cells offer strong tissue-homing capacity, reduced exhaustion, and compatibility with allogeneic use with minimal risk of graft-versus-host disease (GvHD). Early clinical results, including CD20-directed CAR-γδ T cells in B-cell lymphoma, have shown encouraging remission rates without severe GvHD, and phase I trials are ongoing in solid tumours [66].

In current clinical practice, CAR-T therapy remains the reference ACT modality for relapsed or refractory $CD19^+$ B-cell malignancies and $BCMA^+$ multiple myeloma, where the most robust clinical evidence exists. CAR-NK cells are increasingly explored as a safer alternative, particularly in CAR-T–refractory disease or in patients at higher risk of treatment-related toxicities. TCR-T therapies are best suited for targeting intracellular antigens but require careful patient selection due to HLA restriction and potential off-target effects. Tumour-infiltrating lymphocyte (TIL) therapy, such as lifileucel, represents a personalized non-engineered ACT strategy currently used in PD-1–resistant melanoma. Meanwhile, next-generation platforms including CAR-M and CAR-γδ T cells remain experimental but hold considerable promise for solid tumours, where CAR-T efficacy is often limited by poor trafficking and highly immunosuppressive tumour microenvironments [53,61,62,65,66].

3.4 CAR-NK Cells

CAR-NK represent a highly attractive platform for adoptive immunotherapy because they merge innate MHC-independent NK recognition with CAR-driven antigen specificity, creating a dual-targeting modality in which tumour cells can be recognized both through the CAR and through endogenous NK activating pathways.

3.4.1 CAR-NK challenges

Despite the strong biological rationale for NK-based immunotherapy, several translational barriers still limit clinical efficacy, particularly in solid tumours. A major challenge is the limited *in vivo* persistence and expansion of adoptively transferred NK cells: CAR-NK cells typically persist only weeks to months, much shorter than CAR-T cells. This reflects the intrinsically shorter lifespan of NK cells, their dependence on sustained IL-15 signalling for

survival and function, and the risk of activation-induced cell death following chronic CAR stimulation or prolonged receptor engagement. Current strategies therefore aim to enhance persistence through CAR designs incorporating autocrine or inducible IL-15, dual activation circuits, or differentiation protocols that generate memory-like NK cells [67].

Another key obstacle is efficient trafficking and tumour infiltration, as NK cells must reach tumour sites and overcome dense stromal barriers within immunosuppressive TMEs. This is particularly challenging in poorly vascularized solid tumours characterized by immune exclusion, where checkpoint ligands such as PD-L1 and PD-L2 can further impair endothelial adhesion and homing. Once within tumours, NK cells encounter multiple suppressive mechanisms. Hypoxia-driven pathways, including HIF-1α activation, together with metabolic inhibition caused by adenosine accumulation (via the CD39/CD73 axis) and lactate, impair glycolysis, survival, and cytotoxicity. Tumour-derived TGF-β further inhibits NK-cell maturation and reduces expression of natural cytotoxicity receptors, while M2-like tumour-associated macrophages reinforce suppression through IL-10 and TGF-β signalling. Metabolic stress also contributes significantly: TME-derived factors disrupt mitochondrial function, reduce ATP production, and limit oxidative phosphorylation, while glucose depletion by highly glycolytic tumours constrains NK-cell degranulation and cytokine production.

Some of these impairments are partially reversible. IL-15 can restore NK metabolic fitness through mTOR signalling, and several CAR-NK platforms incorporate IL-15 support to improve persistence. However, excessive or continuous IL-15 exposure may paradoxically reduce NK function, an effect known as the “IL-15 dosing paradox”, highlighting the need for careful dosing strategies. Despite these challenges, multiple CAR-NK products are currently being evaluated in Phase I–II clinical trials across hematologic malignancies and solid tumours [68–70].

3.4.2 Engineering Methods: How CAR-NK Cells Are Generated

Viral gene transfer

Lentiviral vectors (LVs) represent the most widely used platform for CAR-NK engineering because they can transduce both dividing and non-dividing cells and support stable genomic integration. However, primary NK cells are intrinsically resistant to lentiviral transduction due to strong antiviral defenses and limited receptor availability, resulting in lower efficiencies than in T cells [32,71]. To improve delivery, vectors are often pseudotyped with alternative

envelopes. While conventional VSV-G vectors rely on LDLR-mediated entry, poorly expressed on NK cells, baboon envelope-pseudotyped vectors (BaEV-LVs) enter through ASCT1/ASCT2 transporters and achieve substantially higher transduction efficiency with favorable safety profiles [71–73].

Transduction efficiency also depends on NK activation status: short IL-2 stimulation or feeder-based expansion increases metabolic activity and receptor expression, enhancing permissiveness to gene transfer [74]. Procedural parameters such as multiplicity of infection (MOI), timing during expansion, and enhancers like Retronectin or Vectofusin-1 can further improve efficiency and reduce viral requirements in GMP manufacturing pipelines [75,76]. Although lentiviral integration ensures durable CAR expression, random insertion introduces potential genotoxicity risks; therefore, clinical platforms employ self-inactivating (SIN) vectors and strict GMP testing for replication-competent lentivirus (RCL) [77]. Gamma-retroviral vectors have historically been used but are less suitable for NK cells due to their requirement for cell division and higher integration bias near proliferation-related genes, leading most manufacturing workflows to move away from them [78,78].

Non-viral gene transfer

Non-viral approaches are increasingly explored to simplify manufacturing and improve safety. mRNA electroporation is a widely used method that enables rapid, transient CAR expression through delivery of *in vitro*-transcribed mRNA using pulsed electric fields. CAR expression appears within hours and peaks around 24 hours, then gradually declines as mRNA degrades; chemically modified transcripts can extend functional activity for several days while maintaining cell viability [68,70].

To achieve longer expression without viral vectors, transposon systems such as Sleeping Beauty and PiggyBac enable genomic integration via a transposase enzyme. For example, hyperactive Sleeping Beauty variants (e.g., SB100X) insert CAR cassettes at TA dinucleotide sites. Although integration efficiency remains lower in NK than in T cells, these systems offer manufacturing advantages because they avoid viral components and associated regulatory testing [79,80]. Hybrid approaches have also emerged, such as MAJESTIC, which combines adeno-associated virus (AAV) delivery of the transposon cassette with transient mRNA expression of the Sleeping Beauty transposase to achieve stable CAR integration while maintaining a non-viral framework [81].

Genome editing with CRISPR-Cas9

CRISPR-Cas9 editing enables next-generation CAR-NK engineering by allowing targeted knock-out of inhibitory pathways or site-specific CAR knock-in. In NK cells, ribonucleoprotein (RNP) electroporation is commonly used because it provides high editing efficiency with limited off-target effects due to the short intracellular half-life of Cas9 [82]. High knock-out efficiencies have been achieved for genes such as KLRC1 (NKG2A), and combined strategies integrating checkpoint deletion with CAR knock-in demonstrate the feasibility of multi-layer engineering in a single workflow [83,84]. Target selection often focuses on removing inhibitory pathways that limit NK activity. For example, KLRC1 deletion disrupts the HLA-E/NKG2A checkpoint exploited by many tumours, enhancing CAR-NK cytotoxicity [84,85]. Similarly, ADAM17 knock-out or engineering of a non-cleavable CD16a variant (S197P) preserves ADCC during NK activation [86,87]. Modulation of cytokine signalling is another strategy: deletion of CISH or SOCS3 enhances IL-15 signalling, improving persistence and metabolic fitness, while TGFBR2 knock-out protects NK cells from TGF-β-mediated suppression within the tumour microenvironment [88–90].

CRISPR editing also enables site-specific CAR knock-in into transcriptionally permissive loci, reducing variability in expression and potentially lowering genotoxic risk compared with random integration. Advanced multiplex strategies combining multiple knock-outs and knock-ins aim to simultaneously enhance tumour recognition, persistence, and resistance to immunosuppression, although editing efficiency decreases as the number of modifications increases [91].

Engineering Method	Approach	Integration Profile	Key Strengths	Main Limitations
Viral Gene Transfer	Lentiviral vectors, BaEV-pseudotyped LV; γ-retroviral vectors	Stable (genomic integration)	Long-term CAR expression; supports extended persistence and serial killing; clinically consolidated GMP workflows	Risk of insertional mutagenesis; NK cells relatively resistant to standard LV entry; longer manufacturing timeline due to viral production and release testing (e.g., RCL)

Non-Viral Gene Transfer	mRNA electroporation (transient CAR), transposons (Sleeping Beauty, PiggyBac), hybrid systems (e.g., AAV-SB "MAJESTIC"-like concepts)	Transient (mRNA); Stable (transposons)	Rapid and flexible manufacturing; avoids RCL testing; reduced genotoxicity	mRNA expression is short-lived, often needs repeated dosing; transposon efficiency lower in NK cells and depends on nucleofection quality; DNA delivery can stress cells
Genome Editing with CRISPR-Cas9	Knock-out (KLRC1/NKG2A, ADAM17, CISH/SOCS3, TGFBR2); knock-in using HDR templates	Stable if knock-in; permanent gene disruption for knock-out	Enables multi-layer engineering (remove inhibition + enhance cytotoxicity + improve persistence); targeted knock-in reduces variability avoiding random integration	Requires rigorous off-target assessment and quality contr**ol**.; HDR-based knock-in has variable efficiency; adds manufacturing complexity and regulatory testing burden compared with simple transduction

Table 4: Comparative overview of the principal genetic engineering platforms used to generate CAR-NK cells, highlighting integration stability (stable, transient, semi-stable) and the main advantages and limitations relevant to clinical translation. HDR = Homology-Directed Repair; RCL testing = Replication-Competent Lentivirus testing.

3.4.3 Safety and Control Engineering

To improve the clinical safety of CAR-NK therapies, particularly in allogeneic, off-the-shelf settings, modern constructs increasingly incorporate built-in control systems that allow physicians to rapidly terminate or modulate the infused cell product in case of unexpected toxicity. These "safety engineering" strategies are especially relevant when treatment complications such as off-target effects, excessive inflammatory reactions, or tumour lysis syndrome require immediate interruption of CAR activity. A leading approach is the inclusion of suicide switches, among which inducible caspase-9 (iCasp9) represents the best characterized translational platform. iCasp9 is based on a modified human caspase-9 that remains inactive under basal conditions but becomes rapidly activated upon administration of a specific dimerizing drug (AP1903/rimiducid), triggering apoptosis of the engineered cells [92–94]. As an alternative control strategy, some engineered products incorporate EGFRt (truncated EGFR) as a non-signalling surface marker. EGFRt allows selective depletion of the infused cells through administration of cetuximab, which triggers immune-mediated killing (including ADCC) of $EGFRt^+$ transduced cells. While less commonly implemented than

iCasp9, EGFRt is attractive because it leverages an already approved monoclonal antibody rather than requiring a dedicated small-molecule activator [95].

3.4.4 Clinical Translation and Therapeutic Advantages of CAR-NK Cell Therapy

A major translational advantage of CAR-NK therapy is their suitability for allogeneic use: unlike CAR-T cells, NK cells lack a TCR and therefore do not rely on peptide–MHC recognition, largely eliminating the risk of graft-versus-host disease (GvHD). This enables the development of "off-the-shelf" CAR-NK products that can be manufactured at scale, cryopreserved, and administered without HLA matching, significantly reducing vein-to-needle time compared with autologous CAR-T therapies [96]. CAR-NK cells also display an improved safety profile, as they generally produce lower levels of inflammatory cytokines and are less associated with immune effector cell–associated neurotoxicity syndrome (ICANS) [97]. Importantly, CAR-NK cells retain their native cytotoxic machinery in addition to CAR-mediated targeting, providing dual mechanisms of tumour recognition that may reduce relapse due to antigen loss [60].

Clinical translation has initially focused on hematologic malignancies, where accessible tumour compartments and well-defined surface antigens provide favourable conditions for evaluation. A landmark Phase I/II study at MD Anderson using cord blood–derived CD19-CAR NK cells expressing IL-15 in relapsed or refractory B-cell malignancies (NHL, CLL, DLBCL) reported an overall response rate of 48.6% at 100 days, with 1-year progression-free and overall survival of 32% and 68%, respectively; notably, CAR-NK persistence was detected for up to 12 months in responding patients, supporting the role of IL-15 in sustaining in vivo activity [98,99]. More recently, scalable platforms have strengthened the clinical rationale for CAR-NK therapies. In a Phase I study, the iPSC-derived product FT596, engineered to express a CD19-CAR, a high-affinity non-cleavable CD16 to enhance ADCC, and an IL-15/IL-15Rα module to promote persistence, produced objective responses, including complete remissions in patients previously treated with CAR-T therapy, while maintaining a highly favourable safety profile with no cytokine release syndrome (CRS), ICANS, or GvHD observed [100, 101]. Other cord blood–derived CAR-NK products, such as TAK-007, have also shown encouraging activity and tolerability in Phase II studies for relapsed or refractory B-cell lymphomas [102].

Although development in solid tumours is still at an earlier stage, progress is increasing. For instance, GPC3-targeted CAR-NK92MI cells have shown potent activity against $GPC3^+$ hepatocellular carcinoma models and retain function after irradiation, an important safety requirement for NK92-derived products [103]. Similarly, NKG2D-based CAR-NK therapy has been explored in advanced colorectal cancer, where repeated infusions proved feasible and well tolerated, and combination with anti-PD-1 therapy appeared to enhance biological activity [104,105]. Reflecting the growing understanding of NK biology, current studies increasingly explore combination strategies; for example, the CAR-NK product FT596 has been tested with rituximab in lymphoma to exploit both CAR-mediated targeting and CD16-driven ADCC [106]. Despite these advances, NK cells have a shorter intrinsic lifespan and limited persistence compared with CAR-T cells. To address this limitation, many CAR-NK platforms incorporate IL-15 or IL-15/IL-15Rα signalling modules to promote survival and expansion, although repeated dosing is often required compared with the single-infusion paradigm typical of CAR-T therapy [107,108].

Advantage of CAR-NK compared with CAR-T		**Rationale**
Allogeneic compatibility	High suitability for allogeneic administration	NK cells do not express a TCR and therefore lack canonical peptide–MHC recognition, largely eliminating the mechanistic basis of alloreactivity and GvHD.
Product accessibility	Enables "off-the-shelf" cell therapy	CAR-NK cells can be manufactured at scale, cryopreserved, and rapidly deployed without HLA matching, resulting in a markedly shortened vein-to-needle time compared with autologous CAR-T production.
Safety profile	Lower toxicities (CRS/ICANS)	NK cells typically release lower levels of inflammatory cytokines than CAR-T cells and are not associated with cytokine programs strongly implicated in ICANS.
Mechanism of action	Dual killing modality (CAR-mediated + innate cytotoxicity)	CAR-NK cells preserve native NK effector pathways in addition to CAR-driven antigen specificity, providing complementary cytotoxic mechanisms.
Resistance to antigen escape	Greater functional resilience to antigen loss	Innate NK recognition provides built-in redundancy, partially mitigating relapse mechanisms driven by single-antigen escape after single-target CAR-T therapy.
Manufacturing	Improved logistical readiness	Centralized production and immediate post-thaw availability can facilitate broader implementation compared with individualized CAR-T manufacturing workflows.

T*able 5. Comparative overview of the main translational advantages of CAR-NK cells over CAR-T cell therapy. The table summarizes key comparison dimensions relevant to clinical translation highlighting the distinctive features that position CAR-NK as a next-generation adoptive cell therapy platform.*

3.4.5 Combination Strategies with CAR-NK Therapy

Because NK cells show limited persistence and operate within highly immunosuppressive tumour microenvironments, CAR-NK therapy is increasingly developed within rational combination strategies designed to improve expansion, trafficking, and antitumor activity. One widely adopted approach is lymphodepleting chemotherapy prior to infusion, which reduces competition for homeostatic cytokines such as IL-15, promotes inflammatory priming, and limits suppressive immune subsets. Clinically, lymphodepletion has been associated with improved CAR-NK expansion and response durability, as observed in the cord blood CD19-CAR-NK study [109].

Radiotherapy also represents a promising partner, as it can reduce tumour burden, promote immunogenic cell death, and increase expression of stress ligands such as MICA/MICB, thereby enhancing NK susceptibility. In addition, irradiation may partially relieve hypoxia-driven immunosuppression within the tumour niche, creating a more permissive environment for NK-cell activity; early clinical programs are currently evaluating CAR-NK combined with radiotherapy [110].

Checkpoint blockade constitutes another key axis of combination. Anti–PD-1/PD-L1 therapies can enhance CAR-NK activity both directly, since PD-1 may be expressed on tumour-infiltrating NK cells, and indirectly by amplifying endogenous T-cell responses triggered by tumour lysis. In colorectal cancer, combining NKG2D CAR-NK cells with serplulimab (anti–PD-1) correlated with improved clinical benefit and increased CAR transgene expansion in vivo [111]. Targeting the HLA-E/NKG2A inhibitory axis is also under investigation: monalizumab (anti-NKG2A) has shown activity with durvalumab (anti–PD-L1), supporting the rationale for restoring NK cytotoxicity against HLA-E–expressing tumours [112,113].

CAR-NK therapy may further synergize with monoclonal antibodies by exploiting NK-mediated ADCC through CD16 engagement. Fc-engineered antibodies, such as the FGFR2b-targeting antibody bemarituzumab, are designed to enhance NK recruitment and tumour killing [114]. This concept is reinforced by CAR-NK engineering strategies that preserve CD16 signalling, including high-affinity non-cleavable CD16 variants or ADAM17 disruption. Clinically, combining the CAR-NK product FT596 with rituximab improved responses in CD19-negative/CD20-positive escape variants, illustrating the complementary action of CAR targeting and antibody-mediated ADCC [104,115,116].

Additional strategies aim to integrate cytokine support directly within NK-cell platforms. For example, PD-L1.t-haNK cells are engineered to target PD-L1–expressing tumours while incorporating cytokine signalling to sustain cytotoxicity and ADCC [117], while memory cytokine-enriched NK cells (m-ceNK) generated through cytokine priming show enhanced persistence and IFN-γ production [118]. Cytokine-based immunotherapies are also being optimized to support NK function in vivo, including DF6002, an extended half-life IL-12 Fc fusion protein designed to enhance inflammatory signalling in the tumour microenvironment [119], and ANKTIVA, a recombinant IL-15 receptor agonist complex recently approved by the FDA that highlights IL-15 signalling as a strategy to restore immune effector activity [120].

Finally, sequential strategies are being explored to combine the rapid cytoreductive capacity of NK cells with the long-term persistence of CAR-T cells. Sequential CAR-NK followed by CAR-T administration may integrate early tumour debulking with durable immune surveillance, with preliminary evidence suggesting improved disease-free survival in high-risk B-ALL. In parallel, the expanding landscape of NK-centred therapies includes engineered innate-like platforms such as KUR-501 (CAR-NKT), which combines GD2 targeting with cytokine support to enhance persistence and activity in solid tumours [60,121].

3.4.6 Emerging Frontiers Beyond CAR-NK

While CAR-NK therapy is rapidly advancing, parallel strategies aim to redirect endogenous NK cells using antibody-based platforms that avoid *ex vivo* genetic modification. These approaches offer key translational advantages, including simplified manufacturing, off-the-shelf availability, and scalability, making them attractive alternatives or complements to CAR-NK therapies.

Bispecific killer cell engagers (BiKEs) are engineered proteins composed of two single-chain variable fragments (scFvs): one binds an activating NK receptor (commonly CD16 or NKp46), while the other targets a tumour-associated antigen (TAA). The 1633 BiKE, for example, redirects NK cells toward $CD33^{+}$ acute myeloid leukemia (AML) by simultaneously engaging CD16 and CD33, forming an artificial immune synapse that triggers NK degranulation and cytokine release (e.g., IFN-γ, TNF-α). Because BiKEs are protein biologics, they can be manufactured rapidly and avoid the logistical complexity of cell therapy; however, they do not provide signals supporting NK persistence or expansion, limiting durability [122–124].

To address this limitation, trispecific killer cell engagers (TriKEs) incorporate cytokine support. The prototypical 161533 TriKE combines CD16 and CD33 targeting with a modified IL-15 linker, enabling simultaneous NK activation and cytokine-driven proliferation. Compared with BiKEs, TriKEs show enhanced cytotoxicity, NK expansion, and cytokine production, as well as improved tumour control and NK persistence in AML models. Early clinical data with GTB-3550 further support safety, NK expansion, and reductions in leukemic burden in AML patients [97,125,126].

More broadly, NK cell engagers (NKCEs) represent a diverse class of multi-specific antibody constructs designed to amplify NK activation. Many platforms simultaneously engage two activating receptors, such as NKp46 with CD16 or NKG2D, together with a tumour antigen, producing synergistic signalling. Examples include DF1001, which targets HER2 while engaging CD16 and NKG2D and is currently in Phase 1/2 studies in advanced solid tumours, and the ANKET platform, which generates multifunctional constructs engaging NKp46 and CD16 while targeting tumour antigens. Some variants, such as ANKET4, also integrate cytokine modules to enhance NK expansion and activity [127,128]. Fc-engineered formats like AbsoluteFc further exploit CD16 recruitment while directing antibody arms to tumour targets such as EGFR and cMET [129].

In parallel, monoclonal antibodies targeting inhibitory NK checkpoints represent another strategy to enhance endogenous NK responses. Monalizumab, an antibody against the inhibitory receptor NKG2A, blocks the HLA-E/NKG2A axis used by tumours to suppress NK surveillance, restoring NK cytotoxicity without depleting effector cells [130]. Clinically, combining monalizumab with the anti–PD-L1 antibody durvalumab has shown increased antitumor activity in solid tumours, reflecting complementary restoration of NK and T-cell effector function. In the NeoCOAST-2 neoadjuvant NSCLC trial, triple therapy with monalizumab, durvalumab, and chemotherapy produced high pathological response rates while remaining compatible with surgery, highlighting the clinical feasibility of NK-directed checkpoint blockade [131,132].

3.5 Artificial Intelligence in Cellular Immunotherapy Design

Artificial intelligence (AI) and machine learning (ML) are increasingly used as decision-support tools in the development of cellular immunotherapies, guiding hypothesis generation, experimental planning, and translational prioritization [133,134]. In oncology, their major

contribution lies in integrating heterogeneous, high-dimensional data and modelling complex biological systems in which cellular responses arise from nonlinear signalling, feedback loops, and context-dependent interactions [135,136]. This systems-level perspective is particularly relevant for cellular therapies, whose efficacy depends on dynamic interactions between engineered immune cells, tumour targets, and the tumour microenvironment.

Unlike traditional precision oncology approaches based on limited biomarkers, tumour–immune interactions involve multiscale processes spanning genomic, transcriptomic, epigenomic, proteomic, metabolic, and spatial determinants. AI frameworks can integrate these multimodal datasets to identify composite biomarkers of response, resistance, and toxicity, improving predictive accuracy beyond single parameters [137,138]. In immuno-oncology, such approaches have already improved patient selection for immune checkpoint blockade, supported outcome prediction through radiomics, and enabled digital pathology analyses that capture spatial features of the immune contexture associated with therapeutic response [135,139].

A key advantage of AI is its ability to inform experimental design before laboratory implementation. Rather than testing large combinatorial spaces empirically, AI models integrate prior knowledge and early experimental data to identify informative experimental conditions [140,141]. This is particularly valuable in cellular immunotherapy, where biological material is limited and donor variability increases complexity. Parameters such as cytokine exposure, activation protocols, culture conditions, and CAR construct design interact in complex ways that traditional design-of-experiments frameworks cannot fully capture. AI models can instead predict how combinations of variables influence cellular phenotypes and functional outcomes.

Bayesian optimization and active learning further operationalize this strategy by iteratively proposing experimental conditions that balance exploration and exploitation, thereby accelerating convergence toward optimal solutions while reducing experimental burden. Bayesian optimization sequentially tests conditions predicted to maximize improvement in a predefined objective, whereas active learning selects experiments that most effectively reduce model uncertainty. Here, exploration involves the systematic testing of underexplored regions of the experimental parameter space to avoid overlooking potentially superior solutions, while exploitation refines combinations that have already demonstrated promising performance [142,143].

In CAR-NK development, these strategies may help co-optimize expansion, memory-like differentiation, metabolic fitness, and effector activity while limiting exhaustion or excessive cytokine release.

AI also enables in silico simulation of cellular behaviour through hybrid mechanistic–ML models that combine known signalling pathways with data-driven learning. Such models can simulate how variables such as antigen density, co-stimulation, cytokine exposure, or CAR architecture influence activation thresholds, persistence, and functional exhaustion [144,145].

The rapid expansion of single-cell and spatial multi-omics technologies has further strengthened the role of AI in immunotherapy research. Deep-learning approaches can integrate transcriptomic, epigenomic, proteomic, and spatial data to identify immune cell states and interaction networks associated with therapeutic response or resistance—insights that are particularly relevant for understanding NK-cell heterogeneity and tumour microenvironment dynamics in CAR-NK development [138,139,146].

From a translational perspective, AI may help shorten the bench-to-bedside trajectory of cellular therapies. By linking in vitro phenotypes to predicted in vivo performance, AI models can prioritize constructs with the highest therapeutic potential while filtering out candidates with limited efficacy or unacceptable toxicity before advancing to animal studies or early clinical trials [147]. Ultimately, integrating preclinical, clinical, and real-world datasets into unified AI frameworks could enable iterative learning systems in which patient-derived data continuously inform experimental design and product optimization.

Overall, AI functions as a decision-support framework that enhances data interpretation and hypothesis generation, while experimental validation remains essential for biological inference [148]. In CAR-NK development, integrating multi-omics profiling, predictive modelling, and AI-guided experimental design provides a powerful framework to improve efficiency, reproducibility, and translational precision [133,134,145].

3.5 NK role in viral infection: ADAM17 regulation

During acute viral infections, NK cells mount rapid effector responses characterized by enhanced activation signalling and cytotoxic granule release. In contrast, chronic infections often drive a progressive state of NK-cell dysfunction or “exhaustion,” marked by reduced cytokine production, impaired degranulation, and altered receptor expression. This transition

reflects the balance between antiviral immune pressure and viral evasion strategies, ultimately shaping viral persistence and disease outcome [149,150].

Within this regulatory landscape, A Disintegrin and Metalloprotease 17 (ADAM17), also known as TNF-α–converting enzyme (TACE), has emerged as an important modulator of NK-cell function during viral infection [151]. ADAM17 regulates the surface availability of several immune receptors through ectodomain shedding. For example, cleavage of CD16 limits ADCC, while shedding of TIM-3 may influence exhaustion-like phenotypes. ADAM17 also processes IL-6R, enabling IL-6 trans-signalling and amplifying inflammatory responses. Importantly, ADAM17-mediated shedding signatures have been associated with immune dysregulation and disease severity in viral infections including SARS-CoV-2, cytomegalovirus (CMV), and Epstein–Barr virus (EBV) [152–155]. Mechanistically, ADAM17 activity is rapidly induced following cellular stimulation. Viral sensing pathways converge on MAPK signalling, where ERK1/2, p38, and JNK phosphorylate the ADAM17 cytoplasmic tail to enhance protease activity, while pattern-recognition receptor signalling (e.g., TLR activation by viral PAMPs) further promotes ADAM17 activation [156].

Structurally, ADAM17 is a type I transmembrane protease (~70 kDa, 824 amino acids) synthesized as an inactive zymogen whose N-terminal pro-domain blocks catalytic activity through a cysteine-switch mechanism. Its maturation requires trafficking from the endoplasmic reticulum to the Golgi via the rhomboid-family protein iRhom2, followed by furin-mediated cleavage that removes the pro-domain and generates the active enzyme [157,158]. Subsequent phosphorylation-dependent conformational changes within the ADAM17–iRhom2 complex expose the catalytic site, allowing rapid shedding of specific substrates such as EGFR ligands (e.g., HB-EGF) [159,160].

Substrate recognition is highly dependent on structural features. For instance, a triple-serine motif (Ser359–Ser361) near the IL-6R cleavage site selectively promotes ADAM17, but not ADAM10, activity, while defined residues within the TIM-3 stalk region (Glu181–Asp190) are required for efficient cleavage. Changes in substrate orientation or stalk length relative to the plasma membrane can abolish shedding through steric constraints. These observations indicate that ADAM17 activity depends not only on expression levels but also on precise structural regulation of enzyme activation and substrate geometry [159,161]

3.5.1 ADAM17 Across NK and Other Immune Populations

Among hematopoietic populations, monocytes and macrophages show particularly high ADAM17 expression, consistent with their central role in inflammatory signalling: in these cells, ADAM17 controls the shedding of key mediators such as TNF-α, TNFR1, TNFR2, and IL-6R following TLR engagement or cytokine stimulation. Granulocytes and neutrophils likewise express abundant ADAM17 and rapidly cleave L-selectin (CD62L) upon activation, a process essential for leukocyte trafficking and emigration toward inflamed tissues. T lymphocytes also express functional ADAM17; both $CD8^+$ and $CD4^+$ T cells increase ADAM17 activity upon TCR activation, enabling the shedding of multiple immune-regulatory ligands that shape downstream immune responses [162–164].

Peripheral blood NK cells maintain modest ADAM17 protein abundance at steady state, but ADAM17 can be rapidly activated upon engagement with antibody-opsonized targets or cytokine-driven stimulation (particularly under IL-15 stimulation), supporting a dynamic "on-demand" model of receptor regulation. Notably, IL-15, the key cytokine controlling NK cell survival and proliferation, exerts a paradoxical effect: it induces ADAM17 expression while, at the same time, suppressing NK-cell proliferation through ADAM17-dependent mechanisms, suggesting that ADAM17 participates in fine-tuning NK-cell homeostasis rather than serving only as an activation marker[165]. Evidence for a direct functional role also comes from human ADAM17 deficiency: NK cells from a patient with complete ADAM17 loss exhibit normal baseline expression of activating receptors, yet fail to downregulate CD16 after antibody-mediated stimulation, indicating that ADAM17 primarily governs activation-induced receptor shedding rather than steady-state receptor expression [154,166].

Beyond NK cells, ADAM17 contributes to immune regulation in additional compartments. Dendritic cells express ADAM17 and shed molecules such as TNF-α, IL-6R, and ICAM-1, thereby influencing DC maturation and their capacity to prime T-cell responses. B cells and plasma cells generally display lower ADAM17 levels than myeloid lineages; nevertheless, ADAM17 still modulates the cleavage of adhesion molecules including L-selectin, with potential implications for B-cell trafficking dynamics. Overall, this hierarchical distribution supports the concept that ectodomain shedding is differentially prioritized across immune subsets: it represents a core regulatory axis in monocytes and neutrophils, whereas NK cells appear to rely on ADAM17 more selectively, primarily as a mechanism to rapidly remodel receptor landscapes during target engagement [167–170].

3.5.2 ADAM17 Shedding of NK Regulatory Molecules

In viral infection, ADAM17-mediated shedding can be viewed as a dynamic “tuning” mechanism that regulates receptor availability and ligand release at the immune synapse, thereby shaping the magnitude and duration of NK-cell responses and influencing antiviral immunity and immunopathology.

A key example is CD16 (FcγRIIIa), the main Fc receptor mediating ADCC. Engagement of CD16 by IgG-opsonized targets triggers NK-cell activation, degranulation, and cytokine release, but activation is rapidly followed by ADAM17-dependent ectodomain shedding that reduces CD16 surface expression. Pharmacologic inhibition of ADAM17 prevents this cleavage. Functionally, CD16 shedding appears to facilitate immune-synapse disengagement and enable efficient serial killing, allowing NK cells to detach from one target and attack others. However, the relationship between CD16 retention and cytotoxicity is context dependent: ADAM17 blockade can increase CD16 levels and IFN-γ production without consistently enhancing overall cytolysis, suggesting that only a threshold level of CD16 is required for maximal ADCC. Conversely, chronic inflammatory conditions may drive excessive ADAM17 activity and pathological CD16 loss, limiting effective antibody-mediated immunity [166,171,172].

ADAM17 also regulates the checkpoint receptor TIM-3, which is associated with NK-cell dysfunction during persistent antigen exposure. TIM-3 expression increases during acute activation but becomes particularly elevated in chronic infections such as HBV, HCV, and HIV, where it correlates with reduced IFN-γ and TNF-α production and an exhausted NK phenotype [40,173–175]. TIM-3 can undergo ectodomain shedding mediated by ADAM17 and ADAM10. Although the functional consequences in NK cells remain incompletely defined, soluble TIM-3 may act as a decoy receptor that binds ligands such as galectin-9, thereby limiting inhibitory signalling. Reduced ADAM17-mediated cleavage during chronic inflammation could instead stabilize TIM-3 at the cell surface and reinforce exhaustion programs. Emerging evidence also links ADAM17 activity to broader inflammatory circuits, including the ADAM17/AREG/EGFR/ERK1/2 axis, suggesting that dysregulation of this pathway may couple NK dysfunction with maladaptive inflammation in chronic infection [166,176,177].

Another important substrate is the IL-6 receptor (IL-6R), which exists as both a membrane-bound receptor (mIL-6R) and a soluble form (sIL-6R) generated primarily by ADAM17-mediated shedding. While classical IL-6 signalling through mIL-6R generally promotes regenerative or anti-inflammatory effects, the IL-6/sIL-6R complex can activate gp130 on IL-6R–negative cells, driving pro-inflammatory transcriptional programs via NF-κB and STAT3. ADAM17-mediated cleavage depends on a triple-serine motif within the IL-6R stalk region. During viral infections, particularly severe COVID-19, circulating IL-6 and sIL-6R increase markedly and correlate with disease severity. Although NK cells express relatively low mIL-6R levels, they produce IL-6 after viral stimulation, and sIL-6R released from other immune cells can amplify inflammatory signalling through feed-forward IL-6/sIL-6R loops [178–183].

Finally, TNF-α represents one of the earliest and most biologically significant ADAM17 substrates. Activated NK cells produce TNF-α during viral infection, and ADAM17 cleaves membrane-bound pro-TNF-α to release soluble TNF-α that signals through TNFR1 and TNFR2 [184–186]. ADAM17 simultaneously sheds TNF receptors themselves, generating soluble TNFR1 and TNFR2 that can buffer TNF-α signalling. This coordinated release of cytokine and receptor produces complex inflammatory dynamics in which the balance between membrane-bound and soluble forms influences immune outcomes. In severe COVID-19, excessive ADAM17 activity contributes to pathological TNF-α and sIL-6R release and the cytokine storm associated with organ damage and mortality. In NK biology, ADAM17-dependent TNF-α shedding supports systemic cytokine availability and facilitates NK–dendritic cell crosstalk, reinforcing antiviral immune activation [153,188,191,192].

3.5.3 ADAM17 in Viral Infection

ADAM17 has increasingly been recognized as a marker of immune activation in viral diseases. Dysregulated sheddase activity can generate measurable soluble mediators that reflect systemic inflammation and immune dysfunction.

SARS-CoV-2

Several studies indicate that ADAM17-dependent shedding pathways are amplified in severe COVID-19 and contribute to hyperinflammation and adverse outcomes [178,193,194]. Viral binding and ACE2 internalization increase circulating angiotensin II, which activates AT1R signalling and downstream ROS, PKC, and MAPK pathways that converge on ADAM17

activation. Activated ADAM17 promotes shedding of inflammatory mediators such as TNF-α, sIL-6R, and EGFR ligands, sustaining the IL-6–amplifier loop associated with severe disease; accordingly, elevated angiotensin II and sIL-6Rα levels have been proposed as biomarkers of systemic inflammation and intensive care need [193,195–198]. Severe COVID-19 is also characterized by increased circulating sCD14 and sCD163, markers of monocyte/macrophage activation generated through shedding programs that correlate with IL-6 levels and poor prognosis, suggesting a broader ADAM17-driven soluble inflammatory signature [199–201]. In lung tissue, ADAM17 expression markedly exceeds ACE2 (~31-fold) and correlates with immune infiltration ($CD4^+$ T cells, $CD8^+$ T cells, NK cells), implying a role in regulating immune recruitment and activation. Elevated ADAM17 expression in cancer patients with COVID-19 has further been linked to worse outcomes, potentially reflecting interactions between inflammatory circuits and tumour-associated immune suppression [197,202–205].

Human cytomegalovirus (HCMV)

HCMV establishes lifelong persistence and strongly reshapes NK-cell biology, notably through the expansion of adaptive NK-cell subsets expressing NKG2C, CD57, and KIRs that respond robustly to CMV-infected cells. ADAM17 has been proposed as a potential regulator within this context, although clinical evidence remains limited. Hypothetically, CMV-associated changes in ADAM17 expression could stabilize NK receptors and alter activation thresholds, while reduced shedding of TNF-α or TNFR2 might modify NK–dendritic cell crosstalk. Similarly, altered CD16 shedding could influence serial killing and ADCC responses mediated by CMV-specific antibodies. Comparative analyses of ADAM17 activity and shedding profiles across different CMV viral loads may help identify soluble markers predictive of reactivation risk or progression to CMV disease [206–210].

Epstein–Barr virus (EBV)

EBV persists lifelong in memory B cells and periodically reactivates. NK cells contribute to viral control by recognizing stress-induced ligands via receptors such as NKG2D and DNAM-1 and through CD16-mediated ADCC against infected B cells [211–215]. EBV evades immune surveillance through multiple mechanisms: during the lytic phase, proteins such as BZLF1 and BHRF1 promote viral reactivation and protect infected cells from NK killing, while in latency EBNA1 downregulates NKG2D ligands (ULBP1–3), reducing NK activation. Although direct

modulation of ADAM17 by EBV has not been demonstrated, NK phenotypes observed in chronic EBV infection, including increased TIM-3 and reduced NKp30/NKp46, suggest altered receptor regulation that could involve dysregulated ADAM17-mediated shedding, potentially linking persistent infection with checkpoint upregulation and NK dysfunction [211,216–218].

Kaposi's sarcoma–associated herpesvirus (HHV-8)

KSHV/HHV-8 drives Kaposi's sarcoma, particularly in immunosuppressed individuals. NK cells normally contribute to immune surveillance, but KSHV interferes with NK recognition by modulating both target-cell ligands and NK receptor expression. Patients often display reduced activating receptors such as NKp30, NKp46, CD161, and in some cases NKG2D. Viral protein K5 downregulates NKG2D ligands (MICA/MICB) and ICAM-1 on infected cells, while Kaposi's sarcoma lesions produce high levels of prostaglandin E2 (PGE2), suppressing NKG2D expression and IL-15–mediated NK activation [219–222]. In transplant recipients, HHV-8 infection can progress from asymptomatic DNAemia to Kaposi's sarcoma inflammatory cytokine syndrome (KICS), characterized by a cytokine-release–like inflammatory profile with elevated IL-6, IL-10, IFN-α, TNF-α, IL-1β, and IL-17A. Increased soluble markers such as sCD14 and sCD163 accompany this inflammatory state, consistent with macrophage-driven remodelling of the tumour microenvironment [223]. Although not uniquely specific to ADAM17, these soluble markers align with the concept that dysregulated ectodomain shedding and inflammatory amplification loops contribute to severe viral disease. Whether ADAM17 directly participates in HHV-8–associated NK dysfunction, for example through modulation of CD16 shedding, TNF-α and IL-6 signalling, or PGE2-driven inhibitory pathways, remains unclear, but altered CD16 expression patterns and CRS-like inflammation in KICS support the hypothesis that ADAM17-dependent shedding may represent an underexplored mechanism linking HHV-8 infection with NK dysregulation and disease progression.

3.5.3 ADAM17 as an Immune Evasion Target: examples from Herpesviruses

Accumulating evidence indicates that several viruses have evolved strategies to manipulate ADAM17, exploiting its central role in immune regulation. HCMV represents a paradigmatic example. In particular, HCMV encodes two proteins (UL148 and UL148D) that downregulate ADAM17 by interfering with its maturation and surface trafficking. As a result, ADAM17

surface expression is reduced and the shedding of multiple immunoregulatory substrates, including TNFR2, is significantly impaired. Functionally, HCMV-mediated ADAM17 downregulation impacts several immune pathways simultaneously. Stabilization of TNFR2 on infected cells may favour pro-survival NF-κB signalling and limit TNF-driven apoptosis, while reduced shedding of ADAM17 substrates can reshape NK-cell regulation and Treg-associated immune control. Mechanistically, UL148/UL148D are thought to disrupt iRhom2-dependent ER-to-Golgi trafficking, leading to intracellular accumulation of immature pro-ADAM17 and limiting the availability of mature catalytically active ADAM17 at the plasma membrane [224–227]. By contrast, ADAM17-targeting mechanisms in EBV and HHV-8 remain less clearly defined. In chronic HBV and HCV infections, reduced CD16 expression and increased TIM-3 expression on NK cells correlate with progressive disease—phenotypes consistent with dysregulated ADAM17-mediated receptor shedding. Whether these patterns reflect direct viral targeting of ADAM17 or represent an indirect consequence of chronic antigen exposure and sustained inflammatory cytokine signalling remains an open question [228–230].

4.AIMS

Overall Objective

The overall objective of this PhD project was to investigate the biology and therapeutic potential of NK cells in two major clinical contexts: cancer immunotherapy and viral infections. Through a translational approach combining cellular characterization, genetic engineering, and functional validation in preclinical and clinical settings, the project aimed to define innovative NK cell–based strategies and identify biomarkers of immune activation.

AIM 1: NK Cells in Immunotherapy

This aim focused on the development and preclinical validation of innovative NK cell–based immunotherapeutic strategies for solid tumors, with particular emphasis on hepatocellular carcinoma (HCC). The project was structured into three interconnected specific aims:

- **Specific Aim 1.1.** Isolation, Expansion, and Phenotypic Characterization of Primary NK Cells. To establish and optimize a robust platform for the isolation and ex vivo expansion of primary human NK cells derived from liver perfusates of deceased brain-dead donors (DBDs), and to longitudinally characterize their phenotype during in vitro culture. This objective included optimizing NK cell isolation and expansion protocols and flow cytometric monitoring of activation, inhibitory, and maturation markers at defined time points, and assessment of phenotypic stability and activation status over time.

- **Specific Aim 1.2**. In Vivo Proof-of-Concept of Cytokine-Activated NK Cells in an Orthotopic HCC Model. To evaluate the anti-tumor efficacy and safety profile of ex vivo cytokine-activated NK cells in a clinically relevant orthotopic xenograft model of HCC. This objective was achieved by orthotopically implanting luciferase-expressing HepG2 cells into immunodeficient NOG mice, the longitudinal monitoring of tumor progression by in vivo bioluminescence imaging (IVIS) and serum alpha-fetoprotein (AFP) quantification, the assessment of therapeutic response following adoptive transfer of activated NK cells. This study was conducted by Dr. Ester Badami (Fondazione Ri.Med) in collaboration with IRCCS ISMETT and IZS Sicilia.

- **Specific Aim 1.3**. Development and Functional Characterization of GPC3-Targeted CAR-NK Cells. To develop and functionally characterize genetically engineered NK cells expressing a fourth-generation anti-GPC3 chimeric antigen receptor (CAR) as an advanced immunotherapeutic strategy for HCC. This included: the genetic modification of primary NK cells using self-inactivating lentiviral vectors encoding anti-GPC3 CAR constructs, the evaluation of CAR variants incorporating cytokine expression modules to enhance cellular persistence and cytotoxic potential, the characterization of transduction efficiency, immunophenotype, and cytokine secretion profile of CAR-NK cell products.

AIM 2: NK Cells in Viral Infections

This aim sought to investigate the regulation of NK cells during viral infections, with particular focus on ADAM17 as a potential biomarker of NK cell activation and immune modulation. Specifically, the study included:

- **Specific Aim 2.1**. Ex vivo evaluation of ADAM17 expression in whole blood samples from HHV-8–positive transplant recipients.

- **Specific Aim 2.2.** Development of an in vitro viral stimulation model using PBMCs isolated from healthy donors and stimulated with viral peptide pools derived from SARS-CoV-2, HHV-8, CMV, and EBV.

- **Specific Aim 2.3.** Longitudinal quantification of cytokine release in culture supernatants to assess NK cell functional responses following viral stimulation.

5.MATERIALS AND METHODS

5.1 Cells and Culture Conditions

Leukocytes were obtained from the perfusion fluid of liver explants, according to a protocol patented by IRCCS-ISMETT and RiMED Foundation [231].Primary $CD3^{-}CD56^{+}$ NK cells were purified from liver perfusate-derived buffy coats by magnetic separation using the human NK cell isolation kit (Miltenyi Biotec, Bergisch Gladbach, Germany, Europe). NK cells were cultured in MACS NK medium (Miltenyi Biotec, Bergisch Gladbach, Germany), supplemented with IL-2 (500 IU/mL; Proleukin, Chiron, Emeryville, CA, USA) and IL-15 (20 ng/mL; Miltenyi Biotec, Bergisch Gladbach, Germany) and were expanded in the presence of NK activation/expansion beads for five days (Miltenyi Biotec, Bergisch Gladbach, Germany). IL-2 and IL-15 concentrations were selected on the basis of previous titration experiments (IL-2: 250–1000 IU/mL; IL-15: 10–30 ng/mL), as reported in earlier studies [36]. When indicated, NK cells were further activated overnight using either the standard IL-2/IL-15 stimulation, IFN-α (1 µg/mL; Origene, Herford, Germany, Europe), or a combination of IL-12 (10 ng/mL; Miltenyi Biotec, Bergisch Gladbach, Germany) and IL-18 (100 ng/mL; D.B.A., Segrate, Italy). Prior to functional assays or subsequent experimental procedures, NK cells were extensively washed to remove residual cytokines.

5. 2 Flow cytometry

Flow cytometry was performed to confirm liver perfusate-derived NK cell identity and to evaluate ADAM17 expression across immune cell subsets from PBMCs. Briefly, aliquots of 0.5 × 10^6 NK cells were stained for surface markers using a panel of prediluted fluorochrome-conjugated anti-human monoclonal antibodies including FITC-CD3, PerCP-Cy5-NKG2D, APC-A-NKp30, PE-A-NKp44, PE-Cy7-A-NKp46, PE-Cy7-A-NKG2A, FITC-PD-1, APC-A-CD137, APC-R700-A-TIM-3, FITC-CD57, and PE-A-TRAIL (BD Biosciences, Milan, Italy), together with PE-CD45 and APC-CD56 (eBioscience, San Diego, CA, USA), anti-Glypican-3 antibodies including FITC-Glypican-3 (D.B.A., Segrate, Italy) Moreover, flow cytometry was used to assess ADAM17 expression across immune cell subsets in PBMCs using the following fluorochrome-conjugated antibodies: PE-ADAM17, BV786-CD4, BV711-CD3, BV421-CD56, PE-CF594-CD16, BV650-CD14, APC-Cy7-CD8, FITC-CD57, APC-CD19, and BV480-CD45 (BD Biosciences, Milan, Italy). Samples were acquired on a 16-color FACS Celesta SORP flow cytometer (Becton Dickinson, San Jose, CA, USA) and analyzed using

FlowJo software (version 10). Immune populations were gated based on lineage markers to identify NK cells ($CD3^{-}CD56^{+}$), NKT cells ($CD3^{+}CD56^{+}$), $CD57^{+}$ exhausted NK cells, as well as T cells ($CD3^{+}$, $CD3^{+}CD4^{+}$, $CD3^{+}CD8^{+}$), B cells ($CD19^{+}$), and monocytes ($CD14^{+}$); ADAM17 expression was assessed on immune subsets as surface expression (reported as MFI and percentage of positive cells).

5.3 Analysis of AFP Levels

Alpha-fetoprotein (AFP) was quantified in conditioned media collected from cultured hepatoma cell lines using the Siemens Dimension™ Vista 1500 Analyzer (Siemens Healthcare Diagnostics S.r.l., Milan, Italy), according to the manufacturer's recommendations. Before analysis, supernatants were centrifuged to eliminate residual cells and debris. For in vivo experiments, human AFP was measured in serum samples obtained from mice bearing orthotopic HepG2-Luc tumors; blood was collected weekly via retro-orbital sampling.

5.4 Plasmid and Viral Production

Two 4th-generation lentiviral CAR constructs targeting Glypican-3 (GPC3) were generated for expression in primary human NK cells. Vector designs were: (1) Lenti-anti-GPC3-h(28BBζ)-3rd-CAR-EGFRt-IL15 (EF-1alpha promoter–Signal peptide–scFv–CD8 hinge–CD28 TM intracellular–4-1BB–CD3zeta–T2AEGFRt–KpnI–IL15–XbaI), referred to as CAR-GPC3-IL15; (2) Lenti-anti-GPC3-h(28BBζ)-3rd-CAR-IFNα-EGFRt-IL15 (EF-1alpha promoter–Signal peptide–scFv–CD8 hinge–CD28 TM intracellular–4-1BB–CD3zeta–T2AIFNα–T2A–EGFRt–KpnI–IL15–XbaI), referred to as CAR-GPC3-IL15-IFNα (Fig. 2). Both vectors encode the suicide gene EGFRt, a truncated and inactive form of the Epidermal Growth Factor Receptor. EGFRt can bind cetuximab in vivo, triggering complement-mediated target cell death, and serves as a safety mechanism to prevent unexpected adverse effects. Both plasmids were commissioned from Creative Biolabs (Shirley, NY, USA).

Lentiviral particles were produced by transient transfection of HEK 293T cells (CRL-3216™, ATCC; LGC Standards S.r.l., Sesto San Giovanni, Italy). A GFP plasmid control (TWEEN) was used to verify transfection efficiency. Virus production was carried out using the LentiArt™ Virus Packaging Kit (Creative Biolabs, Shirley, NY, USA) and Lipofectamine3000 (Life Technologies, Monza, Italy). Plasmid DNA was purified using the EndoFree Plasmid Maxi Kit (QIAGEN, M-MICROMED S.r.l.s., Catania, Italy).

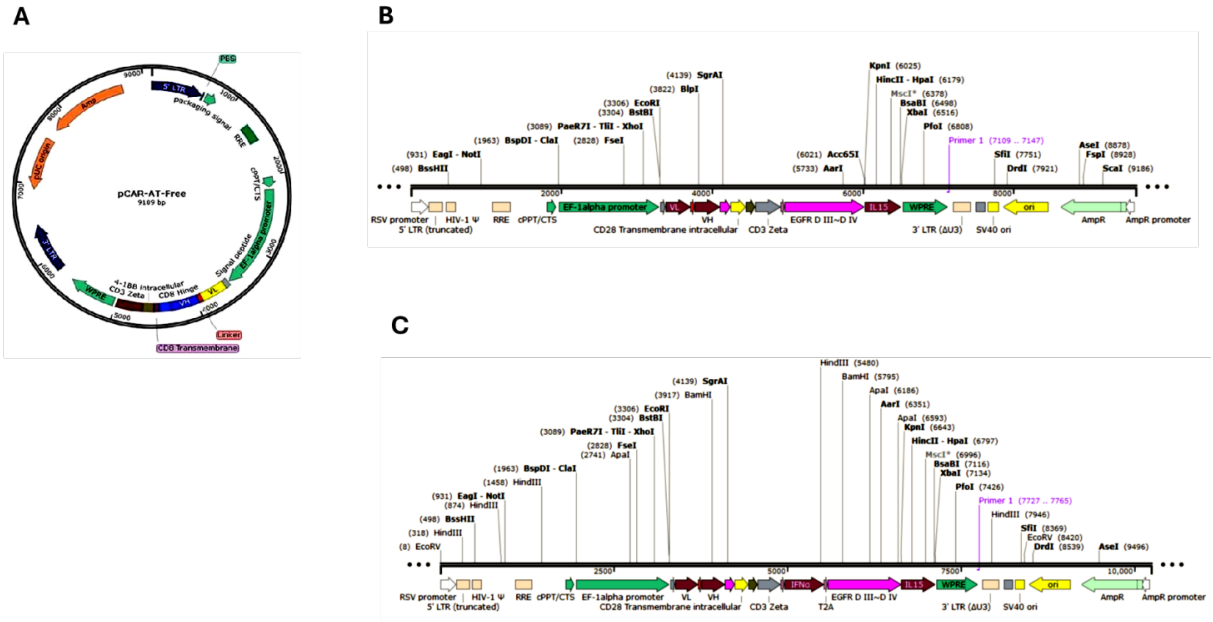

Figure 1: Schematic representation of GPC3-specific CAR construct and the lentiviral vector. (A) GPC3-CAR expression plasmid for lentiviral preparation. (B,C) The construct sequence consisted of a signal peptide, hinge region, transmembrane domain, and intracellular region as follows: Lenti-anti-GPC3-h(28BBζ)-3rd-CAR-EGFRt-IL15 (EF-1alpha promoter-Signal peptide-scFv-CD8 hinge-CD28 transmembrane intracellular-4-1BB-CD3zetaT2AEGFRt-KpnI-IL15-XbaI) (B) and Lenti-anti-GPC3-h(28BBζ)-3rd-CAR-IFNα-EGFRt-IL15 (EF-1alpha promoter-Signal peptide-scFv-CD8 hinge-CD28 transmembrane intracellular-4-1BBCD3zeta-T2AIFNα-T2A-EGFRt-KpnI-IL15-XbaI) (C) [233].

5.5 Viral Transduction

For lentivirus production, 4 × 10^6 HEK 293T cells were seeded in 10 cm dishes 24 h before transfection in DMEM supplemented with 10% FBS and 1% L-glutamine. On the day of transfection, cells were washed twice with PBS and incubated in Optimem (Life Technologies, Monza, Italy) containing Lipofectamine3000 (Thermo Fisher Scientific, Rodano, Italy), LentiArt™ Virus Packaging Kit (Creative Biolabs, Shirley, NY, USA), and the plasmid of interest (TWEEN, CAR-GPC3-IL15, or CAR-GPC3-IL15-IFNα), following the manufacturer's protocol. Medium was replaced after 6–12 h. Viral supernatants were harvested 72 h post-transfection, filtered through a 0.45 µm filter, concentrated using a lentivirus concentration solution (Origene, TEMA Ricerca, Castenaso, Italy), aliquoted, and stored at −80°C.

Primary NK cells were transduced using lentiviral supernatants in the presence of Vectofusin (10 µg/mL; Miltenyi Biotec, Bergisch Gladbach, Germany). Transductions were carried out in untreated 24-well plates (CLEARLine®, Biosigma, Cona, VE, Italy) previously coated with RetroNectin® (7.5 µg/mL; Takara, Diatech Lab Line Srl, Jesi, AN, Italy). After addition of

viral supernatants, 1×10^5 NK cells/well were seeded and subjected to spinoculation (1800 rpm, 1 h, 32°C). Cells were then incubated with the lentiviral vector for 24 h, after which culture medium was replaced with fresh complete medium. Mock-transduced NK cells (empty vector) served as controls. Transduction efficiency was assessed by flow cytometry on days 5 and 10 post-transduction.

5.6 Cytokine detection in CAR-NK conditioned media

Multiplex Analysis of Cytokines Human cytokines IL-2, IL-15, IFN-α, and IFN-γ in CAR-NK cell conditioned media were assessed by ProcartaPlex MixMatch Magnetic bead kit (Affymetrix, Prodotti Gianni, Milan, Italy) following the manufacturer's instructions. Results were obtained with LuminexTM 200 Systems (Luminex Corporation, Austin, TX, USA). Fluorescence intensity (FI) data from the assays were used for further analysis.

5.7 WBC isolated from HHV8-patients

This analysis was conducted at IRCCS-ISMETT using whole blood samples from 10 transplant recipients who developed post-transplant HHV-8 infection. Whole blood aliquots (50 µL/sample) were stained using a panel of fluorochrome-conjugated monoclonal antibodies targeting CD45, CD4, CD8, CD3, CD56, CD16, CD57, CD19, CD14, CD15, and ADAM17. Following surface staining, red blood cell lysis was performed using a lysis buffer. Samples were incubated for 10 min at 37°C, centrifuged at 1800×g for 5 min, washed in PBS, and acquired by flow cytometry. ADAM17 expression was quantified as previously described.

5.8 PBMC isolation from healthy donors

PBMCs were isolated from peripheral blood collected from 15 healthy donors. Whole blood was processed by Ficoll density gradient centrifugation. Briefly, starting from 4 mL of whole blood, samples were diluted 1:2 with PBS-EDTA buffer (2 mM EDTA), and carefully layered onto 3 mL Ficoll. Samples were centrifuged at 800×g for 20 min at 20°C. The opaque interphase containing PBMCs was collected, washed and resuspended in complete RPMI (10% FBS, 1% L-glutamine, 1% penicillin/streptomycin,1% sodium pyruvate) prior to seeding for stimulation assays.

5.9 In vitro PBMC stimulation with viral peptides

To model viral immune stimulation in vitro, freshly isolated PBMCs were cultured and stimulated with viral peptide pools derived from EBV, CMV, SARS-CoV-2, and HHV8. After PBMC isolation, cells were pelleted (1200 rpm for 10 min), and peptides were added to the

cell pellet. Cells were incubated with peptides for 1 h at 37°C and subsequently plated in 96-well U-bottom untreated plates at a density of 2.5×10^5 cells/well. PBMCs were cultured in RPMI supplemented with 10% FBS, 1% penicillin/streptomycin, and 1% L-glutamine. Viral peptides were used at a final concentration of 1 µg/mL. Unstimulated cells cultured in complete medium were included as controls. PBMC stimulation experiments were performed with three sampling time points: Day 1, Day 3, and Day 7. At each time point, PBMCs were collected for flow cytometry analysis of ADAM17 modulation, while culture supernatants were collected and stored for cytokine quantification.

The following peptide pools and viral antigens were used:

- MACS GMP PepTivator EBV Select (Miltenyi Biotec, Bergisch Gladbach, Germany), a pool of 43 lyophilized MHC class I- and class II-restricted peptides derived from 15 EBV proteins, including LMP2a, BRLF1, BMLF1, BNLF1, BERF1/2/3, BALF2, BMRF1, BZLF1, BNRF1, EBNA1/2, and BLLF1.
- PepTivator® CMV pp65 – premium grade and PepTivator® CMV IE-1 – premium grade (Miltenyi Biotec, Bergisch Gladbach, Germany), spanning the complete pp65 sequence (UL83) and the IE-1 immediate-early antigen (UL123), respectively.
- Recombinant SARS-CoV-2 B.1.630 Spike (R&D Systems, Inc., a Bio-Techne brand; Minneapolis, MN, USA). This antigen corresponds to the viral Spike glycoprotein involved in host receptor attachment and membrane fusion, including the S1 and S2 subunits.
- HHV8 peptide pools included latent proteins LANA-1 and K12, and lytic proteins gB (glycoprotein B) and K8.1. HHV8 peptides were kindly provided by Prof. Charles R. Rinaldo (Graduate School of Public Health and School of Medicine, University of Pittsburgh, Pennsylvania, USA).

5.10 Cytokines detection in PBMC activated with viral peptide

Cytokines secreted in response to viral peptide stimulation were quantified in culture supernatants using Luminex™ magnetic bead technology. Supernatants collected at Day 1, Day 3, and Day 7 were analyzed using the Human ProcartaPlex Mix & Match 8-plex kit (Thermo Fisher Scientific, Rodano, Italy), according to the manufacturer's instructions. The panel included 8 analytes: IFNγ, IL-1β, IL-1α, IL-2, IL-6, IL-10, IL-17A, and TNF-α. Samples

were acquired using Luminex-200 instrument (Luminex Corp., Austin, TX, United States). Data was expressed as mean fluorescence intensity (MFI).

5.11 Statistical analysis

Microsoft Office Excel (version 2305) was used for data collection. Statistical analyses were performed using GraphPad Prism (version 8.0.2). Depending on the experimental design and type of comparison, the unpaired t-test, ordinary one-way ANOVA with Tukey's multiple comparisons test, and two-way ANOVA with Sidak's multiple comparisons test were applied. Correlation analyses were performed using Pearson's correlation coefficient. Statistical significance was set at $p < 0.05$. Significance levels were defined as $*p < 0.05$, $**p < 0.01$, $***p < 0.001$, and $****p < 0.0001$.

6. RESULTS

6.1 NK cells in immunotherapy

6.1.1 NK isolation & characterization

In the context of developing and optimizing NK cell–based immunotherapeutic strategies for solid tumours, with a specific focus on HCC, the first experimental phase aimed to establish a robust workflow for the isolation, quality-controlled expansion, and early characterization of primary NK cells. NK cells were purified from liver perfusate-derived buffy coats obtained from DBDs using immunomagnetic separation. The overall isolation and culture workflow is summarized in Fig. 2 A–B. Under the selected expansion conditions (MACS NK medium supplemented with IL-2 and IL-15, with short-term stimulation using activation/expansion beads), liver perfusate-derived NK cells displayed efficient ex vivo growth, reaching ~1.4×10^{10} NK cells after 4 weeks of culture, corresponding to an approximately 280-fold expansion in a representative perfusate-derived NK-cell culture (Fig. 2C). These yields enabled subsequent longitudinal phenotypic monitoring and downstream functional applications.

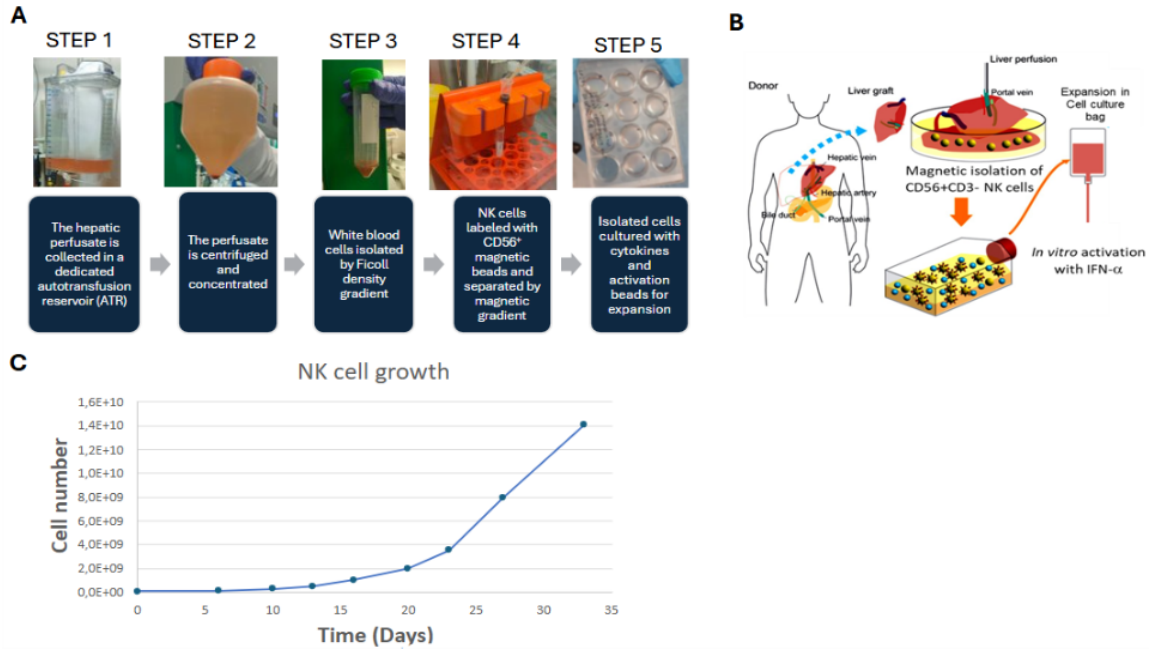

Figure 2: Isolation and expansion workflow of primary NK cells from liver perfusate-derived buffy coats. (A) Graphical representation of the NK-cell isolation procedure from liver perfusate, including magnetic purification of $CD3^{-}CD56^{+}$ NK cells (B) Schematic overview of the experimental pipeline, from perfusate processing to NK-cell culture and subsequent applications, adapted from Ohira et al., 2009. (C) Representative NK-cell expansion curve in culture upon stimulation with IL-2 (500 IU/mL) and IL-15 (20 ng/mL) in MACS NK medium and incubation with NK activation/expansion beads, showing efficient in vitro growth and progressive increase in NK-cell yield over time.

The efficiency of NK-cell isolation from liver perfusate-derived mononuclear cells was assessed across all processed perfusate samples by comparing the expected NK-cell frequency in the starting material with the percentage of NK cells recovered after isolation. Specifically, the expected NK-cell percentage ($CD56^{+}CD3^{-}$) was quantified by flow cytometry on perfusate-derived PBMCs prior to isolation and used to estimate the total number of NK cells in the starting population. As shown in Table 6, the expected NK-cell frequency closely matched the NK-cell percentage measured in the final isolated fraction, indicating high concordance between pre-isolation estimates and post-isolation enrichment. Overall, the isolation procedure yielded a high recovery efficiency, with a median NK yield of 52.1% (Fig. 3), supporting the robustness of the perfusate-based NK isolation protocol. NK yield (%) was calculated as:

NK yield (%) = [real number of NK recovered / (perfusate-derived mononuclear cells × % expected NK)] × 100.

Perfusate N°	Perfusate derived mononuclear cells	Expected NK (%)	Real number of NK recovery	NK recovered (%)	NK yield (%)
1	250000000	28%	50000000	20%	71.40%
2	300000000	20%	50000000	17%	83.30%
3	400000000	22%	50000000	13%	56.80%
4	250000000	30%	61000000	24%	81.30%
5	910000000	10%	29000000	3%	31.90%
6	74400000	49%	24000000	32%	65.90%
7	306000000	62%	65400000	21%	34.50%
8	303000000	36%	81260000	27%	74.50%
9	335000000	31%	50000000	15%	48.20%
10	202500000	18%	19000000	9%	52.10%
11	700000000	14%	62000000	9%	63.30%
12	500000000	38%	96000000	19%	50.50%
13	129400000	24%	10000000	8%	32.20%
14	188000000	19%	35000000	19%	97.90%
15	275200000	27%	70400000	26%	94.70%
16	600000000	34%	94000000	16%	46.10%

17	352500000	34%	55000000	16%	45.90%
18	200000000	26%	26400000	13%	50.80%
19	288000000	28%	14600000	5%	18.10%

Table 6. NK cell isolation efficiency from liver perfusates. The table reports the total number of perfusate-derived mononuclear cells, the expected percentage of NK cells in the starting material (defined as $CD56^+$ $CD3^-$), the absolute number of NK cells recovered after isolation, and the percentage of NK cells in the final isolated fraction. NK yield (%) was calculated as the ratio between the number of recovered NK cells and the estimated number of NK cells in the starting perfusate, multiplied by 100.

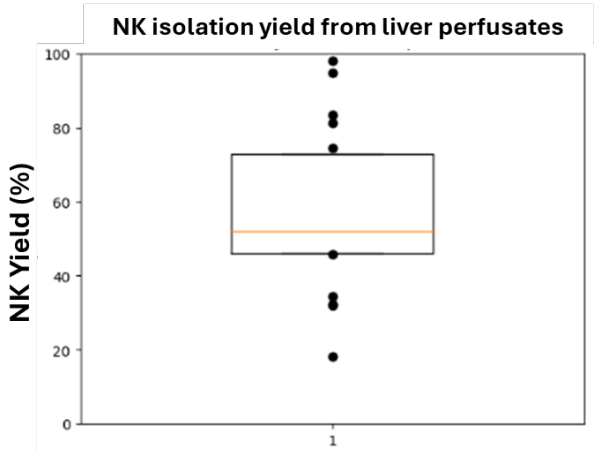

Figure 3: NK cell isolation yield from liver perfusates. Box plot showing the median (horizontal line) and interquartile range (25th–75th percentile) of NK yield (%). Only data points falling outside the interquartile range are displayed as individual dots.

The identity and purity of perfusate-derived NK cells were confirmed by flow cytometry (Fig. 4) using lineage markers to discriminate NK cells ($CD3^-CD56^+$), NKT cells ($CD3^+CD56^+$), and T cells ($CD3^+$). In perfusate-derived buffy coat cells , the lymphocyte gate contained a heterogeneous distribution of lymphoid subsets, including a detectable fraction of NK, NKT, and T cells. Following immunomagnetic isolation, the final cell product consisted of an almost exclusively NK-cell population, with NK cells accounting for 99.3% of gated events, while contaminating NKT (0.59%) and T cells (0%) were negligible. Consistently, histogram analysis confirmed high expression of the NK lineage marker CD56 (98.2%), supporting the high purity of the isolated NK-cell fraction and the effective removal of non-NK lymphocyte subsets.

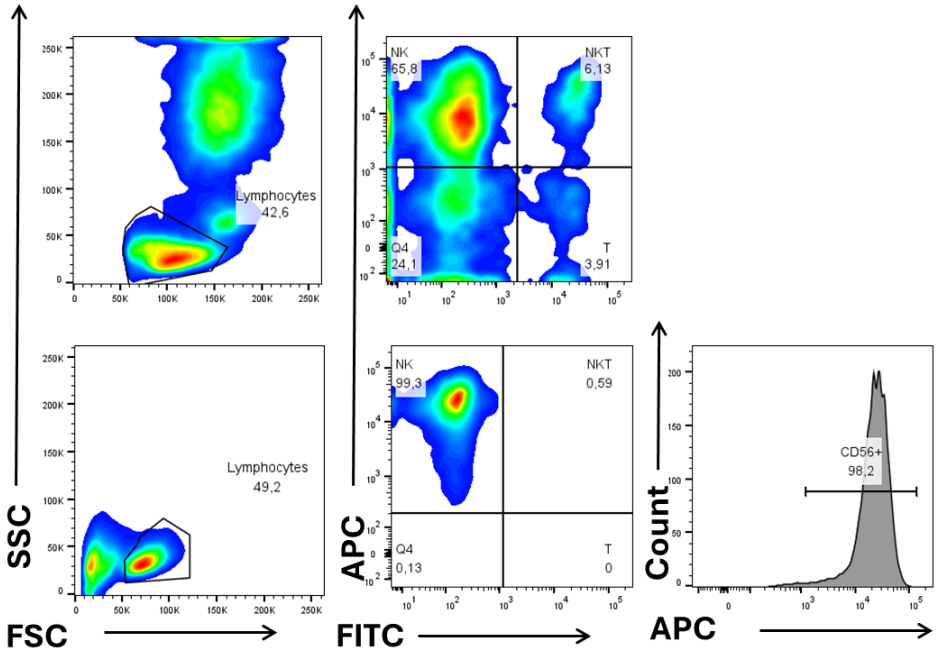

Figure 4: Flow cytometry gating strategy confirming perfusate-derived NK-cell identity and purity after isolation. Representative flow cytometry plots showing lineage-based gating to identify NK cells ($CD3^-CD56^+$), NKT cells ($CD3^+CD56^+$), and T cells ($CD3^+$). Upper panels: perfusate-derived PBMCs within the lymphocyte gate (FSC/SSC) display the coexistence of multiple lymphocyte subsets, including NK, NKT, and T cells. Lower panels: post-isolation analysis demonstrates enrichment of the NK-cell compartment, with a highly pure NK fraction. Histogram plot shows CD56 positivity in the isolated fraction ($CD56^+$ 98.2%).

To monitor the phenotypic profile of perfusate-derived NK cells during ex vivo culture, the expression of selected receptors and differentiation markers was assessed longitudinally at three defined timepoints (T1, T2 and T3, corresponding to weeks 1,2 and 3). The panel included activation/co-stimulatory markers (CD137/4-1BB), inhibitory/checkpoint receptors (TIM-3), natural cytotoxicity receptors (NKp44), inhibitory education-related receptors (NKG2A), and maturation/senescence-associated markers (CD57), together with the ADAM17 sheddase and the Fc receptor CD16 involved in ADCC. Marker expression was reported both as percentage of positive cells (reflecting the frequency of NK cells expressing the marker) and as mean fluorescence intensity (MFI) (reflecting the average signal intensity and thus the relative expression level per cell), moreover histogram plots were reported from a single culture to highlight the positivity for each marker (Fig. 5A–C). Across the examined time points, no statistically significant differences were detected for any of the analysed markers. Nevertheless, the assessment of maturation- and activation-associated markers revealed mild yet appreciable phenotypic oscillations over the culture period.

Expression of the senescence-associated marker CD57 progressively declined over time, with the percentage of positive cells decreasing from 36.32 ± 21.36% at T1 to 17.67 ± 8.30% at T2, remaining low at T3 (19.52 ± 12.58%). In parallel, CD57 MFI showed a marked reduction at T2 (14912.8 ± 12645.7 to 8705.4 ± 6040.7), followed by a partial recovery at T3 (12199.0 ± 12267.2), indicating modulation of expression intensity during culture.

A similar temporal trend was observed for the activation/co-stimulatory marker CD137, which was highly expressed at the early timepoint (48.50 ± 21.49% at T1) and declined at T2 (34.90 ± 19.63%), remaining at comparable levels at T3 (37.78 ± 19.10%). This reduction was accompanied by a progressive decrease in CD137 MFI (4943.0 ± 5231.7 to 4535.0 ± 4506.2 and 1547.4 ± 618.0), suggesting a downmodulation of receptor density over time. In contrast, the inhibitory/checkpoint receptor TIM-3 displayed a transient increase in expression, with the frequency of positive cells rising from 35.08 ± 21.09% at T1 to a peak at T2 (43.80 ± 22.94%), followed by a pronounced decline at T3 (22.34 ± 8.06%). TIM-3 MFI followed a similar pattern, increasing at T2 (4356.4 ± 3927.3) before decreasing at T3 (2421.8 ± 1543.1), indicating a temporary enhancement of inhibitory signaling during intermediate culture. The activating natural cytotoxicity receptor NKp44 remained consistently and highly expressed throughout the culture period. Its frequency increased steadily from 83.16 ± 23.10% at T1 to 95.78 ± 3.14% at T2, reaching 97.00 ± 2.61% at T3. NKp44 MFI also increased at T2 (12941.2 ± 13213.6 to 16268.6 ± 12277.1) and slightly decreased at T3 (13437.0 ± 9171.6), reflecting sustained receptor expression over time. Regarding ADAM17, a gradual increase in the proportion of positive cells was observed from 18.58 ± 11.36% at T1 to 29.18 ± 19.83% at T2, with levels remaining stable at T3 (29.16 ± 17.55%). ADAM17 MFI showed a moderate rise at T2 (1031.0 ± 402.7 to 1429.8 ± 457.2) followed by a slight reduction at T3 (1262.8 ± 429.4), indicating regulated expression during expansion. Expression of the inhibitory receptor NKG2A remained relatively stable in terms of frequency across all timepoints (27.02 ± 23.74%, 26.20 ± 15.61%, and 25.79 ± 18.52% at T1, T2, and T3, respectively). In contrast, NKG2A MFI increased at T2 (7514.2 ± 4348.6 to 12493.8 ± 6088.5) and returned to baseline values at T3 (7555.4 ± 2288.6), suggesting transient modulation of receptor density. Finally, CD16 expression remained high throughout the culture period, with a shift in the distribution of CD16 subsets. The proportion of CD16^bright cells decreased at T2 (49.86 ± 21.50% to 39.28 ± 25.82%) and partially recovered at T3 (42.96 ± 27.48%), whereas CD16^dim cells showed the opposite trend, increasing at T2 (45.62 ± 21.04% to 56.72 ± 24.37%) and remaining elevated at T3 (53.92 ± 26.89%). CD16 MFI increased at T2 (34700.4 ± 16987.8 to 45467.6 ±

44249.1) and remained high at T3 (45342.6 ± 36407.3). Overall, these data document a largely preserved phenotypic signature of perfusate-derived NK cells during the first three weeks of ex vivo culture, providing a reference framework to evaluate potential time-dependent shifts relevant for downstream NK-cell manufacturing steps, including CAR-NK engineering.

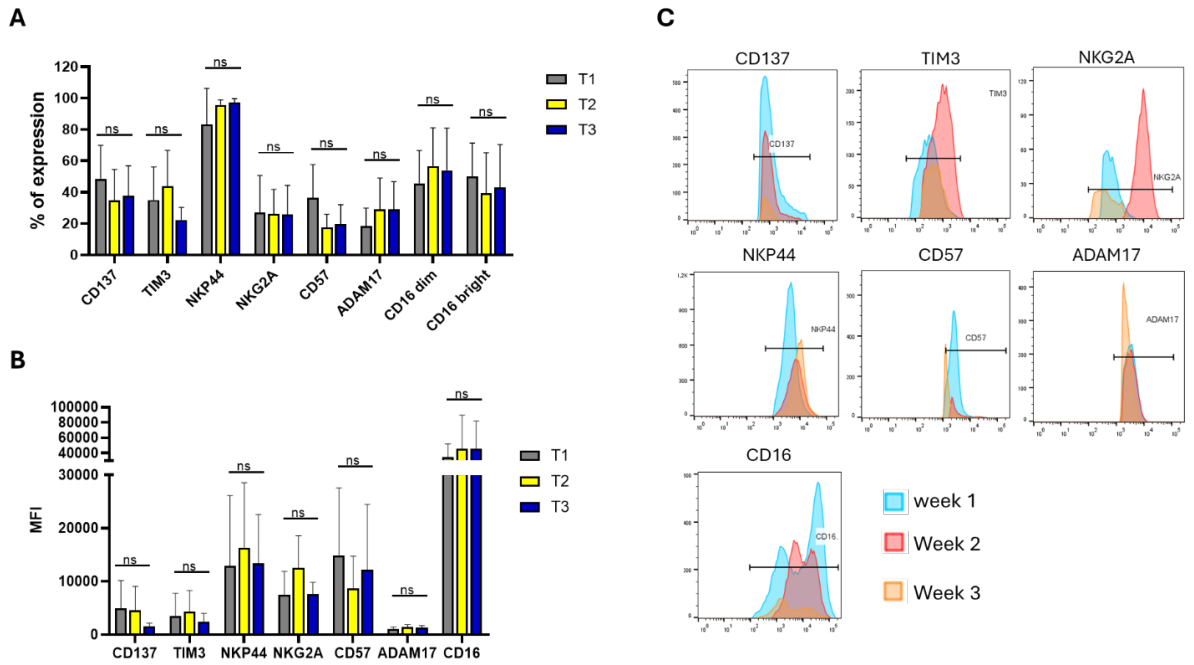

Figure 5: phenotypic profiling of perfusate-derived NK cells during ex vivo culture. Perfusate-derived NK cells expanded in vitro were analyzed by flow cytometry at three culture timepoints (T1, T2, T3; weeks 1, 2, 3) for the expression of key NK-cell markers, including CD137 (activation/co-stimulation), TIM-3 (inhibitory/checkpoint receptor), NKp44 (natural cytotoxicity receptor), NKG2A (inhibitory receptor), CD57 (maturation/senescence-associated marker), ADAM17 (sheddase), and CD16 (Fc receptor mediating ADCC). (A) Marker expression reported as percentage of positive NK cells. (B) Marker expression reported as MFI. (C) Histogram plots from a single culture reporting the positiveness for each marker. Data shown are representative of five NK cell cultures isolated from different perfusate. Statistical comparisons across timepoints were performed using one-way ANOVA with Tukey's multiple comparisons test; statistical significance was set at $p<0.05$, ns non-significant.

6.1.2 *Ex Vivo* Cytokine Activation of Perfusate-Derived NK Cells

Perfusate-derived NK cells were activated overnight with either IFN-α or IL-12/IL-18, and compared with IL-2/IL-15–activated NK cells used as control. IFN-α was selected to enhance NK-cell cytotoxicity through STAT1-dependent pathways and upregulation of activating receptors. In contrast, IL-12/IL-18 stimulation was employed to induce a potent IFN-γ–producing phenotype and promote cytokine-driven functional reprogramming toward a highly inflammatory, memory-like NK-cell profile. IL-2/IL-15 activation was used as a reference

condition, as these cytokines represent the standard platform for NK-cell expansion and survival in adoptive immunotherapy protocols.

To characterize the immunophenotypic impact of *ex vivo* cytokine activation, perfusate-derived NK cells were analysed by flow cytometry following overnight stimulation with either IFN-α or IL-12/IL-18 (Fig. 6). The expression of receptors associated with activation and tumour recognition (NKG2D, NKp30, NKp44, NKp46), inhibitory/suppressive pathways (NKG2A, PD-1, TIM-3), modulation/activation state (CD137), and cytotoxicity-related markers (CD57, TRAIL) was assessed. Overall, the expression levels of most markers were comparable between IFNα-NK and IL-12/IL-18–activated NK cells, indicating broadly similar activation profiles under the two cytokine conditions. Notably, TRAIL expression was increased in NK cells activated with IFN-α compared to IL-12/IL-18–activated NK cells, suggesting enhanced acquisition of a death ligand–associated cytotoxic phenotype in the IFN-α condition.

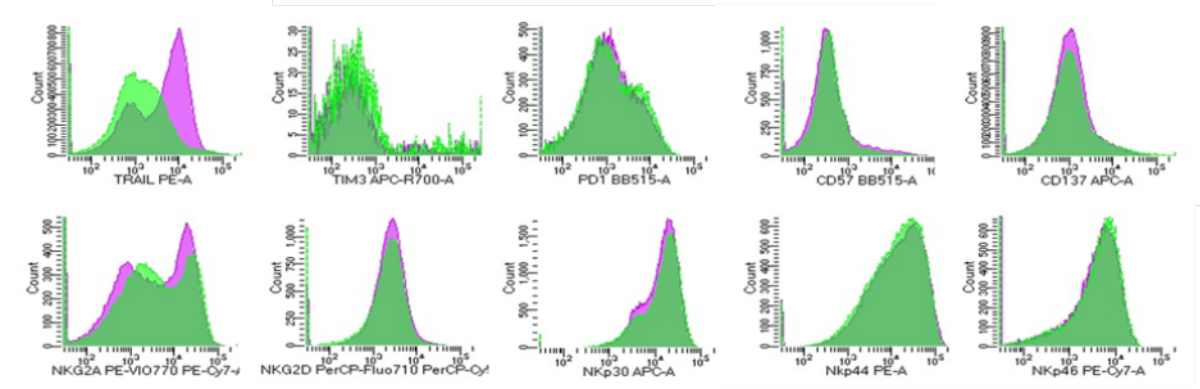

Figure 6: Flow cytometry analysis of IFNα-NK (purple) vs IL12/IL18 NK (green) cells. Comparison of differential expression of NKG2D, NKp30, NKp44, and NKp46 (activating receptors); CD137 (activation-induced co-stimulatory receptor); TRAIL (TNF-related apoptosis-inducing ligand); NKG2A and PD-1 (inhibitory receptors); CD57 (maturation marker); and TIM-3 and PD-1 (exhaustion-associated markers).

6.1.3 *In Vivo* Proof-of-Concept of *Ex Vivo* Activated NK Cell Therapy

This work was conducted at IRCCS ISMETT, a highly specialized transplant and research center and was developed within a research program led by Dr. Badami, Principal Investigator of the project, in which I actively participated during my PhD training. This experimental phase was designed to provide a translational proof-of-concept of cytokine-activated NK-cell therapy in hepatocellular carcinoma, bridging *ex vivo* functional characterization with *in vivo* therapeutic validation in a clinically relevant orthotopic model.

To evaluate the anti-tumour activity and safety of *ex vivo* cytokine-activated NK-cell therapy in a preclinical setting, an orthotopic HCC xenograft model was established in

immunodeficient NOG mice by implanting luciferase-expressing HepG2-Luc cells. This model was selected to enable longitudinal quantification of tumour burden through in vivo bioluminescence imaging (IVIS) following D-luciferin administration, thereby providing a sensitive readout to compare different NK activation regimens. Within this experimental framework (workflow summarized in Fig. 7), NK cells were activated overnight with either IFN-α or IL-12/IL-18 and administered intravenously according to the scheduled infusion protocol. Before initiating *in vivo* treatment, NK-cell functional potency was confirmed *in vitro* against the same target cell line used for tumour engraftment. Both IFNα-NK and IL-12/IL-18-NK displayed significantly higher specific lysis compared to control conditions, confirming effective anti-tumour cytotoxic potential against HepG2-Luc targets

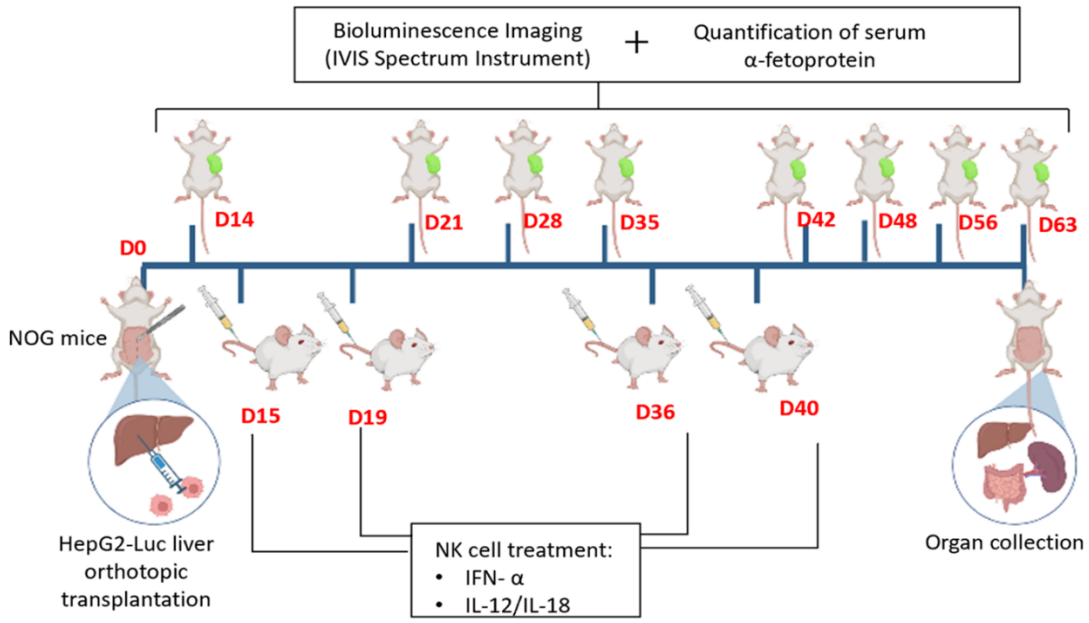

Figure 7 : Experimental design and workflow of the in vivo proof-of-concept study in an orthotopic HepG2-Luc HCC xenograft model. Immunodeficient NOG mice were orthotopically implanted with luciferase-expressing HepG2-Luc cells. Mice received four intravenous NK-cell infusions after overnight activation with either IFN-α or IL-12/IL-18, administered on days 15, 19, 36, and 40 post-implantation. Tumor growth was monitored longitudinally by in vivo bioluminescence imaging (BLI) using the IVIS Spectrum instrument with weekly acquisitions. Serum AFP levels were quantified as an additional readout of tumor burden.

Following the *in vitro* confirmation of cytotoxic potency of cytokine-activated NK cells against HepG2-Luc targets, the anti-tumour efficacy of these NK products was evaluated *in vivo* in an orthotopic HCC xenograft model. NOG mice engrafted with HepG2-Luc cells were treated with intravenously infused NK cells activated *ex vivo* with either IFN-α or IL-12/IL-18, and tumour burden was monitored longitudinally by in vivo BLI. Representative IVIS images revealed a clear reduction of tumour-associated bioluminescent signal in NK-treated animals

compared to untreated controls. In particular, tumour growth appeared most reduced in mice treated with IFNα-activated NK cells, and also reduced, although to a slightly lesser extent, in mice receiving IL-12/IL-18–activated NK cells, whereas the untreated control group displayed the highest bioluminescent signal over time, consistent with uncontrolled tumour progression.

Individual longitudinal trajectories of bioluminescent signal (tracked at days 7, 14, 21, 28, 35, and 42 after tumour cell implantation), showed that tumours in the control group exhibited the steepest signal increase over time, whereas tumour growth dynamics were markedly attenuated in NK-treated groups. In particular, NK cells activated *ex vivo* with IFN-α were associated with the strongest control of tumour progression, with IVIS signals overall approximately 2 log10 lower than controls; NK cells activated with IL-12/IL-18 also slowed tumour progression, with IVIS signals approximately 1 log10 lower than controls. In parallel, serum AFP kinetics (Fig. 8) supported these results. AFP levels of individual animals showed lower AFP levels over time in NK-treated mice compared to controls, consistent with an overall slower tumour growth rate following therapy. Collectively, AFP readouts indicates that *ex vivo* cytokine-activatedNK-cell therapy effectively slowed tumour progression, with the IFNα-NK condition showing stronger anti-tumour activity than IL-12/IL-18-NK cells.

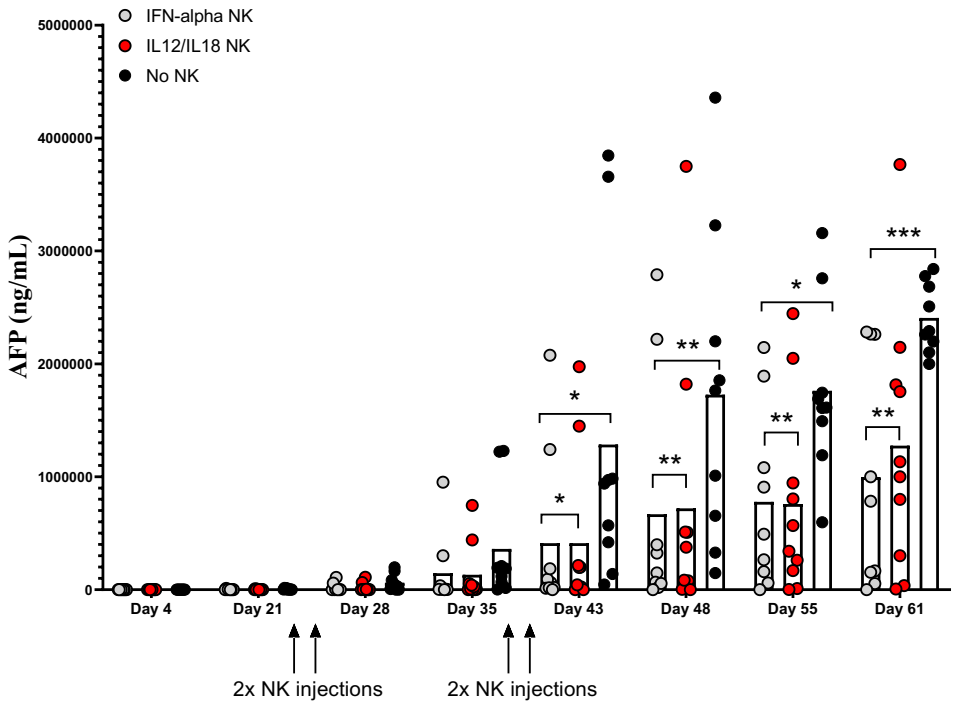

*Figure 8: Tumor growth follow-up by serum AFP levels. Time evolution of serum AFP levels quantified by chemiluminescent assay. Individual AFP level visualized as dot for each acquisition day (one dot per animal/tumor) across timepoints, Data are reported as mean. statistical analysis was done with one-way ANOVA with Tukey's multiple comparisons test. * $p < 0.05$, ** $p < 0.01$, *** $p < 0.001$, **** $p < 0.0001$; ns, non-significant. (n=10).*

6.1.4 Engineering of CAR-NK Cells

To develop CAR-NK cells as an alternative immunotherapeutic strategy for hepatocellular carcinoma, fourth-generation self-inactivating lentiviral vectors encoding an anti-GPC3 CAR were produced and used for NK-cell transduction. Successful lentiviral vector production was supported by the high transfection efficiency achieved in HEK293T packaging cells, as documented by GFP reporter expression. At 72 h post-transfection, a robust GFP signal was observed in HEK293T cells, indicating efficient plasmid delivery and expression and confirming the feasibility of generating lentiviral supernatants for downstream NK-cell transduction (Fig. 9).

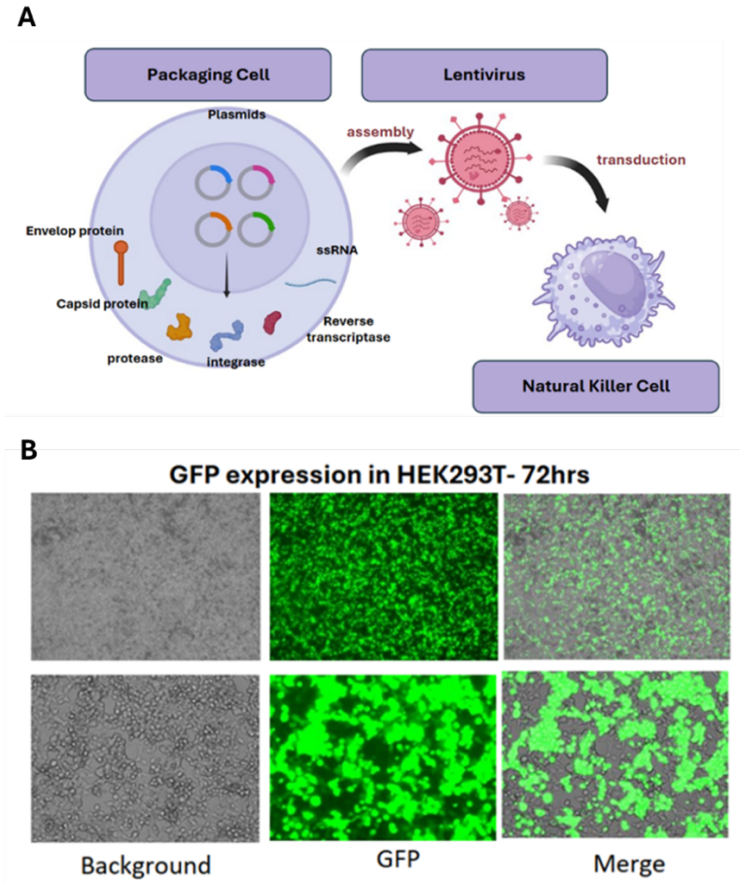

Figure 9: Lentiviral vector production and transduction workflow. (A) HEK293T packaging cells were transiently transfected with the plasmid of interest (TWEEN, CAR-GPC3-IL15, or CAR-GPC3-IL15-IFNα) together with packaging/envelope plasmids to generate CAR-encoding lentiviral particles. Viral supernatants were harvested and used to transduce primary NK cells, in the presence of Vectofusin on RetroNectin-coated plates, resulting in stable transgene expression. (B) GFP expression in HEK293T packaging cells 72 h post-transfection. Representative phase-contrast (background), GFP fluorescence, and merged images showing transfection efficiency in HEK293T cells.

Following lentiviral vector production and delivery, successful transduction of perfusate-derived NK cells was confirmed by detection of GFP reporter expression in the NK-cell

culture. Representative fluorescence imaging (Fig. 10) showed a clear GFP-positive signal in transduced NK cells, indicating effective gene transfer and stable expression of the lentiviral-encoded transgene. The presence of a detectable GFP-positive fraction after transduction supports the overall efficiency of the adopted transduction conditions and confirms the feasibility of genetically engineering primary NK cells within the CAR-NK manufacturing workflow.

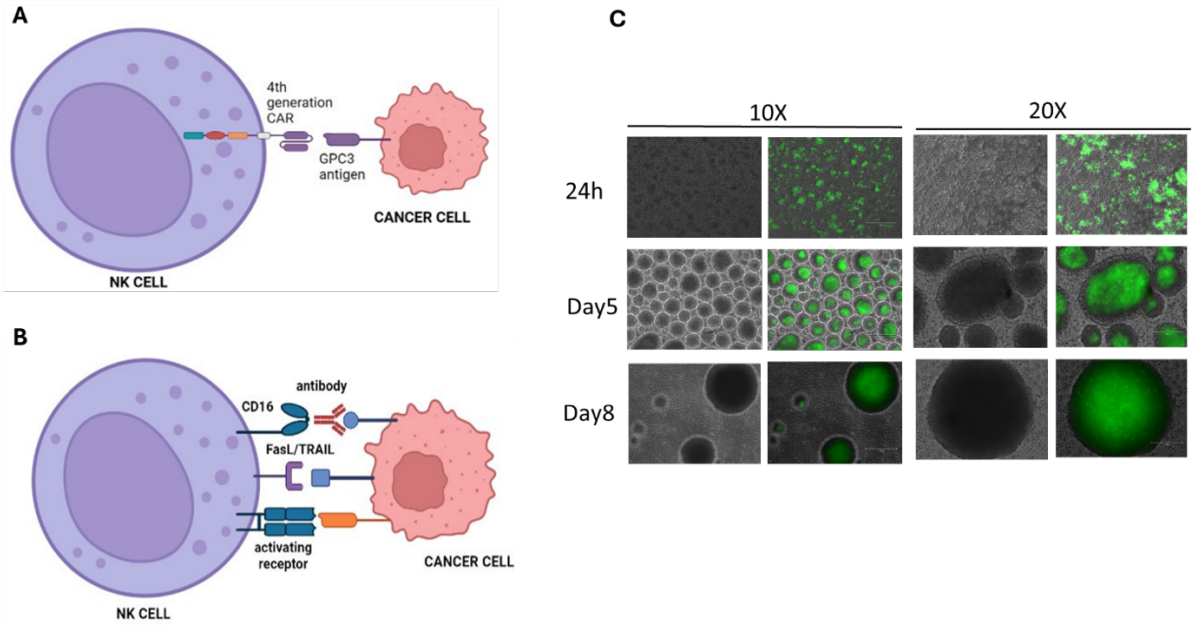

Figure10 : (A–C). CAR-NK design and confirmation of successful lentiviral transduction by GFP reporter expression. (A) Schematic representation of anti-GPC3 CAR-NK cells, showing engineered NK cells expressing a chimeric antigen receptor conferring antigen-specific recognition of glypican-3 (GPC3) on hepatocellular carcinoma cells. (B) Schematic overview of natural NK-cell tumor recognition mechanisms, highlighting innate cytotoxic pathways of target cell killing independently of CAR expression. (C) Representative GFP fluorescence signal in NK cells following lentiviral transduction, confirming transgene acquisition and serving as a qualitative indicator of transduction efficiency.

6.1.5 Quantification of CAR Expression in Engineered NK Cells

Surface expression of fourth-generation GPC3-specific CAR constructs was assessed by flow cytometry in primary NK cells following lentiviral transduction. NK cells were gated on live events based on FSC/SSC morphology and analysed across experimental conditions including non-transduced NK cells (control), GFP-transduced NK cells, and NK cells transduced with CAR-GPC3-IL15 or CAR-GPC3-IL15-IFNα lentiviral vectors. Flow cytometric profiling in Fig. 11 revealed that both GPC3-specific CARs were successfully integrated into the membrane of NK primary cells.

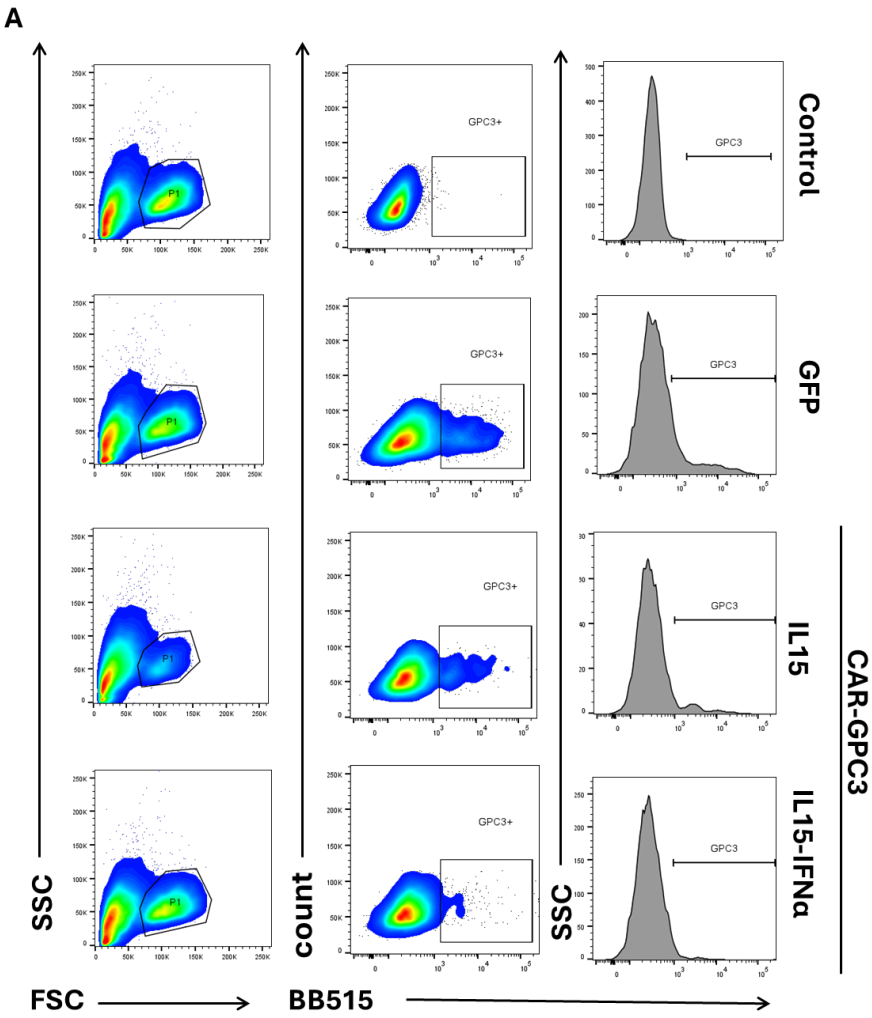

Figure 11: Flow cytometric assessment of surface CAR expression in primary NK cells following lentiviral transduction. Representative flow cytometry plots showing CAR expression in pure primary NK cells under different conditions: non-transduced NK cells (control), GFP-transduced NK cells, and NK cells transduced with CAR-GPC3-IL15 or CAR-GPC3-IL15-IFNα fourth-generation lentiviral vectors. NK cells were gated on live cells based on FSC/SSC morphology.

Cumulative flow cytometric analysis was performed to quantify both the proportion of CAR-expressing NK cells (% transduction) and the level of CAR expression per cell (MFI) at day 5 and day 10 post-transduction, in order to assess early transduction efficiency and persistence over time (Fig. 12).

Among CAR-engineered conditions, at day 5 the percentage of CAR^+ NK cells was comparable between constructs, with CAR-GPC3-IL15 NK cells at 8.2±3.2% and CAR-GPC3-IL15-IFNα NK cells at 10.6±5.3%. Notably, the maximum transduction levels observed at this early timepoint reached 15.1% in the CAR-GPC3-IL15 condition and 25.0% in the CAR-GPC3-IL15-IFNα condition, indicating that high-efficiency events were achievable in individual cultures. At day 10, a reduction in the proportion of CAR^+ cells was observed for both CAR-NK products, with values decreasing to 4.5±2.3% for CAR-GPC3-IL15 and to 2.9±1.4% for

CAR-GPC3-IL15-IFNα; correspondingly, the highest values detected at day 10 were 8.5% and 5.6%, respectively. As expected, non-transduced control NK cells (CTRL) showed only background signal, remaining consistently low at both timepoints (0.3±0.2% at day 5 and 0.2±0.3% at day 10). In the GFP-transduced control, the percentage of GFP^+ cells decreased from 10.2±5.7% (day 5) to 5.6±2.5% (day 10), with a parallel reduction in GFP signal intensity (MFI 3048.0±2649.8 at day 5 vs 1399.0±2275.9 at day 10).

CAR expression intensity, quantified as MFI, showed distinct kinetics across conditions. At day 5, CAR-GPC3-IL15 and CAR-GPC3-IL15-IFNα NK cells displayed comparable signal intensities (MFI 4005.0±2621.6 and 4097.0±3078.6, respectively). At day 10, mean MFI values were 3415.0±2071.1 for CAR-GPC3-IL15 NK cells and 2743.0±1956.0 for CAR-GPC3-IL15-IFNα NK cells, indicating maintenance of measurable CAR expression intensity over time despite a lower CAR-positive fraction. Overall, these data demonstrate successful CAR transduction of primary NK cells with detectable surface expression at early timepoints and partial reduction in the CAR-positive fraction at day 10, while preserving CAR expression levels among transduced cells.

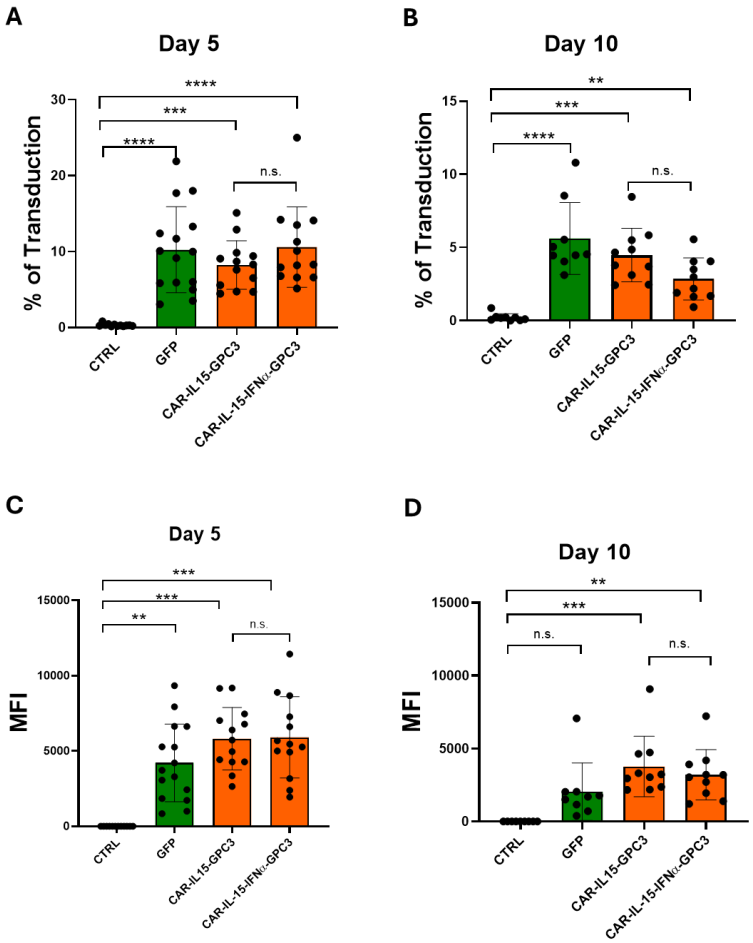

*Figure 12: Longitudinal assessment of CAR transduction efficiency and expression intensity in engineered primary NK cells. Primary human NK cells were transduced with fourth-generation GPC3-specific CAR lentiviral vectors (CAR-GPC3-IL15 and CAR-GPC3-IL15-IFNα) and analysed by flow cytometry at day 5 and day 10 post-transduction to quantify both transduction efficiency and expression intensity. (A) Percentage of CAR-positive cells (% transduction) at day 5 in non-transduced controls (CTRL), GFP-transduced controls, CAR-GPC3-IL15, and CAR-GPC3-IL15-IFNα NK cells; (B) Percentage of CAR-positive cells (% transduction) at day 10 for the same experimental conditions; (C) Mean fluorescence intensity (MFI) of CAR signal at day 5 in GFP, CAR-GPC3-IL15, and CAR-GPC3-IL15-IFNα conditions; (D) MFI at day 10 for the same experimental conditions. Data are reported as mean ± SD. statistical analysis was done with one-way ANOVA with Tukey's multiple comparisons test. * $p < 0.05$, ** $p < 0.01$, *** $p < 0.001$, **** $p < 0.0001$; ns, non-significant (CTRL n=12, CAR-GPC3-IL15 n=13, CAR-GPC3-IL15-IFNα n=13, GFP n=15).*

6.1.6 Cytokine release profiling

CAR-NK cells were tested for the release of cytokines, addressing, in particular, IL-15 and IFN-α, the two soluble factors subcloned in the vector. Addition ally, IL-2 and IFN-γ were also quantified, being involved in the NK-mediated anti-tumor response. As shown in Figure 13, both CAR-NK cells released enhanced levels of IL-15 and IL-2 compared to control and mock NK cells. Interestingly, only CAR-GPC3 IL15-IFNα NK cells produced significantly higher amounts of the cytokine IFN-α, as one would expect. No differences were observed in IFN-γ production.

Collectively, these data confirm enhanced IL-15 secretion by both CAR-NK products versus controls and demonstrate that IFN-α production is restricted to the CAR-IL15-IFNα NK cells, consistent with vector design.

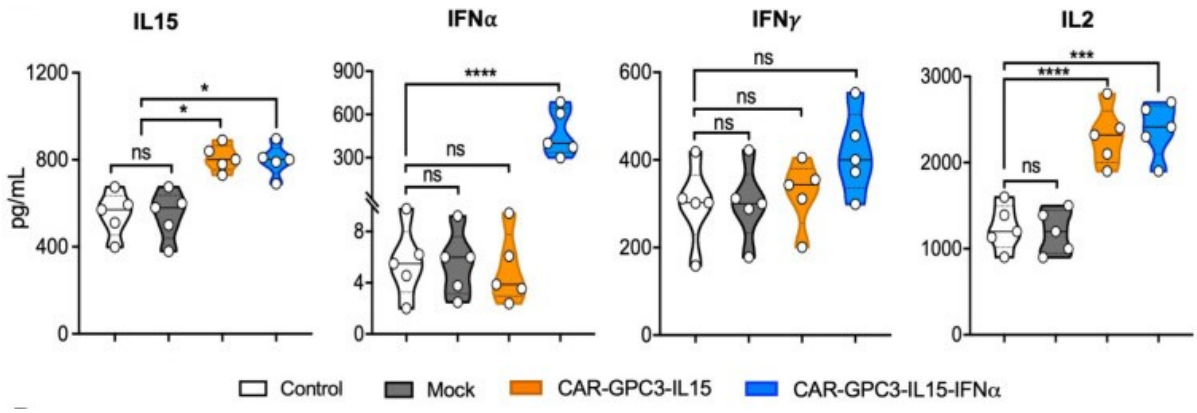

*Figure 13: Characterization of CAR-GPC3-IL15-NK and GPC3-CAR-IL15-IFNα-NK cells. IL-15, IFN-α, IFN-γ and IL-2 production by control, (white), mock control: NK cells transduced with an empty vector (gray), CAR-GPC3-IL15 (orange), and GPC3-CAR-IL15-IFNα NK cells (blue) after 4 h of culture with Huh7 target cells, (n = 5). Mean values ± SEM areshown. Statistical analyses were performed using a two-way ANOVA with Tukey's multiple comparisons test, * $p < 0.05$, ** $p < 0.01$, *** $p < 0.001$, **** $p < 0.0001$; ns, non-significant [233].*

6.2 NK Cells in Viral Infection

6.2.1 ADAM17 expression in HHV-8–positive court

As a second objective of the study, the regulation of NK cells during viral infection was investigated, with a specific focus on ADAM17 as a potential immunological biomarker of NK-cell activation and immune modulation. ADAM17 expression was analysed ex vivo in whole blood samples from HHV-8–positive transplant recipients and compared with healthy controls. Flow cytometric analyses were performed to assess ADAM17 expression across distinct lymphocyte subsets, with particular attention to NK cells, given their central role in antiviral immunity. ADAM17 levels were evaluated both as percentage of positive cells and as MFI, allowing comparative analysis among NK, NKT, exhausted NK ($CD57^+$), and non-exhausted NK ($CD57^-$) populations.

A standardized flow-cytometry gating strategy (Fig.14) was applied to whole-blood samples to identify major leukocyte populations and define NK-cell subsets for subsequent ADAM17 quantification. Doublets were first excluded based on morphological discrimination (SSC-H vs SSC-A), followed by gating on live cells. $CD45^+$ cells were gated to identify lymphocytes, monocytes, and neutrophils. Within the lymphocyte gate, lineage markers were used to define specific subsets: B cells ($CD19^+CD3^-$), NK cells ($CD56^+CD3^-$), NKT cells ($CD56^+CD3^+$), and T cells ($CD3^+CD56^-$). The T-cell compartment was further stratified into T helper cells ($CD3^+CD4^+$) and cytotoxic T cells ($CD3^+CD8^+$). Finally, within the NK gate, expression of CD57 was used to distinguish exhausted/senescent-like NK cells ($CD57^+$) from non-exhausted NK cells ($CD57^-$), enabling downstream comparison of ADAM17 expression across NK and related lymphocyte subsets in HHV-8–positive patients versus controls.

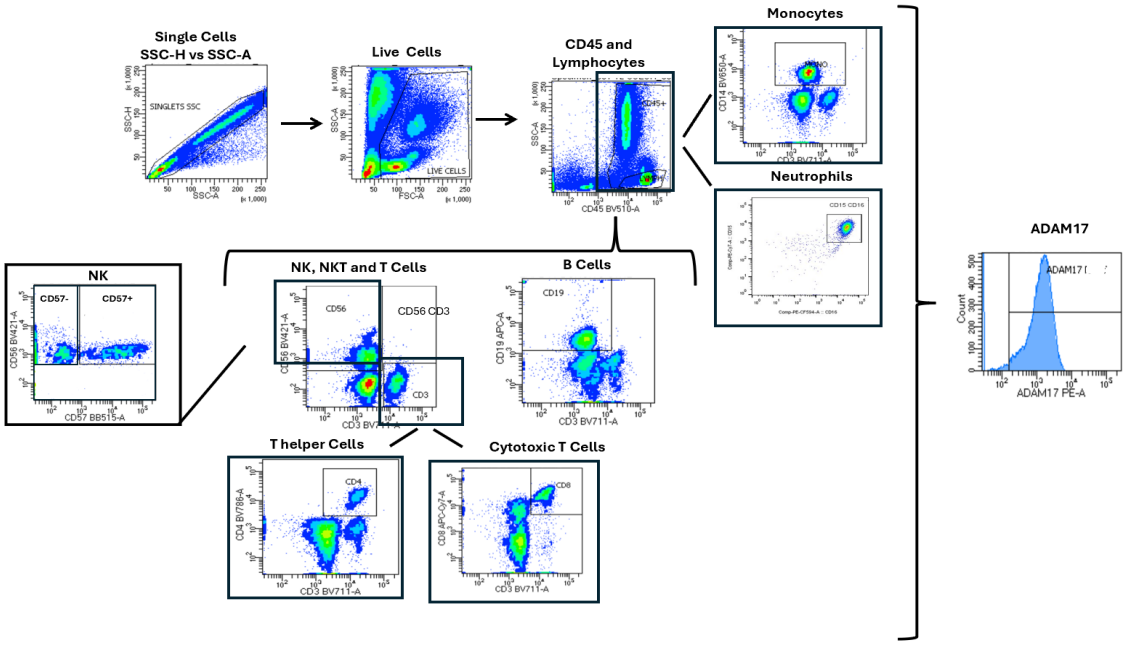

Figure 14: Flow cytometry gating strategy for the identification of NK-cell subsets in HHV-8–positive patients. Representative gating strategy applied to whole-blood samples.

The percentage of ADAM17-expressing cells was evaluated by flow cytometry in whole-blood samples from HHV-8–positive patients and healthy controls, focusing on NK cells and related lymphocyte subsets (Fig. 15). In NK cells, the proportion of ADAM17^{+} cells was comparable between HHV-8–positive patients and healthy donors, with no statistically significant differences detected between the two groups. Similarly, within the NKT cell compartment, the percentage of ADAM17-positive cells did not differ significantly between HHV-8–positive subjects and controls (Fig. 15A). Further stratification of NK cells based on CD57 expression revealed distinct distribution patterns of ADAM17 among maturation/exhaustion subsets. In exhausted NK cells, a higher proportion of ADAM17^{+} cells was observed in HHV-8–positive patients compared with healthy controls; however, this difference did not reach statistical significance. In HHV-8–positive patients, CD57^{-} NK cells displayed lower ADAM17 expression than CD57^{+} NK cells, suggesting that ADAM17 levels increase with NK-cell maturation.

Following the analysis of ADAM17-positive cell frequency, ADAM17 expression was assessed as MFI. Across all analysed populations, ADAM17 MFI was significantly higher in healthy controls compared with HHV-8–positive patients. This difference was observed in total NK cells, NKT cells, and in both exhausted and non-exhausted NK-cell subsets (Fig. 15C).

Overall, HHV-8 infection was associated with a reduced intensity of ADAM17 expression on NK cells, despite comparable frequencies of ADAM17-positive cells between groups.

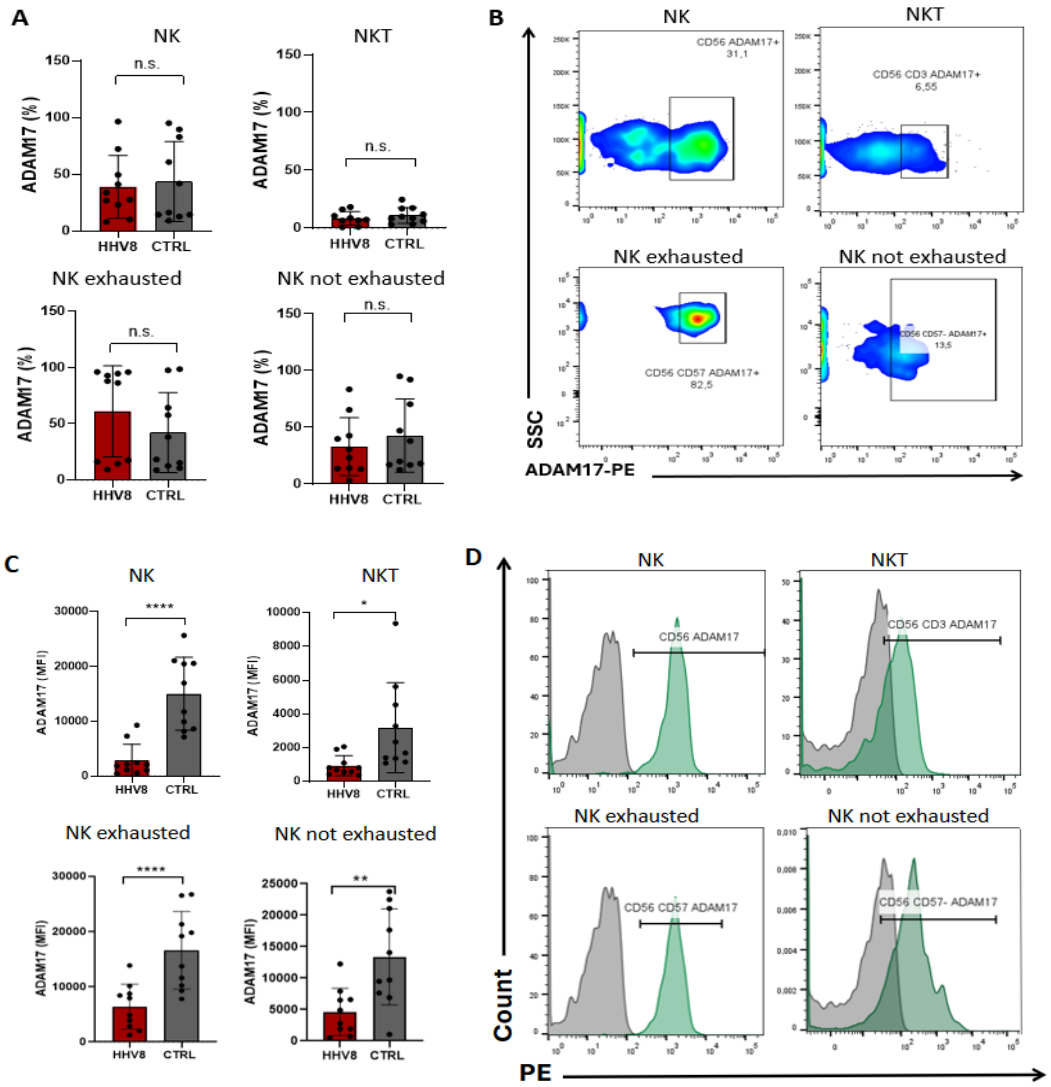

*Figure 15: ADAM17 expression in NK subsets from HHV-8–positive patients and healthy controls. (A) Flow-cytometric quantification of the percentage of ADAM17⁺ (A); MFI (C) in NK cells (CD56⁺CD3⁻), NKT cells (CD56⁺CD3⁺), exhausted NK cells (CD57⁺) and non-exhausted NK cells (CD57⁻) from HHV-8–positive patients and healthy donors. (B) Representative flow-cytometry dot plots from a single HHV-8–positive patient, showing ADAM17 percentage in the same NK subset. (D) Representative histograms of ADAM17 MFI in NK-cell subset from a single HHV-8–positive patient. Statistical analysis was done with one-way ANOVA with Tukey's multiple comparisons test. * $p < 0.05$, ** $p < 0.01$, *** $p < 0.001$, **** $p < 0.0001$; ns, non-significant (n=10).*

The analysis of the percentage of ADAM17-expressing cells and ADAM17 MFI were extended to additional immune cell populations including T cells, CD4⁺ T helper cells, CD8⁺ cytotoxic T cells, B cells, monocytes, and neutrophils (Fig. 16). Within the T helper the percentage of ADAM17⁺ cells was lower in HHV-8–positive patients compared with healthy controls,

whereas no statistically significant differences were detected in total T cells, CD8⁺ cytotoxic T cells, or B cells between the two groups. Monocytes and neutrophils displayed a high proportion of ADAM17-positive cells in both cohorts, with values consistently around ~80% in monocytes and ~90% in neutrophils. No statistically significant differences in ADAM17 MFI were observed between HHV-8–positive patients and healthy controls in any of the analysed populations. Among all subsets, neutrophils exhibited the highest ADAM17 MFI values, consistent with their elevated surface expression of the protease.

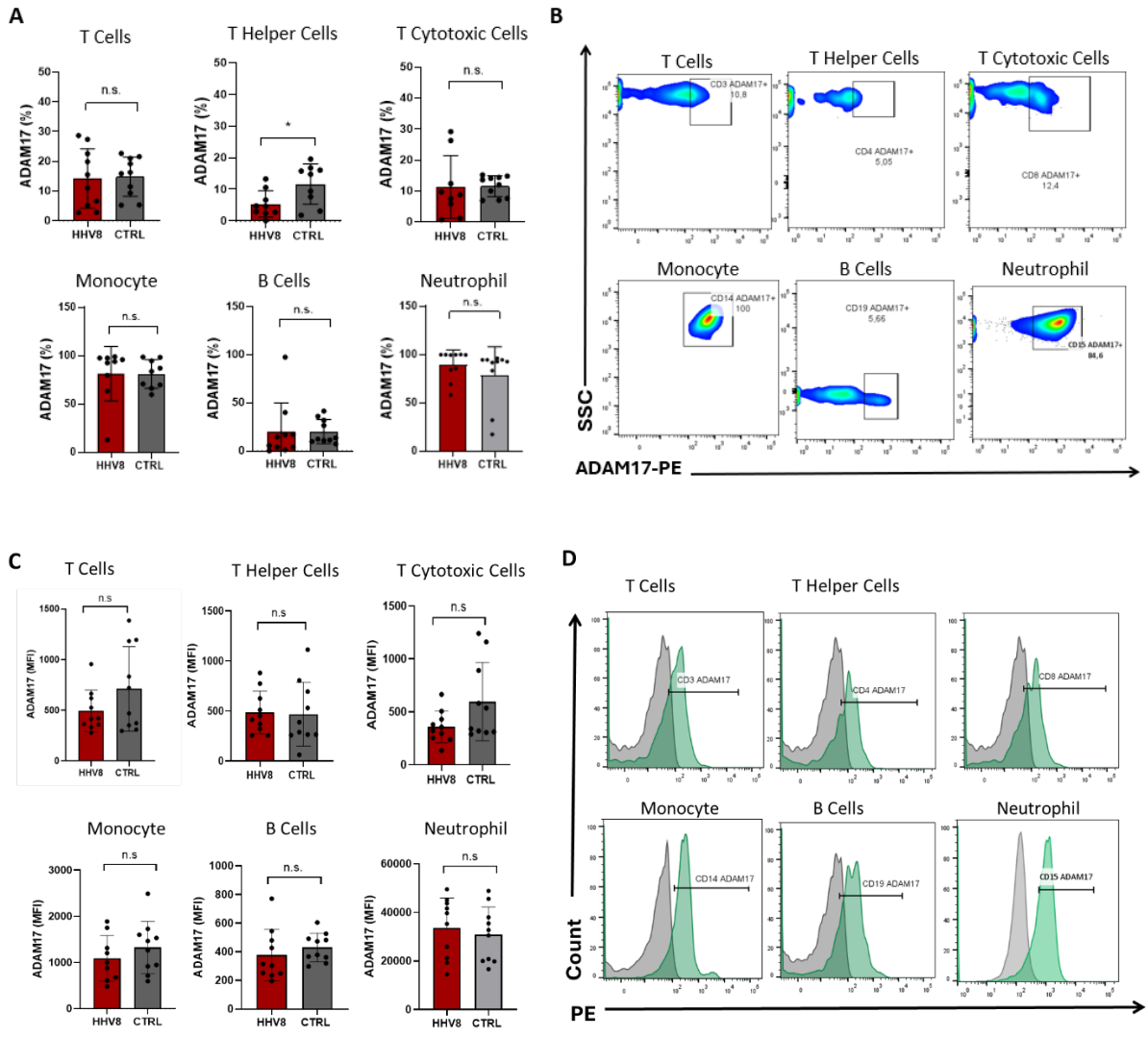

*Figure 16: ADAM17 expression in immune cell subsets from HHV-8–positive patients and healthy controls. Flow-cytometric quantification of the percentage of ADAM17⁺ (A); MFI (C) in T cells (CD3⁺), CD4⁺ T helper cells (CD3⁺CD4⁺), cytotoxic T cells (CD3⁺ CD8⁺), B cells (CD19⁺), monocytes (CD14⁺) and neutrophils (CD15⁺), from HHV-8–positive patients and healthy donors. (B) Representative flow-cytometry dot plots from a single HHV-8–positive patient, showing ADAM17 percentage in the same subsets. (D) Representative histograms of ADAM17 MFI in the same subsets from a single HHV-8–positive patient. statistical analysis was done with one-way ANOVA with Tukey's multiple comparisons test. * $p < 0.05$, ** $p < 0.01$, *** $p < 0.001$, **** $p < 0.0001$; ns, non-significant (n=10).*

The relative distribution of major immune cell subsets was compared between HHV-8–positive patients and healthy controls (Fig. 17). Within the NK-cell compartment, a higher proportion of total NK cells, NKT cells, and non-exhausted NK cells was observed in HHV-8–positive patients compared with healthy donors. A similar increase was detected for B cells and monocytes in the HHV-8 cohort. In contrast, the relative frequency of total T cells, including both $CD4^+$ T helper and $CD8^+$ cytotoxic T-cell subsets, was lower in HHV-8–positive patients than in controls. The distribution of neutrophils was comparable between the two groups. Overall, HHV-8 infection was associated with a shift in immune-cell composition characterized by enrichment of NK-related and innate immune populations and a relative reduction of T-cell subsets.

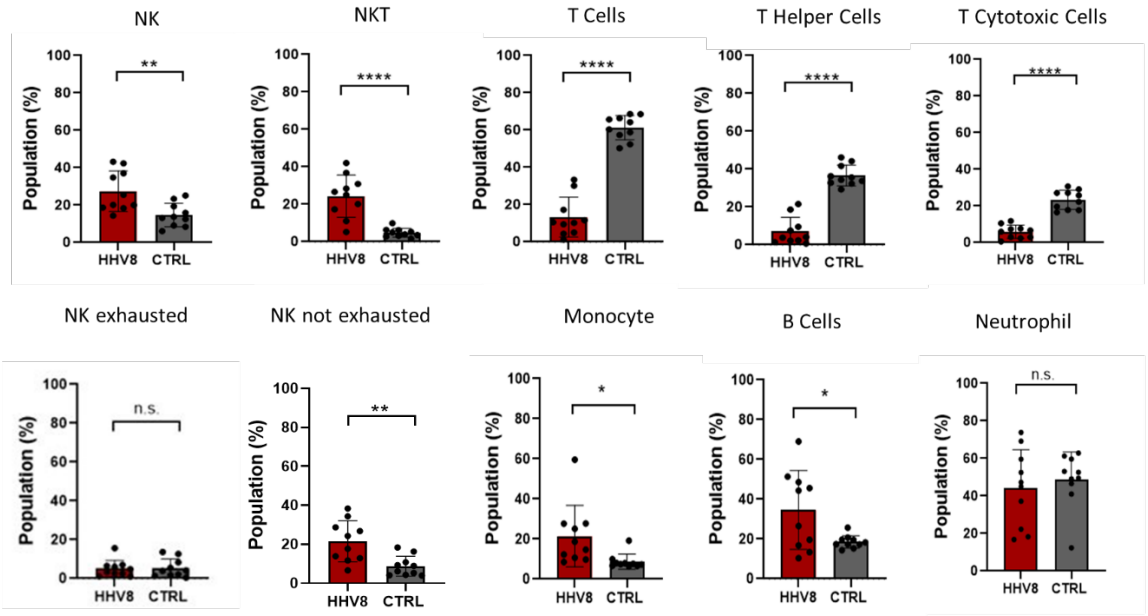

*Figure 17: Distribution of immune cell subsets in HHV-8–positive patients and healthy controls. Flow-cytometric analysis showing the relative frequency (%) of major immune cell populations, including NK cells ($CD56^+CD3^-$), NKT cells ($CD56^+CD3^+$), exhausted NK cells ($CD56^+CD57^+$), non-exhausted NK cells ($CD56^+CD57^-$), T cells ($CD3^+$), T helper cells ($CD3^+CD4^+$), cytotoxic T cells ($CD3^+CD8^+$), B cells ($CD19^+$), monocytes ($CD14^+$), and neutrophils ($CD15^+$) in whole-blood samples from HHV-8–positive patients and healthy donors. Data are presented as individual values with group comparison between the two cohorts. Statistical analysis was done with one-way ANOVA with Tukey's multiple comparisons test. * $p < 0.05$, ** $p < 0.01$, *** $p < 0.001$, **** $p < 0.0001$; ns, non-significant (n=10).*

6.2.2 ADAM17 expression in NK subsets following In Vitro Viral Peptide Stimulation

To further investigate the role of ADAM17 in NK-cell regulation during viral infections, its expression was analysed in an in vitro viral stimulation model. PBMCs isolated from healthy donors were stimulated with viral peptide pools derived from SARS-CoV-2, HHV-8, CMV,

and EBV, allowing direct comparison of ADAM17 modulation in response to distinct viral antigens under controlled experimental conditions. A flow-cytometry gating strategy analogous to that applied to HHV-8 patient samples was used for PBMCs subjected to in vitro viral stimulation (Fig. 18). Doublets were excluded based on scatter properties, followed by gating on live CD45$^+$ cells. Lymphocyte populations were identified and further resolved into NK cells (CD56$^+$CD3$^-$), NKT cells (CD56$^+$CD3$^+$), T cells (CD3$^+$CD56$^-$), subdivided into CD4$^+$ T helper and CD8$^+$ cytotoxic T cells, and B cells (CD19$^+$CD3$^-$). Within the NK compartment, CD57 expression was used to distinguish exhausted (CD57$^+$) from non-exhausted (CD57$^-$) NK cells. Unlike the ex vivo HHV-8 analysis, neutrophils were not included, as samples underwent Ficoll-based whole-blood processing (rather than red blood cell lysis) prior to acquisition.

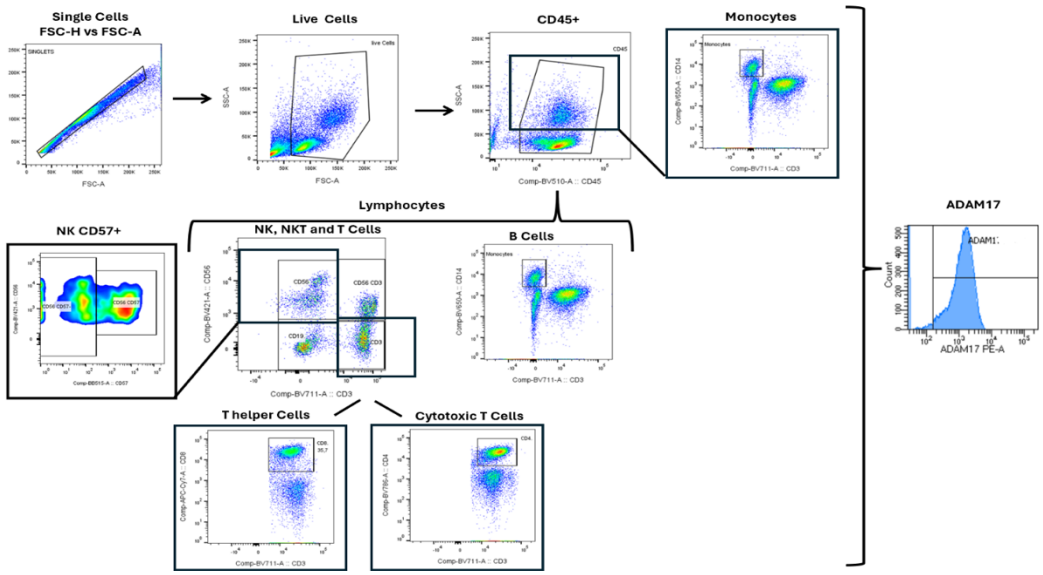

Figure 18: Flow cytometry gating strategy for in vitro viral stimulation assays. Representative gating strategy applied to PBMCs from healthy donors following in vitro stimulation with viral peptide pools.

6.2.3 SARS-CoV-2 Stimulation

ADAM17 expression was analysed as MFI and as percentage of expression in PBMCs from healthy donors following in vitro stimulation with SARS-CoV-2 peptide pools, focusing on NK-cell subsets (Fig. 19). Evaluation of total NK cells, NKT cells, exhausted NK cells, and non-exhausted NK cells did not reveal statistically significant differences in ADAM17 MFI between unstimulated control PBMCs and SARS-CoV-2–stimulated samples. Likewise, no significant differences were observed across the analysed time points (day 1, day 3, and day 7 post-stimulation). Despite the lack of statistically significant changes, a progressive decrease in ADAM17 MFI over time was observed across NK-cell subsets, not related to SARS-CoV-2 stimulation, with a more pronounced reduction in exhausted NK cells. In parallel, analysis of

ADAM17 expression as percentage of positive cells did not show statistically significant differences between unstimulated controls and SARS-CoV-2–stimulated samples. Across conditions, exhausted NK cells consistently displayed the highest proportion of ADAM17-expressing cells, moreover ADAM17 positivity within this subset, as well as in NKT cells, remained largely stable over time.

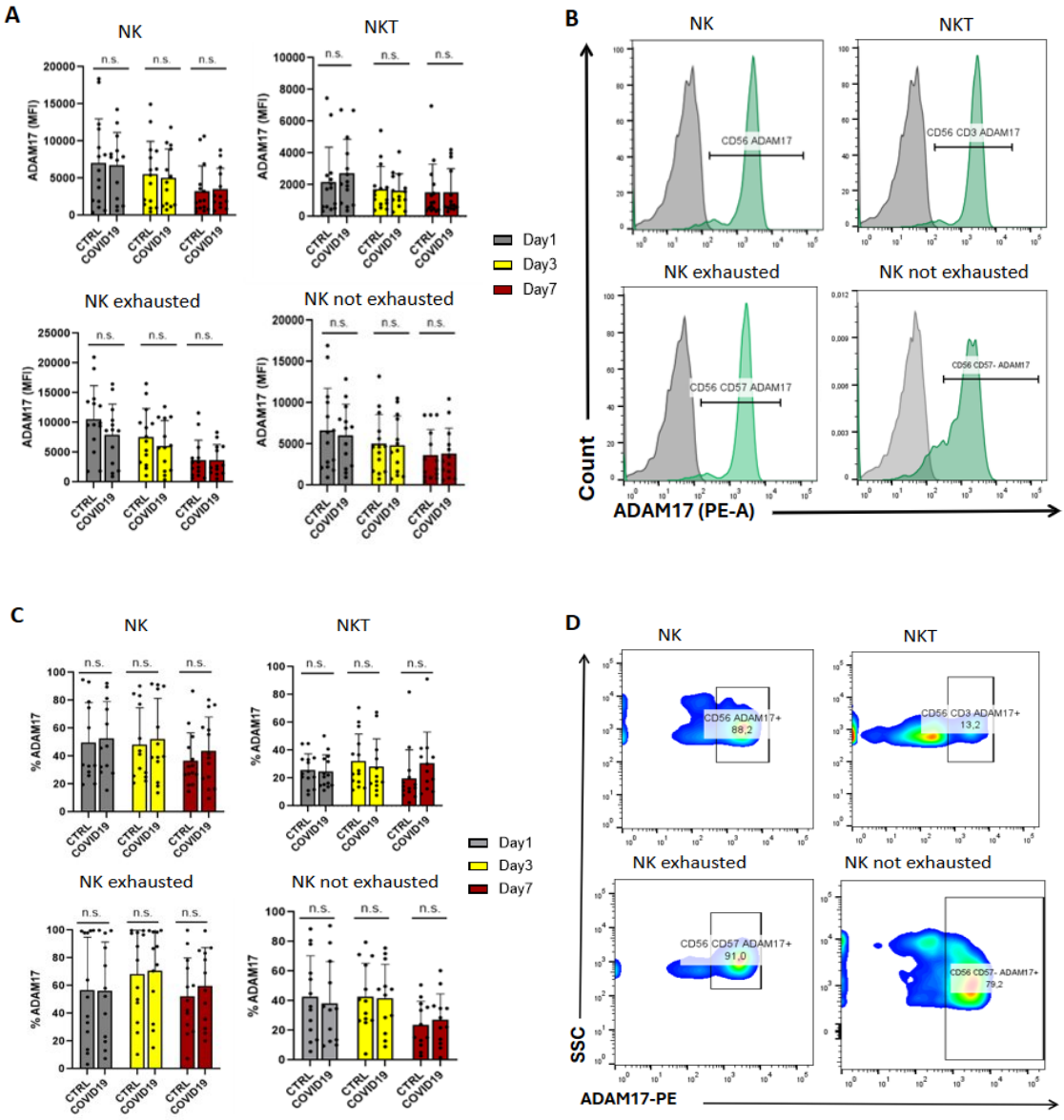

*Figure 19: ADAM17 expression in NK-cell subsets following in vitro stimulation with SARS-CoV-2 peptides. PBMCs from healthy donors were stimulated in vitro with SARS-CoV-2 peptide pools and analysed at day 1, day 3, and day 7 post-stimulation. ADAM17 expression measured as MFI (A) and % of expression (C) in NK cells ($CD56^{+}CD3^{-}$), NKT cells ($CD56^{+}CD3^{+}$), exhausted NK cells ($CD57^{+}$), and non-exhausted NK cells ($CD57^{-}$) compared with unstimulated controls. Representative histograms of ADAM17 MFI (B) and representative flow-cytometry dot plots (D) in NK-cell subset from a single sample of PBMC in vitro stimulated with SARS-CoV-2 at day 1. Statistical analyses were performed using a two-way ANOVA with Tukey's multiple comparisons test. * $p < 0.05$, ** $p < 0.01$, *** $p < 0.001$, **** $p < 0.0001$; ns, non-significant (n=14).*

6.2.4 HHV-8 stimulation

ADAM17 expression was evaluated in PBMCs from healthy donors following in vitro stimulation with HHV-8 peptide pools, focusing on NK-cell subsets and analysing both MFI and percentage of positive cells (Fig.20). Assessment of total NK cells, NKT cells, exhausted NK cells, and non-exhausted NK cells showed no statistically significant differences in ADAM17 MFI between HHV-8–stimulated samples and unstimulated controls at any of the three time points analysed (day 1, day 3, and day 7 post-stimulation). Although not statistically significant, ADAM17 MFI exhibited a progressive decline over time across all NK-cell subsets, indicating a time-dependent modulation of expression, independently of HHV-8 stimulation. Consistently, analysis of ADAM17 expression as percentage of positive cells did not reveal significant differences between stimulated and control conditions. Across all time points, exhausted NK cells displayed a higher proportion of ADAM17-positive cells compared with non-exhausted NK cells. In both exhausted NK cells and NKT cells, the percentage of ADAM17-expressing cells remained largely stable over time, suggesting maintenance of ADAM17 positivity within these subsets independently of viral peptide stimulation.

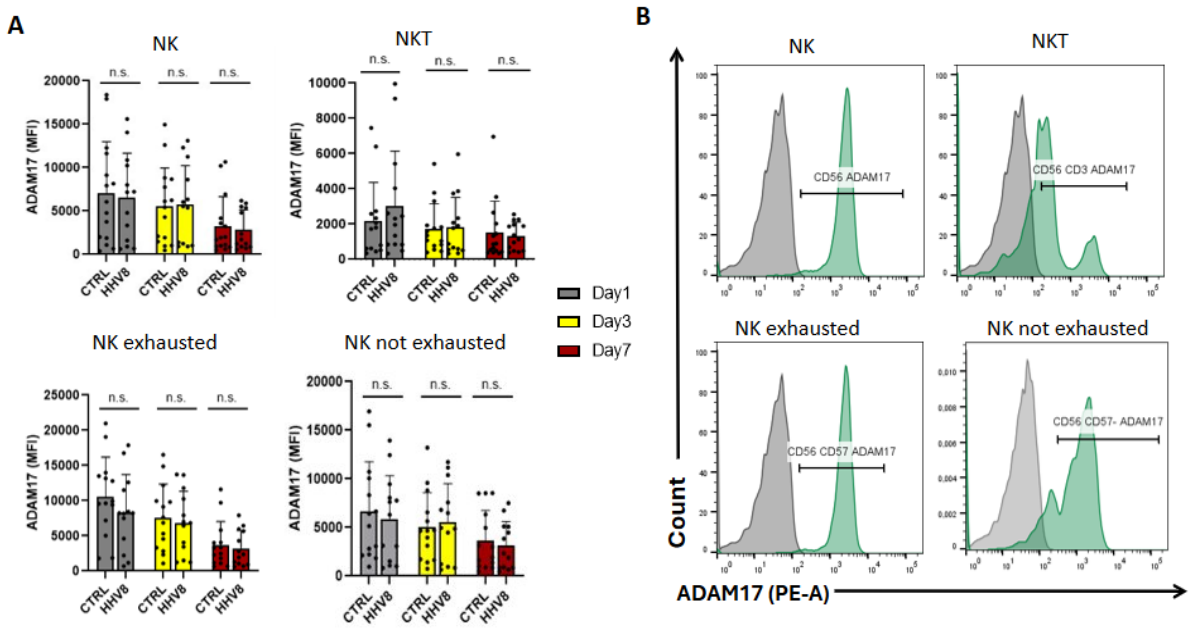

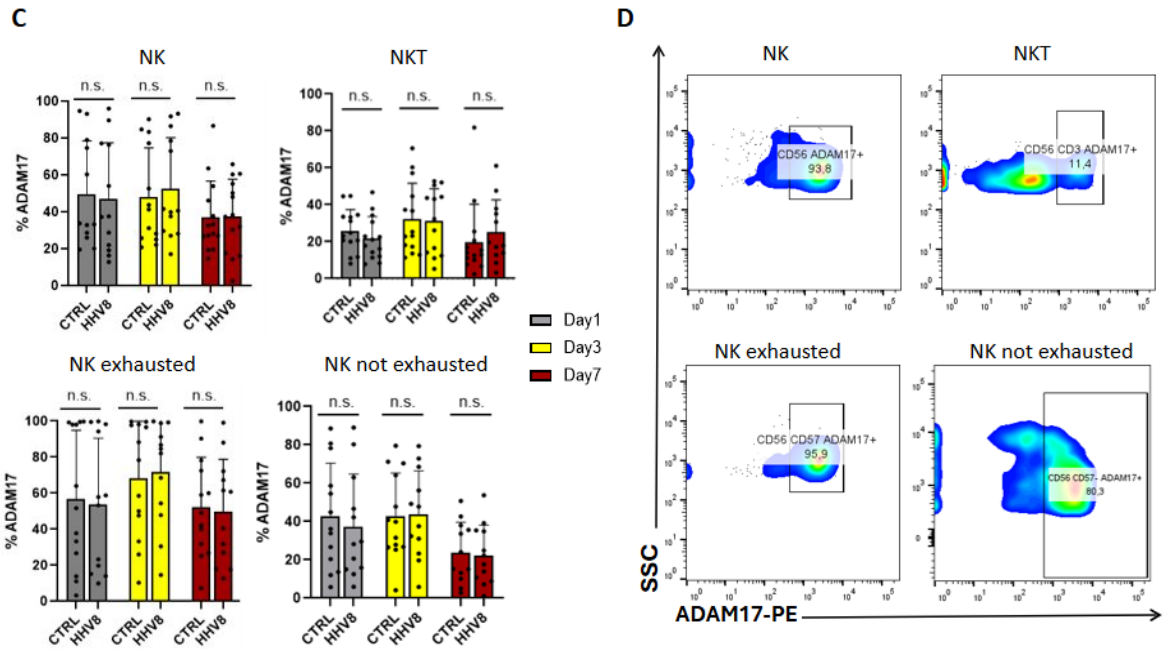

*Figure 20: ADAM17 expression in NK-cell subsets following in vitro stimulation with HHV8 peptides. PBMCs from healthy donors were stimulated in vitro with HHV8 peptide pools and analysed at day 1, day 3, and day 7 post-stimulation. ADAM17 expression measured as MFI (A) and % of expression (C) in NK cells ($CD56^{+}CD3^{-}$), NKT cells ($CD56^{+}CD3^{+}$), exhausted NK cells ($CD57^{+}$), and non-exhausted NK cells ($CD57^{-}$) compared with unstimulated controls. Representative histograms of ADAM17 MFI (B) and representative flow-cytometry dot plots (D) in NK-cell subset from a single sample of PBMC in vitro stimulated with HHV8 at day 1. Statistical analyses were performed using a two-way ANOVA with Tukey's multiple comparisons test. * $p < 0.05$, ** $p < 0.01$, *** $p < 0.001$, **** $p < 0.0001$; ns, non-significant (n=14).*

6.2.5 CMV stimulation

A temporal modulation of ADAM17 expression was observed in CMV-stimulated samples, particularly within the NK subset, both in exhausted and non-exhausted NK cell compartments (Fig. 21A). In these subsets, ADAM17 MFI values tended to be slightly lower than in unstimulated controls at all analysed time points (day 1, day 3, and day 7 post-stimulation). Although these differences did not reach statistical significance, a subtle downward trend in ADAM17 expression was observed in CMV-stimulated PBMCs compared with controls.

In addition, analysis of ADAM17 MFI revealed a mild and progressive reduction over time across all NK-related populations, including total NK cells as well as exhausted and non-exhausted subsets (Fig. 21C). Notably, this temporal decline was observed both in CMV peptide–stimulated samples and in unstimulated controls, indicating that the downward trend was independent of viral stimulation.

Consistent with the MFI analysis, evaluation of ADAM17 expression as percentage of positive cells did not reveal statistically significant differences between CMV-stimulated PBMCs and controls. In NKT cells, ADAM17 expression was slightly higher in CMV-stimulated PBMCs

compared with controls. Similarly, in total NK cells, as well as in both exhausted and non-exhausted NK subsets, a mild increase in ADAM17 expression could be observed at day 3, although this difference did not reach statistical significance.

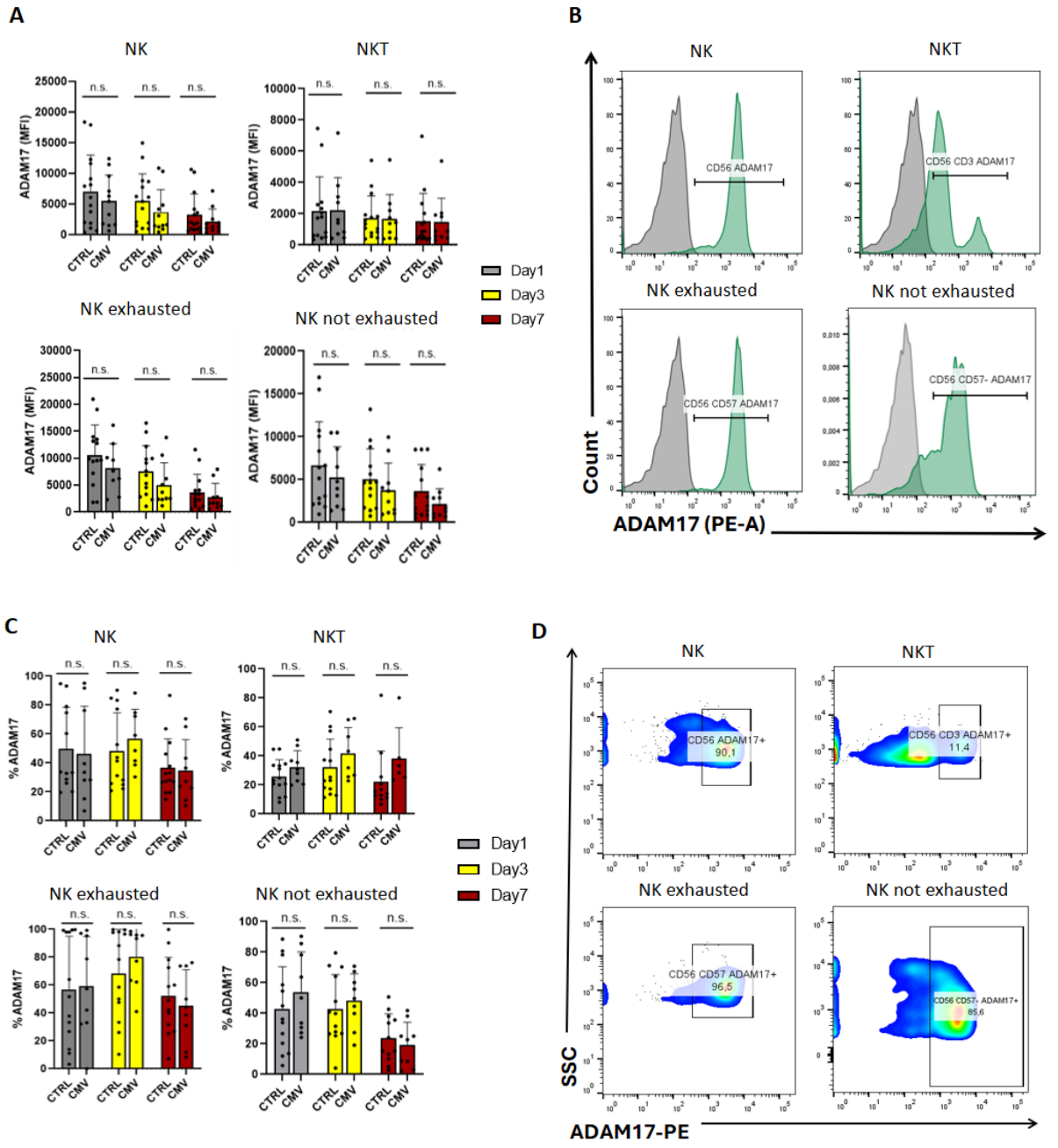

*Figure 21: ADAM17 expression in NK-cell subsets following in vitro stimulation with CMV peptides. PBMCs from healthy donors were stimulated in vitro with CMV peptide pools and analyzed at day 1, day 3, and day 7 post-stimulation. ADAM17 expression measured as MFI (A) and % of expression (C) in NK cells ($CD56^{+}CD3^{-}$), NKT cells ($CD56^{+}CD3^{+}$), exhausted NK cells ($CD57^{+}$), and non-exhausted NK cells ($CD57^{-}$) compared with unstimulated controls. Representative histograms of ADAM17 MFI (B) and representative flow-cytometry dot plots (D) in NK-cell subset from a single sample of PBMC in vitro stimulated with CMV at day 1. Statistical analyses were performed using a two-way ANOVA with Tukey's multiple comparisons test. * $p < 0.05$, ** $p < 0.01$, *** $p < 0.001$, **** $p < 0.0001$; ns, non-significant (n=14).*

6.2.6 EBV stimulation

Across all three analysed time points (day 1, day 3, and day 7 post-stimulation), ADAM17 MFI values in NK cells, including exhausted and non-exhausted subsets, were consistently lower than those observed in unstimulated controls; however, no statistically significant differences were detected between EBV-stimulated and control conditions. Conversely, within the NKT cell compartment, ADAM17 MFI remained comparable between EBV-stimulated samples and controls and did not display relevant temporal variation. A time-dependent trend was observed in ADAM17 expression during in vitro culture. ADAM17 MFI showed a progressive decline over time in total NK cells, as well as in exhausted and non-exhausted subsets, regardless of EBV peptide stimulation. A comparable reduction was observed in both stimulated and unstimulated control conditions (Fig. 22A). In contrast, NKT cells maintained relatively stable ADAM17 MFI levels throughout the observation period. Evaluation of ADAM17 expression as percentage of positive cells revealed a distinct behaviour across NK-cell subsets (Fig. 22B). In NKT cells, ADAM17 positivity showed a time-dependent increase in EBV-stimulated samples compared with controls, culminating in a higher proportion of ADAM17-expressing cells at day 7.

In contrast, within NK cells and exhausted NK cells, the percentage of ADAM17-positive cells remained largely stable over time, with no statistically significant differences between EBV-stimulated and control samples. In non-exhausted NK cells, a reduction in ADAM17-positive cells over time was observed in both EBV-stimulated PBMCs and unstimulated controls, indicating that this trend was not driven by viral stimulation.

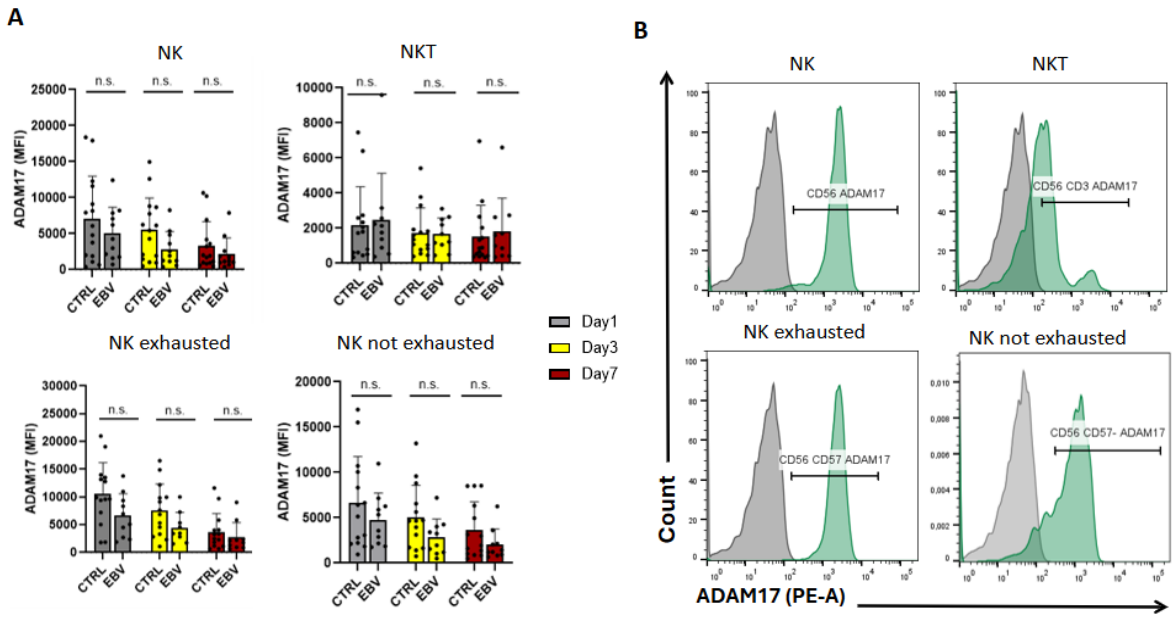

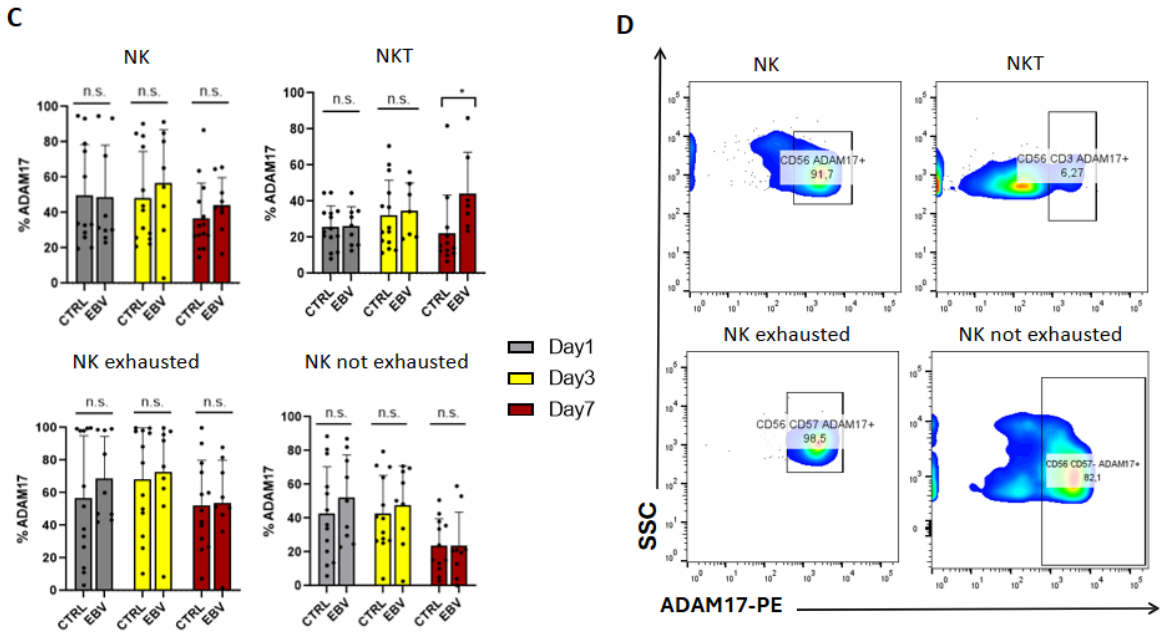

*Figure 22: ADAM17 expression in NK-cell subsets following in vitro stimulation with EBV peptides. PBMCs from healthy donors were stimulated in vitro with EBV peptide pools and analyzed at day 1, day 3, and day 7 post-stimulation. ADAM17 expression measured as MFI (A) and % of expression (C) in NK cells ($CD56^+CD3^-$), NKT cells ($CD56^+CD3^+$), exhausted NK cells ($CD57^+$), and non-exhausted NK cells ($CD57^-$) compared with unstimulated controls. Representative histograms of ADAM17 MFI (B) and representative flow-cytometry dot plots (D) in NK-cell subset from a single sample of PBMC in vitro stimulated with EBV at day 1. Statistical analyses were performed using a two-way ANOVA with Tukey's multiple comparisons test. * $p < 0.05$, ** $p < 0.01$, *** $p < 0.001$, **** $p < 0.0001$; ns, non-significant (n=14).*

6.2.7 Frequency of NK-Cell Subsets

The relative frequency of NK cells, NKT cells, exhausted NK cells, and non-exhausted NK cells was evaluated in PBMCs stimulated in vitro with viral peptide pools derived from SARS-CoV-2 (Fig. 23A), HHV-8 (Fig. 23B), CMV (Fig. 23C), and EBV (Fig. 23D). For all conditions, subset frequencies were calculated as a percentage of total lymphocytes.

Across the four stimulation models, differences in subset distribution emerged over time. In particular, NKT cells displayed marked modulation depending on the viral stimulus. A reduction in the proportion of NKT cells over time was observed in PBMCs stimulated with HHV-8, CMV, and EBV peptides, whereas this decrease was less evident following SARS-CoV-2 stimulation. Notably, among all conditions, the highest proportion of NKT cells was consistently detected in SARS-CoV-2–stimulated PBMCs. Analysis of total NK cells revealed a progressive decrease of frequencies over time in PBMCs stimulated with CMV and EBV peptides; in contrast, under SARS-CoV-2 and HHV-8 stimulation, NK-cell frequencies remained largely stable over time. This pattern was observed in both exhausted and non-exhausted NK cells within CMV- and EBV-stimulated PBMCs.

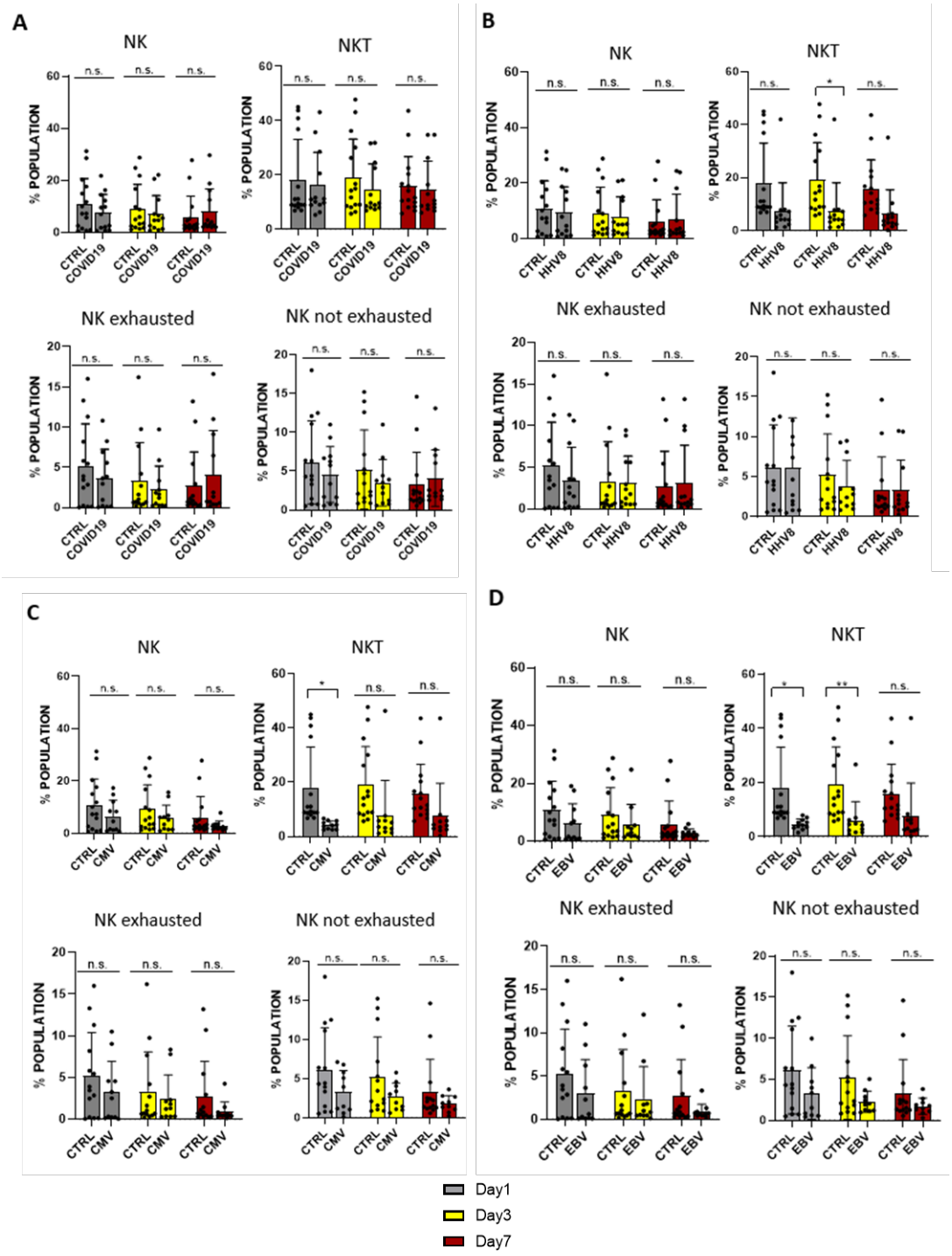

*Figure 23: Distribution of NK-cell subsets in PBMCs following in vitro viral peptide stimulation. PBMCs from healthy donors were stimulated in vitro with viral peptide pools derived from SARS-CoV-2 (A), HHV-8 (B), CMV (C), and EBV (D). The relative frequency (%) of NK cells ($CD56^+CD3^-$), NKT cells ($CD56^+CD3^+$), exhausted NK cells ($CD56^+CD57^+$), and non-exhausted NK cells ($CD56^+CD57^-$) was calculated as a percentage of total lymphocytes at the indicated time points. Data are shown as individual values over time and illustrate virus-dependent modulation of NK-cell subset distribution following in vitro stimulation. Statistical analyses were performed using a two-way ANOVA with Tukey's multiple comparisons test. * $p < 0.05$, ** $p < 0.01$, *** $p < 0.001$, **** $p < 0.0001$; ns, non-significant (n=14).*

6.2.8 ADAM17 Expression in T Cells, B Cells, and Monocytes

ADAM17 expression was additionally evaluated as percentage of positive cells and MFI in immune cell populations other than NK cells, including total T lymphocytes ($CD3^+$), T helper cells ($CD3^+CD4^+$), cytotoxic T cells ($CD3^+CD8^+$), monocytes ($CD14^+$), and B cells ($CD19^+$), in PBMCs stimulated *in vitro* with viral peptide pools derived from SARS-CoV-2 (Fig. 24), HHV-8 (Fig. 25), CMV (Fig. 26), and EBV (Fig. 27). Analyses were performed at day 1, day 3, and day 7 post-stimulation. Across all four viral conditions, no statistically significant differences were detected between peptide-stimulated PBMCs and unstimulated controls in terms of either ADAM17 MFI or % of ADAM17-expressing cells at any time point.

In all stimulation models, monocytes consistently exhibited the highest proportion of ADAM17-positive cells, with values around ~80%, and maintained stable ADAM17 expression over time. In contrast, T and B lymphocytes showed comparable and lower percentages of ADAM17 expression, averaging around ~20%, irrespective of the viral stimulus.

Regarding expression intensity, in CMV- and EBV-stimulated PBMCs, a mild time-dependent reduction in ADAM17 MFI was observed in monocytes, although this trend did not reach statistical significance. Moreover, ADAM17 MFI progressively decreased over time in T lymphocytes, while remaining largely stable in B cells. This temporal trend was observed in both peptide-stimulated and unstimulated PBMCs, indicating that it was not attributable to viral stimulation.

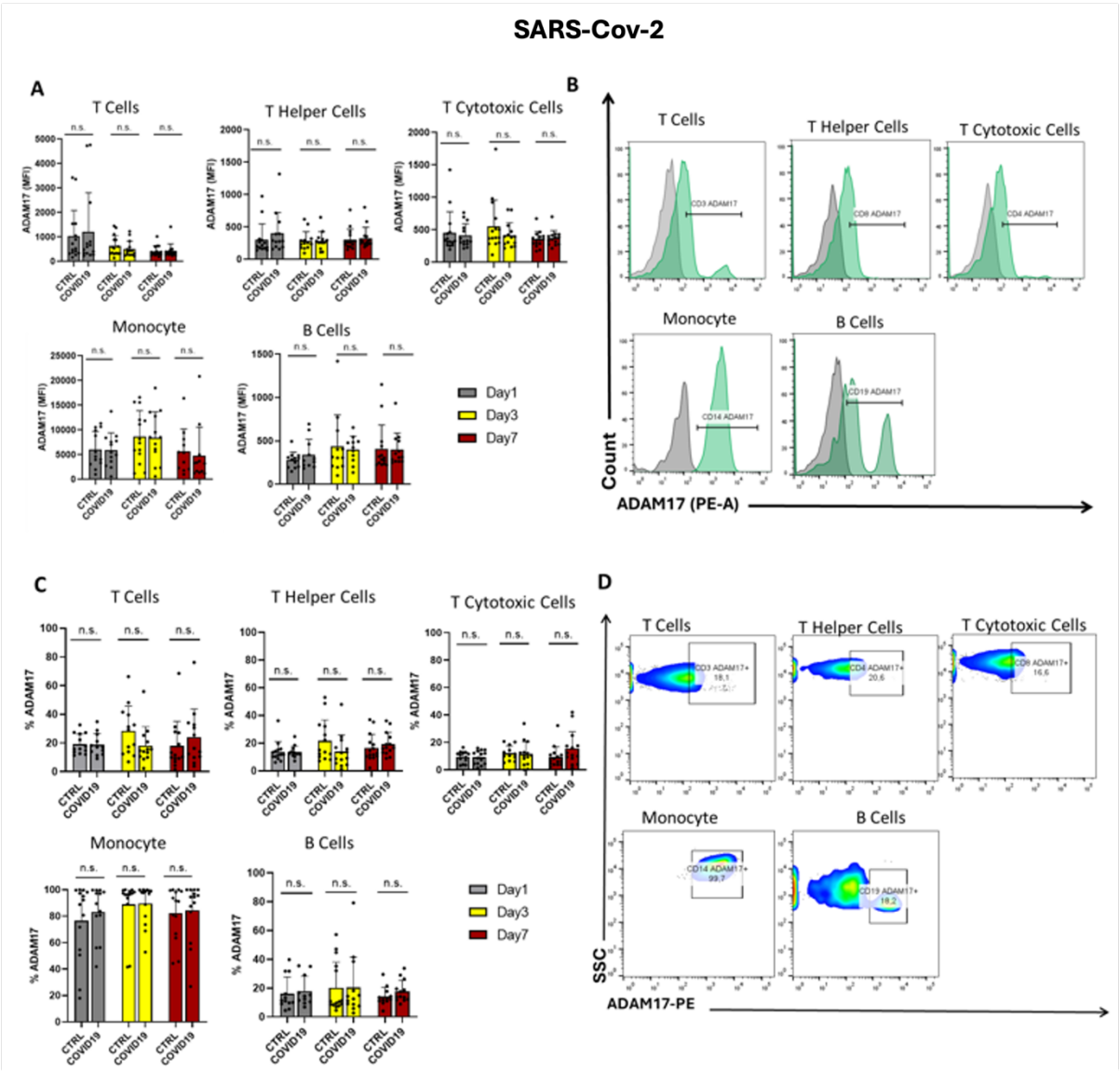

*Figure 24: ADAM17 expression in immune cell subsets following in vitro stimulation with SARS-CoV-2 peptides. PBMCs from healthy donors were stimulated in vitro with SARS-CoV-2 peptide pools and analyzed at day 1, day 3, and day 7 post-stimulation. ADAM17 expression measured as MFI (A) and % of expression (C) in T cells ($CD3^+$), T helper cells ($CD3^+CD4^+$), cytotoxic T cells ($CD3^+CD8^+$), B cells ($CD19^+$), monocytes ($CD14^+$), compared with unstimulated controls. Representative histograms of ADAM17 MFI (B) and representative flow-cytometry dot plots (D)in the same immune cell subset from a single sample of PBMC in vitro stimulation with SARS-CoV-2 at day 1. Statistical analyses were performed using a two-way ANOVA with Tukey's multiple comparisons test. * $p < 0.05$, ** $p < 0.01$, *** $p < 0.001$, **** $p < 0.0001$; ns, non-significant (n=14).*

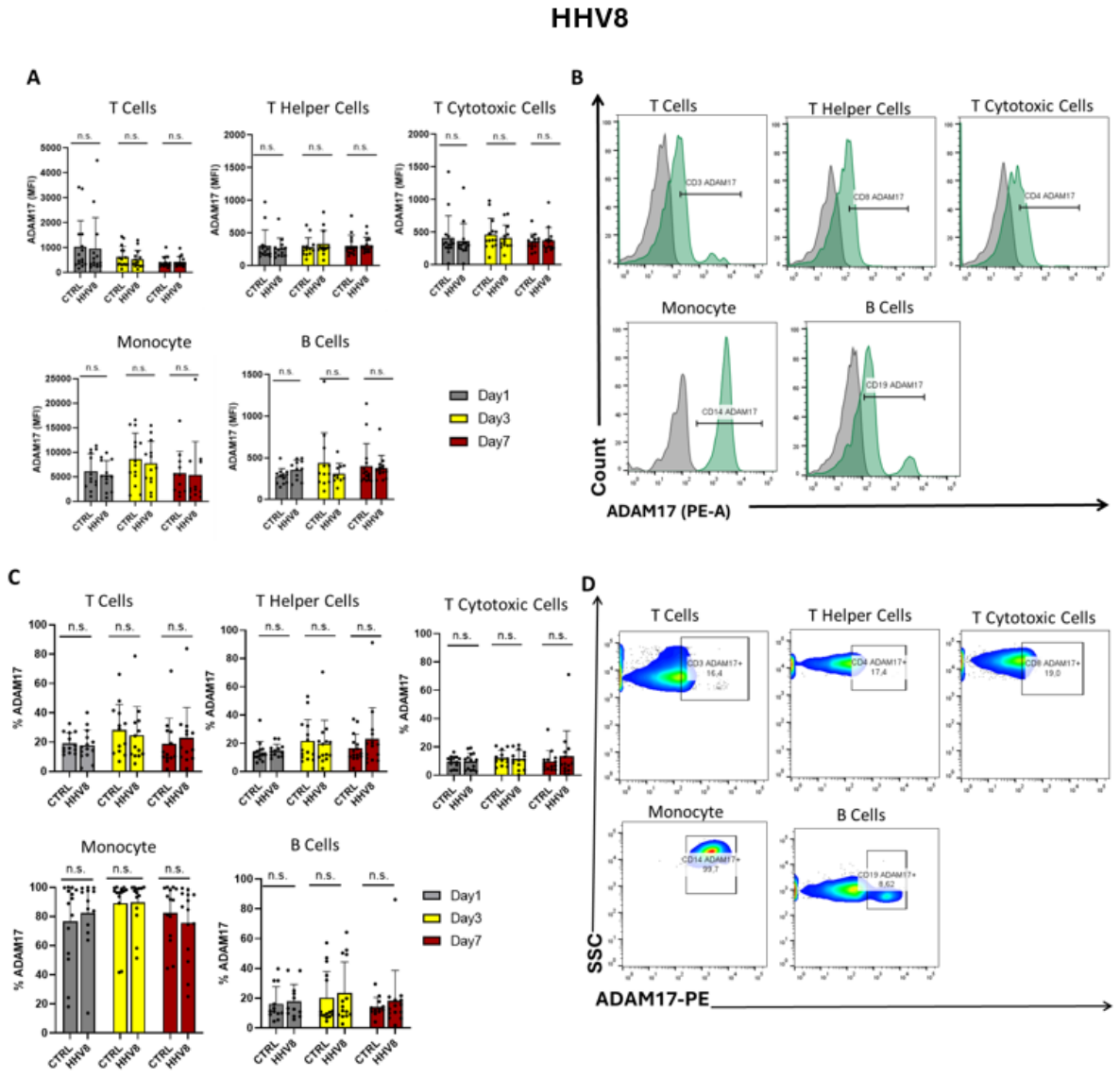

*Figure 25: ADAM17 expression in immune cell subsets following in vitro stimulation with HHV8 peptides. PBMCs from healthy donors were stimulated in vitro with HHV8 peptide pools and analyzed at day 1, day 3, and day 7 post-stimulation. ADAM17 expression measured as MFI (A) and % of expression (C) in T cells ($CD3^+$), T helper cells ($CD3^+CD4^+$), cytotoxic T cells ($CD3^+CD8^+$), B cells ($CD19^+$), monocytes ($CD14^+$), compared with unstimulated controls. Representative histograms of ADAM17 MFI (B) and representative flow-cytometry dot plots (D)in the same immune cell subset from a single sample of PBMC in vitro stimulation with HHV8 at day 1. Statistical analyses were performed using a two-way ANOVA with Tukey's multiple comparisons test. * $p < 0.05$, ** $p < 0.01$, *** $p < 0.001$, **** $p < 0.0001$; ns, non-significant (n=14).*

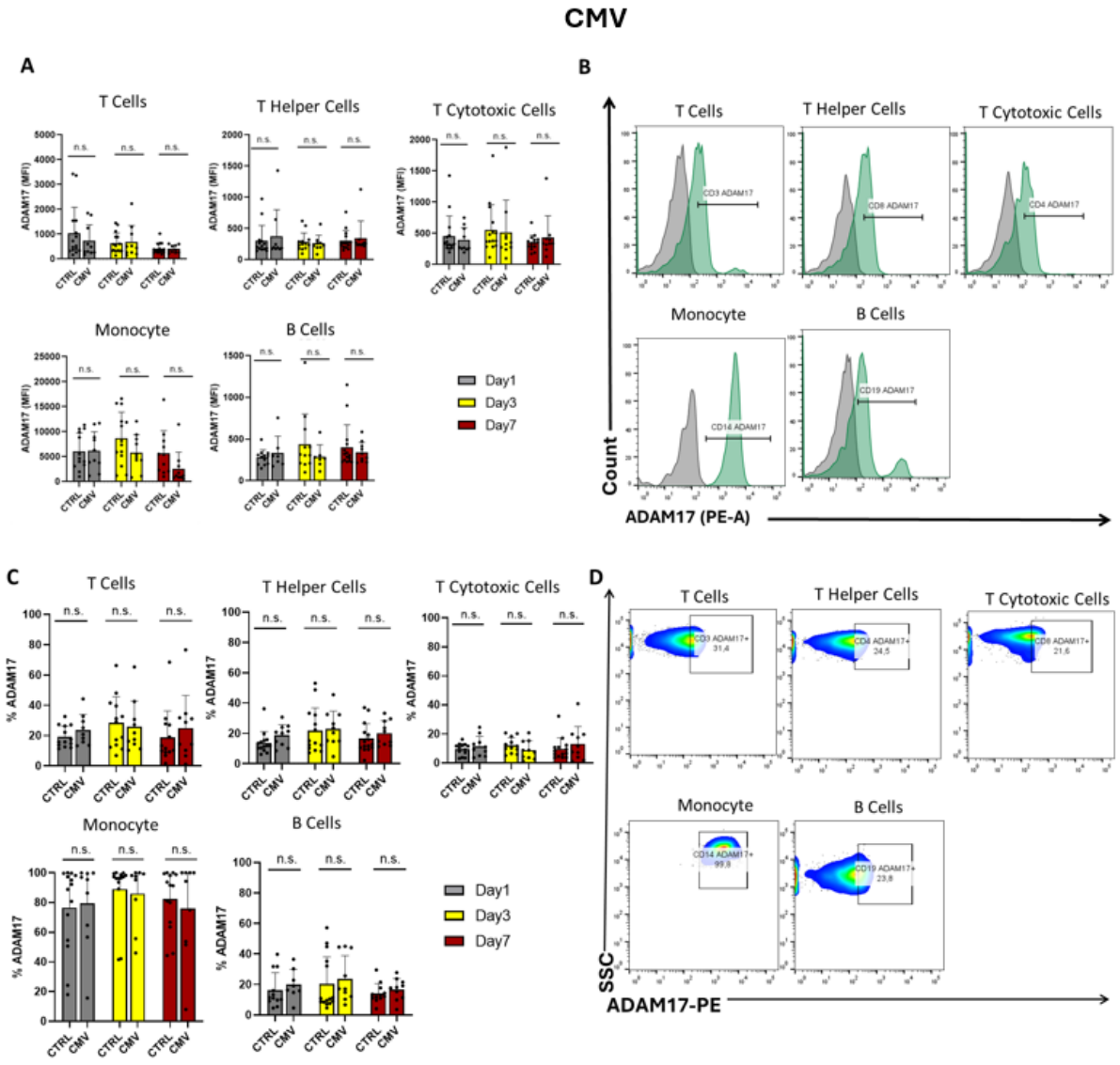

*Figure 26: ADAM17 expression in immune cell subsets following in vitro stimulation with CMV peptides. PBMCs from healthy donors were stimulated in vitro with CMV peptide pools and analyzed at day 1, day 3, and day 7 post-stimulation. ADAM17 expression measured as MFI (A) and % of expression (C) in T cells ($CD3^+$), T helper cells ($CD3^+CD4^+$), cytotoxic T cells ($CD3^+CD8^+$), B cells ($CD19^+$), monocytes ($CD14^+$), compared with unstimulated controls. Representative histograms of ADAM17 MFI (B) and representative flow-cytometry dot plots (D)in the same immune cell subset from a single sample of PBMC in vitro stimulation with CMV at day 1. Statistical analyses were performed using a two-way ANOVA with Tukey's multiple comparisons test. * $p < 0.05$, ** $p < 0.01$, *** $p < 0.001$, **** $p < 0.0001$; ns, non-significant (n=14).*

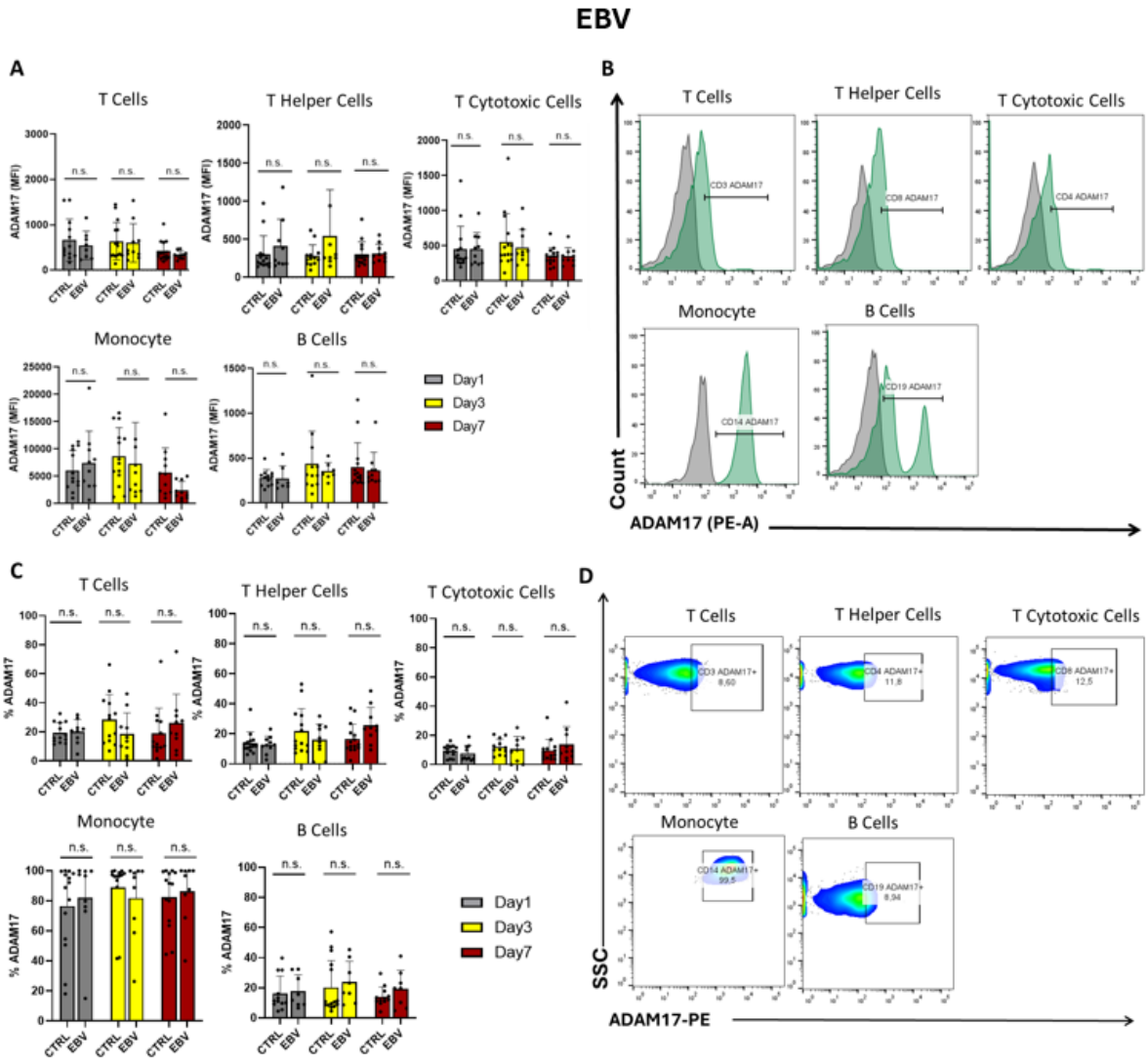

*Figure 27: ADAM17 expression in immune cell subsets following in vitro stimulation with EBV peptides. PBMCs from healthy donors were stimulated in vitro with EBV peptide pools and analyzed at day 1, day 3, and day 7 post-stimulation. ADAM17 expression measured as MFI (A) and % of expression (C) in T cells ($CD3^+$), T helper cells ($CD3^+CD4^+$), cytotoxic T cells ($CD3^+CD8^+$), B cells ($CD19^+$), monocytes ($CD14^+$), compared with unstimulated controls. Representative histograms of ADAM17 MFI (B) and representative flow-cytometry dot plots (D)in the same immune cell subset from a single sample of PBMC in vitro stimulation with EBV at day 1. Statistical analyses were performed using a two-way ANOVA with Tukey's multiple comparisons test. * $p < 0.05$, ** $p < 0.01$, *** $p < 0.001$, **** $p < 0.0001$; ns, non-significant (n=14).*

6.2.9 Distribution of T Cells, B Cells, and Monocytes Populations

The relative frequency of T lymphocytes ($CD3^+$), T helper cells ($CD3^+CD4^+$), cytotoxic T cells ($CD3^+CD8^+$), monocytes ($CD14^+$), and B cells ($CD19^+$) was assessed in PBMCs activated ex vivo with viral peptide pools derived from SARS-CoV-2, HHV-8, CMV, and EBV (Fig. 30). The proportion of T and B lymphocytes was calculated relative to the total lymphocyte population, whereas monocyte frequency was expressed as a percentage of total $CD45^+$ cells. In PBMCs stimulated with SARS-CoV-2 peptides, no statistically significant differences were

observed in the distribution of these populations compared with unstimulated controls at any time point.

PBMCs stimulated with HHV-8, CMV, and EBV peptides displayed a mild reduced proportion of monocytes at day 1 compared with controls. In EBV-stimulated PBMCs (Fig.28D), an increase in total T lymphocytes was observed relative to controls, reaching statistical significance at day 3 and being detectable also at day 1 and day 7; this increase was more evident within the T helper subset (although it did not reach statistical significance). Across CMV and EBV stimulated PBMCs, a slightly lower proportion of B cells, without reaching statistical significance, was detected compared with unstimulated controls, and this reduction was maintained throughout the observation period.

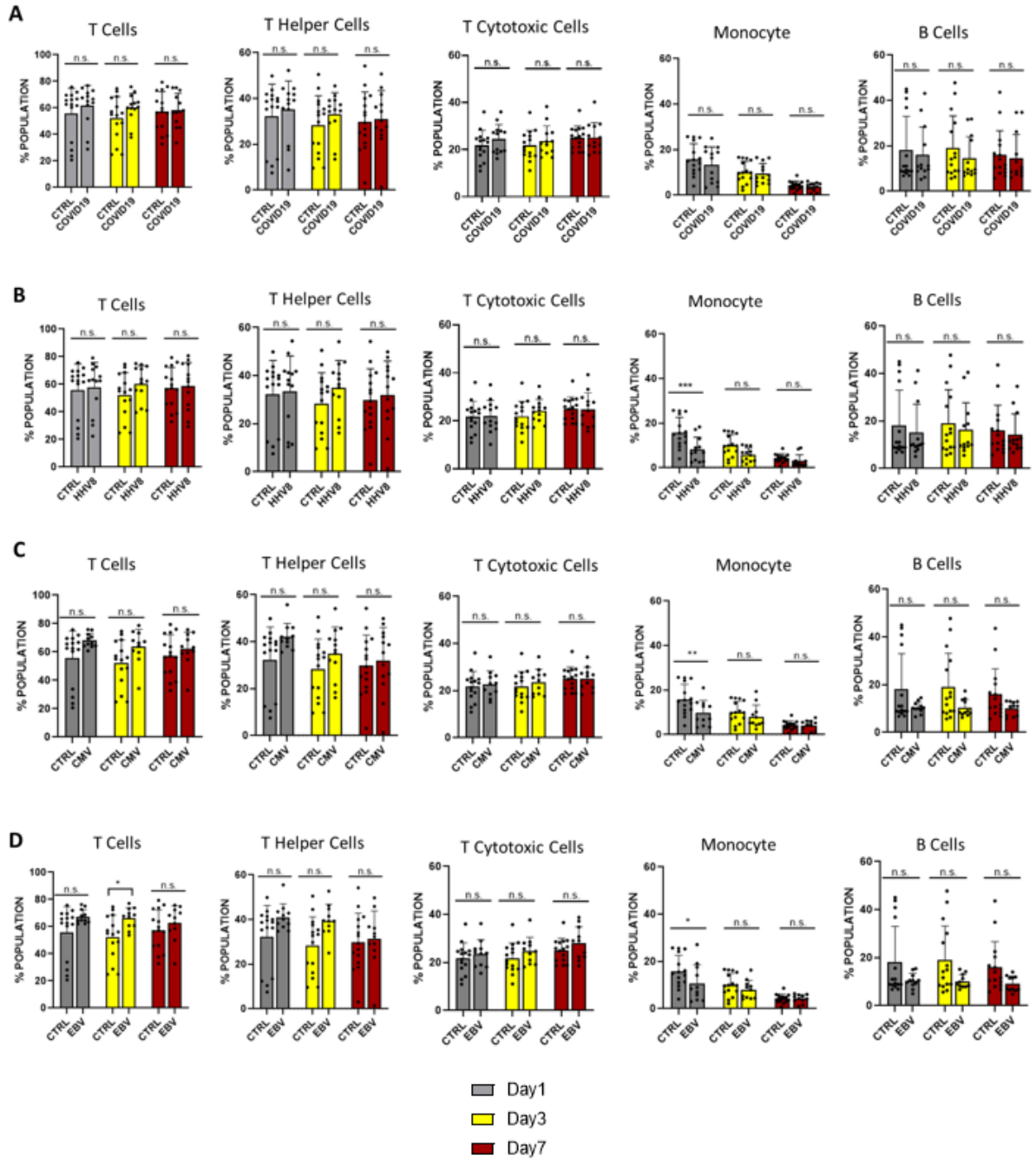

*Figure 28: Distribution of immune cell subsets following in vitro viral peptide stimulation. PBMCs from healthy donors were stimulated in vitro with viral peptide pools derived from SARS-CoV-2 (A), HHV-8 (B), CMV (C), and EBV (D), and analyzed at day 1, day 3, and day 7. The relative frequency (%) of T cells ($CD3^+$, $CD3^+CD4^+$, $CD3^+CD8^+$) and B cells ($CD19^+$) are shown as a percentage of total lymphocytes, while monocytes ($CD14^+$) are expressed as a percentage of $CD45^+$ cells. Data are shown as individual values over time and illustrate virus-dependent modulation of immune cell subsets distribution following in vitro stimulation. Statistical analyses were performed using a two-way ANOVA with Tukey's multiple comparisons test. * $p < 0.05$, ** $p < 0.01$, *** $p < 0.001$, **** $p < 0.0001$; ns, non-significant (n=14).*

6.2.10 In Vitro Cytokine Response of PBMCs to Viral Peptide Stimulation

To complement the cellular phenotypic analyses, cytokine secretion was evaluated in culture supernatants to assess the inflammatory and immunomodulatory response induced by viral peptide stimulation (SARS-CoV-2, HHV-8, CMV, and EBV). Culture supernatants from in vitro-stimulated PBMC were collected at defined time points (day 1, day 3, and day 7 post-stimulation) to assess a comprehensive evaluation of the inflammatory and immunomodulatory milieu induced by different viral peptide stimulations (Fig. 31). The analysis focused on a panel of eight soluble mediators representative of pro-inflammatory (TNF-α, IL-1β, IL-1α, IL-6), immunoregulatory (IFN-γ, IL-2), anti-inflammatory (IL-10), and Th17-associated (IL-17A) cytokines.

TNF-α production displayed a time-dependent increase in PBMCs stimulated with SARS-CoV-2, HHV-8, and CMV peptides. In SARS-CoV-2–stimulated samples, TNF-α levels rose markedly from day 1 (18.7 ± 7.2 MFI) to day 3 (295.9 ± 369.9 MFI) and remained elevated at day 7 (325.5 ± 442.8 MFI). A similar kinetic was observed in CMV-stimulated PBMCs, with TNF-α increasing from 26.5 ± 29.5 MFI at day 1 to 57.9 ± 75.2 MFI at day 3 and reaching 313.2 ± 326.4 MFI at day 7. In HHV-8 stimulation, TNF-α levels were low at day 1 (19.8 ± 30.3 MFI), showed minimal variation at day 3 (16.8 ± 14.1 MFI), and increased at day 7 (123.5 ± 119.0 MFI). EBV-stimulated PBMCs also showed an upward trend (from 17.1 ± 10.7 MFI at day 1 to 177.2 ± 134.8 MFI at day 7), although this increase did not reach statistical significance.

Analysis of IFN-γ revealed virus-specific kinetics. In SARS-CoV-2–stimulated PBMCs, IFN-γ progressively increased over time, peaking at day 3 (91.8 ± 82.0 MFI) and remaining elevated at day 7 (186.1 ± 150.3 MFI) compared with day 1 (37.5 ± 25.9 MFI). A similar trend was observed in EBV stimulation, with IFN-γ reaching its highest levels at day 3 (196.3 ± 459.9 MFI), followed by sustained expression at day 7 (162.8 ± 195.1 MFI). In contrast, HHV-8 stimulation did not induce a comparable IFN-γ response, with values remaining low and relatively stable across time points (6.5 ± 1.2 MFI at day 1; 5.9 ± 1.5 MFI at day 3; 11.4 ± 6.5 MFI at day 7). CMV stimulation induced only a modest increase at day 3 (37.7 ± 51.2 MFI) compared with day 1 (17.8 ± 13.1 MFI), followed by a slight reduction at day 7 (23.9 ± 25.8 MFI).

Distinct profiles were also observed for IL-6. In CMV-stimulated PBMCs, IL-6 levels were already elevated at day 1 (102.6 ± 191.6 MFI) compared with the other viral conditions and

remained relatively stable over time (94.5 ± 127.5 MFI at day 3; 270.6 ± 241.3 MFI at day 7). In contrast, SARS-CoV-2, EBV, and HHV-8 stimulations showed a progressive increase in IL-6 over time. SARS-CoV-2–stimulated samples increased from 41.2 ± 49.1 MFI at day 1 to 158.2 ± 159.0 MFI at day 7, while EBV stimulation led to a marked rise from 38.2 ± 43.8 MFI at day 1 to 295.6 ± 242.4 MFI at day 7. In HHV-8–stimulated PBMCs, IL-6 levels increased more moderately, reaching 73.3 ± 42.8 MFI at day 7, remaining lower than those observed in the other viral conditions.

Levels of IL-1β and IL-1α remained low and largely unchanged over time in SARS-CoV-2, HHV-8, and CMV stimulations, indicating limited induction of these cytokines under these conditions. In contrast, EBV stimulation was associated with a transient increase of both IL-1β and IL-1α at day 3, suggesting a short-lived pro-inflammatory response specific to EBV exposure.

IL-2 and IL-17A concentrations were consistently low across all viral stimulations and time points analysed, with no appreciable trends or significant differences compared with control conditions.

Finally, IL-10 displayed distinct kinetics depending on the viral stimulus. In CMV-stimulated PBMCs, IL-10 levels were already elevated at day 1 (54.5 ± 70.4 MFI) and increased further over time, reaching 136.3 ± 133.7 MFI at day 7. In SARS-CoV-2 and EBV conditions, IL-10 induction was delayed, with relatively low levels at day 1 (68.8 ± 66.1 MFI and 21.0 ± 16.8 MFI, respectively), followed by a marked increase at day 3 (180.0 ± 153.2 MFI for SARS-CoV-2; 69.2 ± 85.5 MFI for EBV) that was maintained at day 7. In contrast, HHV-8 stimulation did not induce a substantial IL-10 response, with values remaining low and stable across all time points (31.6 ± 54.1 MFI at day 1; 40.6 ± 36.1 MFI at day 7).

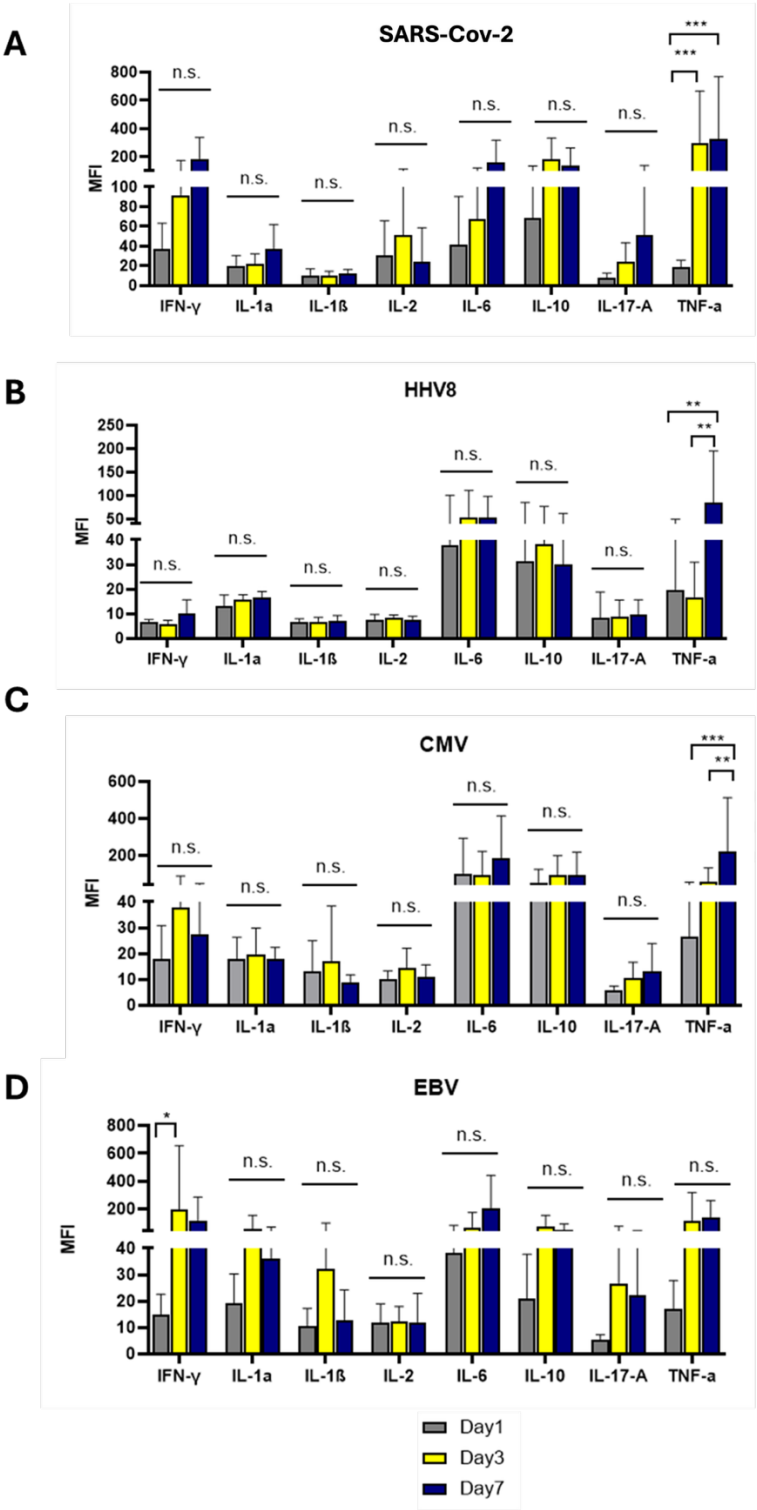

*Figure 29: Cytokine release profiles in PBMCs following in vitro viral peptide stimulation. Cytokine levels were quantified in culture supernatants from PBMCs stimulated with viral peptide pools. Supernatants were collected at day 1, day 3, and day 7 post-stimulation and analyzed by multiplex bead-based assay. Panels report cytokine secretion following stimulation with SARS-CoV-2 (A), HHV-8 (B), CMV (C), and EBV (D) peptide pools. Data are shown for pro-inflammatory and regulatory cytokines, including TNF-α, IFN-γ, IL-6, IL-1β, IL-1α, IL-2, IL-10, and IL-17A, highlighting virus-specific and time-dependent cytokine secretion patterns. Statistical analyses were performed using a two-way ANOVA with Tukey's multiple comparisons test. * $p < 0.05$, ** $p < 0.01$, *** $p < 0.001$, **** $p < 0.0001$; ns, non-significant (n=7).*

7. DISCUSSION

7.1 NK cells in immunotherapy

7.1.1 NK isolation & characterization

The development of effective NK cell–based immunotherapies require access to scalable and biologically relevant sources of primary human NK cells. In this study, liver perfusate from deceased brain-dead donors emerged as a highly efficient starting material, enabling robust isolation and expansion of primary NK cells through a standardized and reproducible workflow. Using an immunomagnetic separation strategy developed and patented by ISMETT and RiMED Foundation (WO 2018/099988), NK cells were consistently isolated with very high purity (>99% $CD3^{-}CD56^{+}$) and negligible contamination by T or NKT cells (Fig.2)[231].

The strong concordance between expected and recovered NK-cell frequencies, together with isolation yields reaching values above 70% in individual perfusate samples (Fig.3), highlights the robustness and predictability of the procedure. Compared with peripheral blood–derived PBMCs, liver perfusate provides a clear quantitative advantage, as it is intrinsically enriched in NK cells, allowing recovery of large absolute NK-cell numbers from a single donor. This feature has been previously documented, as reported by Pagano et al., who demonstrated substantially higher NK-cell yields from liver perfusate compared with matched peripheral blood samples[232].

Importantly, the high isolation efficiency combined with IL-2/IL-15–based expansion enabled robust NK-cell amplification (~280-fold, up to ~1.4×10^{10} cells), (Fig. 2C), supporting the suitability of perfusate-derived NK cells for downstream functional characterization and genetic engineering. Collectively, these findings establish liver perfusate as a uniquely advantageous and clinically relevant source for NK-cell–based immunotherapy development.

Perfusate-derived NK cells expanded ex vivo with IL-2 and IL-15 maintained a largely stable phenotypic profile over the first three weeks of culture (Fig.5). This stability is consistent with cytokine-driven expansion of highly proliferative, activation-competent NK cells rather than with progressive terminal maturation or acquisition of dysfunctional features. IL-2/IL-15–based protocols are known to preferentially sustain immature or early differentiated NK-cell subsets with preserved responsiveness to activating signals[234].

Accordingly, the absence of statistically significant changes across timepoints reflects an equilibrium between activation, proliferation, and receptor turnover under sustained γ-chain cytokine signaling, rather than phenotypic inertia. Among the analysed receptors, NKp44 showed the highest and most consistent expression. This dominant expression underscores the strong activation imprint induced by IL-2/IL-15 and supports preservation of natural cytotoxicity receptor–mediated tumour recognition[234,235].

In contrast, NKG2A, while stable over time, was expressed in a substantially smaller fraction of cells than NKp44 (Fig.5A), indicating that inhibitory signalling is retained but does not prevail over activating inputs in the expanded NK-cell compartment. CD16 remained highly expressed throughout culture and displayed the highest MFI among all markers, despite modest redistribution between CD16dim and CD16bright subsets. This pattern suggests activation-associated tuning rather than sustained shedding, supporting preservation of ADCC competence during prolonged expansion [86,152,166,236–238].

The proportion of $CD57^+$ NK cells progressively decreased over time, while CD57 MFI remained relatively stable. This finding is consistent with selective expansion dynamics rather than active downregulation of this maturation marker. CD57 identifies terminally differentiated NK cells characterized by limited proliferative capacity and high cytotoxic potential [2,24]. Under IL-2/IL-15 stimulation, less differentiated $CD57^-$ NK cells preferentially expand, leading to a relative dilution of the $CD57^+$ subset over time. In addition, the higher $CD57^+$ frequency observed at early timepoints may partly reflect transient stress associated with the isolation procedure, with subsequent recovery and re-equilibration under optimized culture conditions [239,240].

CD137 and TIM-3 showed only mild, transient oscillations in both frequency and MFI, and their surface density remained markedly lower than that of NKp44, CD16, and NKG2A. CD137 (4-1BB) is a co-stimulatory receptor transiently induced upon NK-cell activation and involved in amplifying cytotoxic and cytokine responses, whereas TIM-3 functions as an activation-associated checkpoint receptor that modulates NK-cell responsiveness during sustained stimulation. The observed fluctuations in CD137 and TIM-3 expression reflect fine-tuning of NK-cell activation in response to sustained cytokine stimulation. In the absence of persistent inhibitory receptor upregulation or loss of activating signals, these changes do not support an exhaustion phenotype [241–246].

ADAM17 expression showed low surface MFI throughout culture. This dissociation highlights the critical distinction between ADAM17 expression and enzymatic activity. Although ADAM17 can be transiently activated during early NK-cell stimulation to mediate shedding of selected substrates, sustained high surface expression or persistent proteolytic activity was not observed. The maintenance of low ADAM17 MFI, together with preserved CD16 expression, suggests that ADAM17-mediated feedback is tightly regulated and does not impose a limiting constraint on NK-cell expansion or receptor integrity under these conditions[86,166,236].

Overall, the observed marker dynamics, dominant and sustained NKp44 expression, preserved CD16, stable NKG2A, gradual reduction of $CD57^{+}$ cells, transient modulation of CD137 and TIM-3, and restrained ADAM17 expression, define a stable, activation-oriented NK-cell phenotype. These features reflect physiological adaptation to cytokine-driven expansion rather than maturation-associated decline or exhaustion, supporting the suitability of perfusate-derived NK cells for downstream applications, including CAR-NK manufacturing.

7.1.2 *Ex vivo* cytokine activation of perfusate-derived NK cells

Short-term *ex vivo* activation of perfusate-derived NK cells revealed comparable surface immunophenotypes. Indeed, expression of major activating and inhibitory receptors (NKG2D, NKp30, NKp44, NKp46, NKG2A, PD-1, TIM-3) and of the activation marker CD137 was largely comparable between IFN-α– and IL-12/IL-18–activated NK cells (Fig.6). IFN-α–activated NK cells are consistently reported in the literature to exhibit potent antitumour activity against hepatoma cell lines, maintaining robust effector function even at low effector-to-target ratios. This enhanced functional profile is mechanistically supported by the rapid engagement of IFN-I signaling pathways, which directly activate STAT1 and promote early transcriptional programs associated with cytolytic competence within a 24-hour timeframe [247–251]. By contrast, IL-12/IL-18–driven activation is primarily mediated through STAT4-centered signaling cascades, which generally require more prolonged stimulation to reach peak functional output and are more closely associated with sustained cytokine production rather than immediate cytolytic readiness [252–254]. Moreover, IFN-I signalling has been shown to increase intracellular stores of perforin and granzyme B and to promote a “serial killer” phenotype, enabling individual NK cells to efficiently engage and lyse multiple target cells sequentially [248,255,256].

A central mechanistic distinction between the two activation conditions was the selective upregulation of TRAIL in IFN-α–activated NK cells (Fig.6). TRAIL is a key death ligand in

liver-associated NK-cell immunity and plays a prominent role in the elimination of virus-infected hepatocytes and transformed cells [257–260]. IFN-α directly induces TRAIL transcription through STAT1- and ISGF3-dependent mechanisms, as well as via induction of IRF-1, allowing rapid accumulation of TRAIL at the NK-cell surface[247]. In contrast, IL-12/IL-18–mediated TRAIL induction is indirect and largely dependent on secondary IFN-γ signaling, a multistep process that is kinetically disadvantaged during short-term stimulation [260-262].

7.1.3 In *vivo proof-of-concept* of *ex vivo*–activated NK-cell therapy

The anti-tumor activity and safety of *ex vivo* cytokine-activated NK cells were evaluated in a preclinical orthotopic HCC xenograft model (workflow summarized in Fig. 7). The study was conducted at IRCCS ISMETT within a research project led by Dr. Badami, in which I actively participated during my PhD training.

Luciferase-expressing HepG2 cells were orthotopically implanted into immunodeficient NOG mice, and tumor progression was longitudinally monitored through *in vivo* bioluminescence imaging (IVIS) together with serial quantification of serum AFP [263,264], enabling dynamic and complementary assessment of tumor burden.

Following isolation of NK cells from liver perfusate and detailed phenotypic characterization, the experimental strategy moved toward functional optimization. Based on their baseline profile, NK cells were subjected to short-term *ex vivo* activation using two distinct cytokine regimens, IFN-α or IL-12/IL-18, with the aim of enhancing their effector competence prior to systemic administration. Consistent with the established capacity of IFN-α and IL-12/IL-18 combinations to potentiate NK-cell activation, promote granule polarization, and amplify effector molecule release, cytokine priming generated functionally competent cytotoxic effectors capable of recognizing HepG2-Luc targets.

In the orthotopic xenograft setting, *ex vivo* cytokine–activated human NK cells exerted measurable antitumor effects, demonstrating that primed innate effectors can significantly limit tumor progression *in vivo*. Because NOG mice lack endogenous T, B, and NK cells, the reduction in tumor burden observed following NK-cell infusion can be directly attributed to the activity of the administered human NK cells, thereby confirming their intrinsic capacity to recognize and control hepatoma growth independently of adaptive immunity [265–268].

Among the two activation strategies, IFN-α–activated NK cells consistently achieved superior tumor control compared with IL-12/IL-18–activated cells, as reflected by an approximate ~2 $\log_{10}$ reduction in bioluminescent signal versus an intermediate ~1 $\log_{10}$ reduction, respectively. This *in vivo* hierarchy aligns with the well-characterized biology of IFN-I–driven activation programs. IFN-α rapidly induces STAT1-dependent transcriptional pathways that enhance intracellular cytotoxic readiness and TRAIL-mediated effector mechanisms, which are particularly relevant in HCC [172,251,261,269,270]. In contrast, IL-12/IL-18 predominantly engage STAT4-dependent signaling, favoring IFN-γ production and inflammatory amplification but typically requiring more sustained stimulation to reach maximal cytotoxic output [269,270].

The combined use of bioluminescence imaging and serum AFP quantification strengthened the interpretation of tumor control dynamics. BLI provided a quantitative readout of viable tumor burden, whereas AFP reflected both tumor mass and functional tumor cell activity. The concordant suppression of BLI signal and AFP levels (Fig. 8), most pronounced in the IFN-α–treated group, supports effective NK-cell engagement with the tumor *in vivo* and provides robust evidence of biologically meaningful antitumor activity [264,271–274]. Importantly, tumor control in this model manifested primarily as tumor growth delay rather than complete regression. In the context of NK-cell–based immunotherapy for solid tumors, growth delay represents a biologically meaningful endpoint, reflecting sustained immunological pressure that counterbalances tumor proliferation without achieving total eradication. Such outcomes are consistent with the known constraints imposed by solid tumor microenvironments, including limited NK-cell trafficking, progressive hypoxia, and metabolic stress that restrict NK persistence and function over time [172,269,270,275]. Although the liver constitutes a relatively permissive immunological niche, characterized by high physiological NK-cell density, constitutive IL-15 and IL-2 availability, and reliance on death receptor–mediated cytotoxic pathways, hypoxia-driven dysfunction and tumor-intrinsic resistance mechanisms remain critical barriers to durable tumor control in established HCC [276].

7.1.4 Engineering and *in vitro* validation of anti-GPC3 CAR-NK cells

Given the limited persistence and lack of intrinsic antigen specificity that constrain unmodified NK-cell therapies in solid tumours, genetic engineering approaches have been developed to enhance tumour-directed activity while preserving native cytotoxic pathways. In this study, we

established a CAR-NK platform targeting glypican-3 (GPC3), a clinically relevant antigen in HCC, through the generation of fourth-generation self-inactivating lentiviral vectors.

Efficient lentiviral production was first confirmed in HEK293T packaging cells, where robust GFP expression at 72 h post-transfection demonstrated effective plasmid delivery and vector generation (Fig. 9). Subsequent transduction of perfusate-derived primary NK cells resulted in detectable GFP-positive populations (Fig. 10C), confirming successful gene transfer within the adopted manufacturing workflow. The CAR construct design (Fig. 10A), integrated with cytokine armouring modules, enabled stable transgene expression while preserving endogenous NK-cell recognition mechanisms (Fig. 10B).

Surface CAR expression was subsequently confirmed by flow cytometry, demonstrating successful membrane localization of both GPC3-specific constructs in primary NK cells (Fig. 11). The detection of CAR-positive populations in the CAR-GPC3-IL15 and CAR-GPC3-IL15-IFNα conditions, in contrast to non-transduced controls, confirms effective genomic integration and stable surface expression of the engineered receptor. Importantly, verification of surface expression is a critical step in CAR-NK manufacturing, as functional activity depends not only on transgene delivery but also on proper receptor trafficking and membrane presentation. The flow cytometric profiling shown in Figure 11 therefore supports the structural integrity of the fourth-generation constructs and indicates that cytokine-armored designs did not impair receptor expression at the cell surface.

Quantitative flow cytometric analysis further characterized the kinetics of CAR expression over time (Fig. 12). At day 5 post-transduction, both fourth-generation constructs achieved comparable transduction efficiencies, confirming effective lentiviral gene delivery in primary liver-derived NK cells. CAR surface expression was clearly detectable at early time points, followed by a reduction in the proportion of CAR^+ cells by day 10. However, measurable CAR MFI was preserved within the transduced fraction. This pattern is consistent with the proliferative behaviour of primary NK cultures, in which rapidly expanding non-transduced cells progressively dilute the relative frequency of CAR^+ cells, while transgene expression remains stable in successfully engineered NK cells. Overall, these findings indicate that although the CAR-positive fraction decreases in bulk culture, receptor expression remains stable at the single-cell level within engineered NK cells, supporting the structural integrity and persistence of the transgene in transduced populations.

IL-15 armoring emerged as a central feature of the CAR-NK platform. Sustained IL-15 secretion by both CAR constructs (Fig.13A) aligns with the established role of IL-15 as the dominant homeostatic cytokine for NK-cell survival, metabolic fitness, and proliferative capacity, acting through STAT5-dependent pathways that sustain cytotoxic competence during ex vivo expansion [277–280]. From a translational perspective, endogenous IL-15 production reduces dependence on exogenous cytokine supplementation and enhances manufacturing robustness, while providing a mechanistic basis for improved *in vivo* persistence, a known limitation of unarmed CAR-NK cells [281]. The addition of IFN-α co-expression represents a rational, but more complex, armoring strategy. IFN-I signaling activates STAT1-driven interferon-stimulated gene programs that enhance cytolytic readiness, including perforin, granzyme B, and TRAIL expression [248,261,282–284].

In this study, IFN-α production was restricted to the CAR-GPC3-IL15-IFNα construct and declined over time (Fig.13B), a kinetic that may be advantageous by providing early activation without prolonged exposure that could promote compensatory immunoregulatory pathways. Nevertheless, IFN-α armoring introduces potential trade-offs, including induction of PD-L1 or feedback inhibition under sustained signaling, underscoring the importance of temporal control in cytokine-armored designs [284,285].

Overall, these findings support the feasibility of anti-GPC3 CAR-NK engineering from perfusate-derived NK cells and position IL-15–armored CAR-NK cells, with optional IFN-α co-expression, as a flexible and biologically sound platform for HCC immunotherapy[233].

7.2 NK Cells in Viral Infection

7.2.1 ADAM17 modulation and NK-cell immune tuning in HHV-8 infection

Ex vivo analysis of whole-blood samples from HHV-8–positive transplant recipients reveals a selective remodeling of the NK-cell compartment characterized by preserved ADAM17 expression frequency but reduced surface expression intensity. ADAM17 frequency represents the proportion of cells within a subset expressing detectable ADAM17 on the surface, whereas ADAM17 mean fluorescence intensity (MFI) reflects the average density of ADAM17 molecules per cell. Importantly, frequency and MFI are independent parameters: two populations may display similar frequencies of $ADAM17^{+}$ cells but differ markedly in MFI, indicating comparable proportions of expressing cells but different expression levels per cell.

As shown in Figure 15, the frequency of ADAM17 within total NK and NKT populations is comparable between HHV-8–positive patients and healthy controls, whereas ADAM17 MFI is consistently reduced in HHV-8–positive patients across all NK-cell subsets. This pattern suggests that HHV-8 infection maintains the proportion of ADAM17-expressing cells while reducing its surface abundance at the single-cell level, consistent with a functional downregulation of ADAM17 rather than loss of expression [169,286–288].

Importantly, ADAM17 MFI can be considered an indirect indicator of surface abundance of ADAM17, which influence (but does not directly measure) the NK cell's shedding potential, as it mediates the cleavage of multiple critical surface receptors and ligands, including CD16, L-selectin, TNFα, TNFR1, and TNFR2 [287,289,290]. A reduction in ADAM17 MFI reflects diminished per-cell sheddase activity, which would be expected to favour the preservation of activation receptors such as CD16 on the cell surface [286,291].

The reduced ADAM17 MFI observed in NK cells, NKT cells, and exhausted-phenotype NK cells from HHV-8–positive patients suggests regulated modulation rather than simple loss of expression. Several non–mutually exclusive mechanisms may explain this pattern.

First, the IL-18/ADAM17 axis has been described as a key pathway in NK-cell immune tuning during chronic viral infections [169,292,293]. In HIV-1 infection, sustained IL-18 signalling through the MyD88–IRAK–TRAF6 pathway activates NF-κB and MAPK cascades, promoting ADAM17-dependent shedding of receptors such as CD16 and substrates including L-selectin, TNFα, TNFR1, and TNFR2, thereby modulating NK cytotoxicity, trafficking, and inflammatory responses [171,294]. This mechanism balances antiviral activity with prevention of immunopathology [293,295]. In HHV-8 infection, however, the reduced ADAM17 MFI suggests that IL-18–driven ADAM17 regulation may be attenuated or temporally uncoupled. Possible explanations include transient IL-18 responses not captured by cross-sectional sampling, viral interference with IL-18 signalling, or immunosuppressive therapy in transplant recipients reducing IL-18 production [223,296]. In this context, it should also be considered that HHV-8–positive samples were analysed after virological confirmation of infection, at a stage at which the effects of IL-18–driven signalling may may have already subsided or may no longer be readily detectable

Second, reduced ADAM17 expression may represent a counter-regulatory adaptation to chronic immune activation, limiting excessive receptor shedding and preserving activation

receptors such as CD16 on NK cells, thereby maintaining antiviral responsiveness while preventing excessive inflammation [293,297].

Finally, ADAM17 surface levels depend on protein maturation and trafficking, involving chaperones (iRhom1, iRhom2, FRMD8) and furin-dependent processing [158,160,298]. HHV-8 immunomodulatory proteins (K3, K5, K6, RTA) can broadly alter immune receptor trafficking and degradation pathways [299–302], and may therefore indirectly reduce ADAM17 delivery to the plasma membrane, lowering surface MFI without necessarily changing ADAM17 transcription or total protein levels.

Stratification of NK cells by CD57 expression in HHV-8–positive patients revealed reduced ADAM17 MFI in both $CD57^+$ and $CD57^-$ NK cells (Fig. 17C), although the difference was not statistically significant. The parallel reduction across maturation states argues against a mechanism specifically linked to CD57-associated terminal differentiation or exhaustion. Indeed, $CD57^+$ NK cells are better interpreted as differentiated or "adaptive-like" cells with enhanced antiviral responsiveness rather than classical exhausted cells defined by impaired function and checkpoint upregulation [239,303,304]. The absence of subset-specific differences therefore suggests that ADAM17 downmodulation reflects a global regulatory process affecting the NK compartment.

Mechanistically, ADAM17 surface abundance depends on iRhom2-mediated maturation and dynamic membrane trafficking [305]. Chronic inflammation and herpesvirus-driven remodelling of trafficking pathways may therefore reduce steady-state delivery or retention of ADAM17 at the plasma membrane across NK subsets [306]. Accordingly, the uniform reduction of ADAM17 MFI in $CD57^+$ and $CD57^-$ NK cells is more consistent with systemic modulation of protease trafficking or stability than with CD57-defined exhaustion.

ADAM17 expression was subsequently analysed in circulating lymphoid ($CD3^+$, $CD4^+$, $CD8^+$ T cells and $CD19^+$ B cells) and myeloid ($CD14^+$ monocytes and $CD15^+$ neutrophils) populations (Figure 16). HHV-8–positive individuals showed a reduced frequency of $ADAM17^+$ $CD4^+$ T cells, while MFI remained unchanged. Given that chronic HHV-8 infection is known to remodel $CD4^+$ T-cell composition and activation states through persistent antigenic stimulation and viral immune evasion strategies [288,291], the reduced proportion of $ADAM17^+$ $CD4^+$ T cells is most plausibly interpreted as a redistribution in the proportion of $CD4^+$ T cells expressing detectable surface ADAM17 rather than intrinsic suppression at the

single-cell level. Indeed, preserved MFI indicates that, among ADAM17-positive cells, surface protease density is maintained.

In contrast, monocytes and neutrophils displayed high ADAM17 frequency and MFI, consistent with their established role as major sources of this sheddase in inflammatory regulation [286,287,289]. Experimental models confirm that ADAM17 deficiency in myeloid cells disrupts TNF and adhesion molecule shedding without affecting cell viability [169,287]. Importantly, no differences were observed between HHV-8–positive patients and controls, indicating that chronic HHV-8 infection does not significantly alter baseline ADAM17 expression in circulating myeloid subsets.

Across all analysed populations, ADAM17 MFI remained comparable between HHV-8–positive patients and controls, indicating preserved per-cell surface abundance of the protease despite viral infection.

As shown in Figure 17, HHV-8–positive transplant recipients exhibited enrichment of NK cells, NKT cells, non-exhausted NK cells, B cells, and monocytes, together with reduced $CD4^+$ and $CD8^+$ T-cell subsets. The most direct explanation for this pattern is the iatrogenic immunosuppression associated with transplantation, as drugs such as calcineurin inhibitors, corticosteroids, antimetabolites, and mTOR inhibitors preferentially suppress T-cell proliferation and IL-2–dependent signalling pathways [306,307]. In contrast, innate immune populations, including NK cells, monocytes, and neutrophils, are less directly affected and can persist through alternative innate immune mechanisms [308]. Consequently, the reduction of T-cell subsets observed in HHV-8–positive transplant recipients is consistent with the established effects of transplant immunosuppression on adaptive immunity.

NK-cell enrichment in HHV-8–positive patients can be explained by cytokine-driven expansion during viral infection, primarily mediated by IL-15 and IL-18. IL-15, produced by macrophages, dendritic cells, and epithelial cells, together with IL-18 induced by viral pathogen-associated molecular patterns and early IFN-γ responses, promotes NK-cell proliferation and survival [293,297]. While transplant immunosuppression effectively suppresses T-cell responses, NK cells remain responsive to IL-15– and IL-18–mediated signalling, resulting in expansion of the NK-cell compartment during chronic HHV-8 infection [309–311].

During viral infections, including herpesvirus infections, type I interferons (IFN-I; IFN-α and IFN-β) further shape hematopoiesis by promoting preferential expansion of myeloid and

granulocyte lineages [312,313]. Consistent with this mechanism, the increased monocyte frequency observed in Figure 17, together with the strong ADAM17 surface expression detected in monocytes and neutrophils (Fig. 16), supports a state of persistent innate immune activation. These cells physiologically maintain high ADAM17 levels to enable rapid shedding of inflammatory mediators and receptors, while sustained IFN-I signalling during infection promotes emergency myelopoiesis and granulopoiesis, maintaining expansion and activation of myeloid populations [313,314].

The enrichment of B cells in HHV-8–positive patients may reflect polyclonal B-cell activation driven by chronic viral antigen exposure and pro-inflammatory cytokines such as IL-6, TNF-α, and IL-1β produced by innate immune cells [306]. HHV-8–specific B-cell responses have been described in infected individuals, and persistent antigenic stimulation may sustain virus-specific populations. In addition, bystander activation through TLR signalling and IFN-I may expand non-specific B cells as part of the innate response to persistent viral infection [306,315,316].

Consistent with previous observations, chronic viral infections, particularly those caused by persistent herpesviruses, often drive a shift from adaptive toward innate immune responses. HHV-8 (KSHV), a lymphotropic gammaherpesvirus that establishes predominantly latent infection, has likely co-evolved with the innate immune system as a primary immunological barrier, especially during early phases of infection when adaptive responses are not yet fully mobilized [306,317,318].

Collectively, these data support a model of "innate immune dominance" during chronic HHV-8 infection in transplant recipients. In this context, adaptive T-cell immunity is strongly suppressed by immunosuppressive therapies required for graft tolerance, whereas innate immune pathways, driven by IFN-I signalling, IL-15, IL-18, and persistent viral stimulation, remain relatively active and promote the expansion of NK cells, monocytes, neutrophils, and B cells. Although HHV-8–specific $CD8^+$ T cells play a key role in controlling viral replication and preventing Kaposi sarcoma in immunocompetent individuals, their reduced function in transplant recipients likely shifts antiviral pressure toward the innate immune compartment [306,319]. Consequently, the enrichment of innate immune cells observed in HHV-8–positive patients is consistent with a compensatory response, as these populations are relatively resistant to pharmacologic immunosuppression and remain responsive to chronic viral signals through IFN-I pathways, IL-15/IL-18–mediated expansion, and trained immunity–like mechanisms.

7.3 Viral Peptide–Based *In Vitro* Model

7.3.1 ADAM17 modulation in NK-Cell Subsets

Across the 7-day culture period, ADAM17 surface density in NK cells, measured by MFI, showed a progressive and reproducible decline in both viral peptide–stimulated PBMC cultures and time-matched unstimulated controls (Fig. 19–22), indicating a time-dependent rather than stimulus-specific modulation. In contrast, ADAM17 MFI in NKT cells remained stable, revealing a lineage-specific difference in ADAM17 regulation. Importantly, the overall frequency of ADAM17^{+} NK cells remained largely unchanged, suggesting a dissociation between the proportion of expressing cells and the per-cell surface abundance of the protease.

The decline in ADAM17 MFI likely reflects activation-dependent regulation of ADAM17 trafficking and turnover. Previous studies show that cellular activation induces rapid, actin-dependent mobilization of ADAM17 from intracellular compartments to the plasma membrane, followed by internalization, recycling, or shedding despite stable transcript levels [292,298,320]. During prolonged PBMC culture, NK cells experience persistent low-level activation from residual cytokines and cell–cell interactions, repeatedly engaging this mobilization–turnover cycle and progressively reducing steady-state surface ADAM17. In addition, sustained enzymatic activity may promote auto-cleavage or membrane shedding of ADAM17 itself, further contributing to the observed decline in MFI [292,298,320]. These changes occur within the broader phenotypic remodeling known to occur during in vitro PBMC culture, where lymphocyte activation states and membrane protein expression gradually shift over time [321,322].

In contrast, the stability of ADAM17 MFI in NKT cells suggests a distinct regulatory mechanism. NKT cells rely on rapid, high-affinity TCR recognition of CD1d-presented lipid antigens, generating a dominant activation signal that reduces the need for dynamic receptor tuning typical of NK cells. Whereas NK cells integrate multiple activating and inhibitory pathways, NKT activation is more pulsatile and TCR-driven, which may allow maintenance of relatively stable ADAM17 surface levels while preserving sheddase activity that supports their role as early cytokine producers rather than serial cytotoxic effectors [292,295,320].

Notably, the reduction of ADAM17 MFI in NK cells occurs uniformly across maturation states. Both CD57^{+} (mature) and CD57^{-} (immature) NK-cell subsets display parallel kinetics of MFI decline (1–3, 6). At all time points, CD57^{+} NK cells maintain higher ADAM17 MFI than

$CD57^-$ cells, consistent with maturation-associated amplification of immune machinery rather than exhaustion [239,303,304,323]. This pattern aligns with cumulative IL-18–driven maturation during chronic antigen exposure, mediated through IL-18 receptor signalling via the MyD88/IRAK/TRAF6 axis and downstream NF-κB/MAPK activation that upregulates ADAM17 as part of the mature NK-cell effector program [192,292,293,297]. Functionally, higher ADAM17 expression in mature NK cells supports rapid tuning of activation receptor density, particularly CD16, allowing efficient antiviral responses while preventing excessive inflammatory signalling [166,239].

Comparison between NK and NKT compartments shows that NK cells consistently exhibit a slightly higher proportion of ADAM17 positivity than NKT cells, independent of viral peptide stimulation (Fig. 19–22), indicating a modest lineage-specific difference in ADAM17 regulation. This distinction is largely preserved across conditions; however, in CMV- and EBV-stimulated cultures, NKT cells display a late increase in ADAM17 expression at day 7, approaching the levels detected in NK cells. In these conditions, ADAM17 expression in NKT cells is higher than in time-matched unstimulated controls, although the difference does not reach statistical significance. No comparable trend is detected following SARS-CoV-2 or HHV-8 stimulation. This delayed increase is compatible with progressive CD1d upregulation on antigen-presenting cells and incremental NKT-cell engagement, leading to enhanced ADAM17 expression only at later time points, in line with the lower baseline levels characteristic of this compartment [324–328]. Such a pattern may reflect virus-specific imprinting of the NKT compartment by persistent herpesviruses, resulting in phenotypic adaptation in response to prolonged antigenic stimulation.

A virus-specific pattern of ADAM17 modulation in NK cells may emerge following viral peptide stimulation. A modest, time-dependent reduction in ADAM17 MFI is observed after CMV and EBV stimulation, whereas no comparable modulation is detected following SARS-CoV-2 or HHV-8 stimulation; notably, ADAM17 MFI in NKT cells remains largely unchanged across conditions. This pattern suggests that CMV and EBV may more effectively engage NK-cell regulatory pathways that promote progressive ADAM17 feedback modulation, even in the absence of live viral replication. In peptide-based PBMC cultures, CMV and EBV stimulation may sustain cytokine-mediated NK-cell activation through antigen-presenting cell signals, favouring repeated cycles of ADAM17 activation and surface regulation over time

[236,325,329,330]. In contrast, SARS-CoV-2 and HHV-8 peptides appear less capable of maintaining the cytokine signalling required to drive similar temporal modulation.

From a methodological perspective, the lack of statistical significance in ADAM17 MFI differences after CMV or EBV stimulation warrants cautious interpretation. The modest effect size may reflect inter-donor variability, limited sample size, baseline time-dependent modulation inherent to PBMC cultures, or intrinsic limitations of peptide stimulation compared with live infection. These findings should therefore be considered descriptive trends rather than definitive evidence of discrete regulatory mechanisms, highlighting the need for validation in complementary experimental systems.

7.3.2 Virus-Specific Immune Tuning of NK and NKT Cell Compartments

Following *in vitro* stimulation with viral peptide pools (SARS-CoV-2, HHV-8, CMV, EBV), distinct virus-specific patterns of immune-cell redistribution emerge, reflecting differential engagement of lymphocyte compartments.

A mild reduction in NKT-cell frequencies (Fig. 23) is observed after HHV-8, CMV, and EBV stimulation, whereas SARS-CoV-2 induces minimal NKT-cell loss, highlighting differences in viral interaction with the NKT compartment. NKT cells recognize lipid antigens presented by CD1d, a pathway preferentially exploited by persistent herpesviruses that sustain CD1d-mediated antigen presentation by dendritic cells and B cells. Chronic CD1d-mediated TCR engagement may therefore drive activation-induced apoptosis of NKT cells [324,327,331,332]. Similar patterns have been described in chronic viral infections such as HCV, where prolonged NKT activation initially contributes to inflammation but ultimately correlates with reduced NKT-cell frequencies, likely due to exhaustion-related apoptosis [333,334]. In contrast, SARS-CoV-2 is less likely to generate strongly immunogenic CD1d-restricted lipid antigens, resulting in weaker NKT-cell activation and limited apoptotic loss in this model [331,332]. Within the 1–7 day culture system, repeated exposure to CMV-, EBV-, or HHV-8–derived CD1d-presented antigens in the absence of survival cytokines such as IL-15, IL-7, or IL-21 may create a pro-apoptotic environment that progressively reduces NKT-cell numbers, highlighting virus-specific susceptibility to stimulation-driven contraction [335,336,336].

Total NK-cell frequencies tend to decline over time after CMV and EBV stimulation, although this trend does not reach statistical significance, whereas they remain largely stable following

SARS-CoV-2 and HHV-8 stimulation (Fig. 23). These patterns suggest virus-specific effects on NK-cell dynamics. CMV is known to drive expansion of adaptive NK cells *in vivo*, particularly $NKG2C^{+}CD57^{+}$ populations that accumulate during chronic infection. However, this process requires prolonged antigenic stimulation over months or years and cannot be reproduced within the short timeframe (3–10 days) of peptide-based in vitro stimulation. The modest decline in NK-cell frequencies observed here likely reflects activation-induced cell death during acute stimulation, rather than the development of stable adaptive NK-cell expansion.

7.3.3 ADAM17 Expression in T Cells, B Cells and Monocytes

PBMCs were stimulated *in vitro* with viral peptide pools derived from SARS-CoV-2 (Fig. 24), HHV-8 (Fig.25), CMV (Fig.26), and EBV (Fig.27), with ADAM17 expression subsequently assessed at day 1, day 3, and day 7. Across all conditions and time points, ADAM17 expression in T Cells, B Cells and Monocytes remained stable, with no statistically significant differences between stimulated and unstimulated cultures, reflecting intrinsic cell-type–specific patterns of ADAM17 regulation.

Monocytes displayed the highest proportion of ADAM17-positive cells with stable expression across all viral conditions, consistent with their established role as producers of TNF-α, whose release requires ADAM17-mediated proteolytic cleavage, and supports ADAM17 as a constitutive feature of monocyte identity rather than a stimulus-dependent marker [290,337].

A modest, although not statistically significant, reduction in monocyte ADAM17 MFI was observed at later time points following CMV and EBV stimulation and may reflect partial activation or differentiation associated with minor ADAM17 internalization or auto-cleavage as a feedback mechanism limiting excessive TNF-α release [337,338].

Although CMV is known to target ADAM17 through UL148 and UL148D during live infection, the use of peptide pools precludes direct viral interference, indicating that any observed modulation likely reflects secondary activation-driven regulation [206]. In contrast, T and B lymphocytes displayed low baseline surface ADAM17 expression across all experimental conditions. In these lineages, ADAM17 is not constitutively expressed at high levels but can be transiently mobilized upon activation to mediate regulated shedding of selected substrates, such as CD62L or FasL in T cells and BAFFR/TACI in B cells. This pattern

reflects tight temporal control of sheddase activity rather than sustained surface availability. Accordingly, the primary effector functions of T and B cells rely predominantly on receptor-mediated signalling and secretion of soluble cytokines rather than on ADAM17-dependent shedding. The maintenance of stable, low ADAM17 surface expression irrespective of viral peptide stimulation supports a cell-type–specific model of ADAM17 regulation distinct from that observed in NK cells [339,339–342].

Finally, the progressive reduction of ADAM17 MFI observed in T cells over time in both stimulated and unstimulated PBMC indicates a culture-dependent rather than virus-specific effect. Gradual lymphocyte activation and phenotypic evolution during in vitro culture promote transient ADAM17 mobilization followed by auto-cleavage and internalization, resulting in a mild decline in surface MFI over time[156].

7.3.4 Distribution of T Cells, B Cells and Monocytes

Changes in immune-cell frequencies observed after in vitro viral peptide stimulation (Fig. 28) are more plausibly explained by activation-driven remodelling of the PBMC compartment than by overt cellular dysfunction. The early decrease in monocyte frequencies following HHV-8, CMV, and EBV peptide stimulation likely reflects rapid monocyte activation and engagement in antigen sensing/processing pathways, including cytokine production, together with phenotypic modulation that can affect how monocytes are captured by conventional flow-cytometric gates. In particular, inflammatory cues can be associated with down-modulation of CD14 and other surface markers and with rapid shifts toward dendritic cell–like phenotypes, which can make “monocyte frequency” appear reduced even when viability is preserved [343–345]. In parallel, expansion or increased activation of other immune subsets may further influence relative proportions within the PBMC compartment. Consequently, the observed reduction most plausibly represents a proportional and activation-associated shift rather than impaired viability or true monocyte loss.

A slightly increase in total T lymphocytes, particularly $CD4^+$ T helper cells, is observed at early time points, consistent with activation-induced proliferation driven by viral peptide presentation on MHC-II molecules by monocytes and dendritic cells, together with CD80/CD86-mediated costimulation [346,347]. This expansion represents an expected and adaptive engagement of the antigen-specific immune response rather than an indicator of altered T-cell function.

A mild reduction in B-cell frequencies, although not statistically significant, can be observed in CMV and EBV stimulation. This effect may result from multiple non-mutually exclusive mechanisms, including preferential proliferation of activated T cells, which dilutes the relative contribution of B cells within the PBMC population. Whereas T cells directly recognize peptide–MHC complexes through the TCR, B-cell activation generally requires T-cell help via CD40–CD40L interactions or occurs indirectly through bystander activation mediated by pro-inflammatory cytokines [348–350]. In addition, B cells are more prone than T cells to apoptosis under in vitro culture conditions in the absence of optimal survival signals [351].

7.3.5 In Vitro Cytokine Response of PBMCs to Viral Peptide Stimulation

Cytokine release was longitudinally assessed at days 1, 3, and 7 in supernatants from PBMCs activated in vitro with viral peptide pools (SARS-CoV-2, HHV8, CMV, EBV) enabling evaluation of immune responses (Fig.29). Analysis of a broad panel of pro-inflammatory (TNF-α, IL-1β, IL-1α, IL-6), immunoregulatory (IFN-γ, IL-2), anti-inflammatory (IL-10), and Th17-associated (IL-17A) mediators revealed a distinctly virus-specific temporal architecture of cytokine production, rather than a convergent activation pattern across different viral stimuli.

Longitudinal analysis of cytokine revealed virus-specific kinetic patterns rather than uniform inflammatory trajectories, indicating that the temporal architecture of immune activation differs across pathogens.

TNF-α displayed a time-dependent increase following SARS-CoV-2, CMV, and HHV-8 stimulation, consistent with progressive activation of the monocyte compartment in PBMC cultures and with secondary amplification driven by antigen-specific lymphocyte–monocyte cross-talk. TNF-α is released as a soluble cytokine through ADAM17-mediated proteolytic cleavage [290,352–354].

The gradual increase in TNF-α over time may therefore reflect secondary autocrine and paracrine amplification loops, potentially mediated by TNFR1 signalling on neighbouring monocytes and downstream NF-κB and MAPK pathway activation, rather than a single early burst of cytokine release [355,356].

IL-6 also displayed antigen-dependent kinetics and may act as a secondary amplifier of TNF-α initiated inflammation. Notably, CMV peptide stimulation induced earlier and more sustained IL-6 production, whereas SARS-CoV-2 and EBV peptide stimulation showed more

delayed IL-6 increases with higher levels at later time points. In a peptide-based PBMC assay, these differences are more plausibly attributed to (i) antigen processing requirements (e.g., immediate MHC loading for exogenous peptides vs. uptake/processing for recombinant protein), (ii) inter-individual variation in functional state of antigen-specific memory T cells, and (iii) the timing of lymphocyte--monocyte cross-talk (including IFN-γ and TNF-α -driven monocyte activation and contact-dependent signals), rather than by direct differential engagement of innate pattern-recognition receptors by the antigens themselves [354,354,357].

Virus-dependent IL-6 and IL-10 kinetics further highlighted divergent immune regulatory strategies. CMV stimulation induced early and sustained IL-6 and IL-10 production, generating a persistence-permissive cytokine environment in which inflammation is balanced by IL-10–mediated suppression of Th1 adaptive immunity. This IL-6/IL-10 equilibrium favours viral persistence through controlled immune activation rather than full adaptive clearance and has been directly implicated in CMV persistence in vivo [358–361]. In contrast, SARS-CoV-2 and EBV exhibited delayed IL-6 and IL-10 induction, consistent with acute infection contexts in which regulatory mechanisms develop later and do not prevent effective adaptive immune engagement [357,362,363]. HHV-8 showed minimal IL-10 induction despite its persistent nature, suggesting reliance on immune evasion strategies distinct from the IL-10–dependent mechanisms characteristic of CMV[352].

A moderate variation was observed in IFN-γ production: EBV peptide stimulation induced robust and sustained IFN-γ responses, whereas HHV8 and CMV peptide stimulation elicited more modest induction. Because the EBV stimulus consisted of defined MHC class I/II–restricted peptides rather than viral nucleic acids, the observed response may reflect a relatively strong antigen-specific recall component in the studied donors. EBV peptide pools commonly include multiple well-characterized immunodominant epitopes from both lytic and latent proteins, which could efficiently restimulate pre-existing memory T cells in EBV-seropositive individuals. In this context, the enhanced IFN-γ production may be attributable to a higher precursor frequency and/or greater functional competence of EBV-specific T cells [364].

IL-1β and IL-1α remained largely low across all conditions, with only a transient IL-1α increase observed following EBV stimulation, indicating limited inflammasome activation in this peptide-based in vitro system. This finding is consistent with the absence of viral replication–associated danger signals required to fully engage the inflammasome–caspase-1

axis, despite preserved NF-κB activation as evidenced by TNF-α and IL-6 production [352,353,365–367].

Finally, persistently low IL-2 and IL-17A levels across all viral stimulations argue against robust Th1 or Th17 polarization within this experimental setting. IL-2 production requires strong $CD4^+$ T-cell activation supported by adequate costimulation and IL-12 signalling, while IL-17A generation depends on specific Th17-polarizing cytokine milieus that were not provided in this model [368–370].

Collectively, these findings indicate that viral peptide stimulation elicits pathogen-specific cytokine programs that may recapitulate key aspects of *in vivo* immune modulation, highlighting distinct strategies of immune engagement and regulation across viral infections. This experimental system represents a short-term in vitro model (1–7 days) that is well suited to capture early immune responses, however, it remains inherently limited in its ability to reproduce the full complexity and chronicity of immune dynamics observed *in vivo*.

7.3.6 TNF-α and IL-6 Signalling in the Regulation of ADAM17 Activity in NK Cells

TNF-α produced by monocytes upon viral stimulation engages TNFR1 on NK cells and other immune populations, activating downstream NF-κB and MAPK signalling pathways that critically regulate ADAM17 function [355,356]. A key mechanistic step in this process is the TNF-α–dependent upregulation of iRhom2, an essential regulator of ADAM17 trafficking and maturation to the cell surface [298]. Once activated, ADAM17 rapidly mediates shedding of key NK-cell surface receptors, including CD16 and CD62L, which are central to ADCC and lymphoid tissue homing, respectively [171,236].

Inflammatory activation–induced receptor shedding represents a sophisticated adaptive mechanism through which TNF-α signalling simultaneously promotes NK-cell activation while limiting excessive receptor availability and uncontrolled trafficking to inflamed tissues. In this context, the mild time-dependent reduction in ADAM17 MFI on NK cells after CMV and EBV stimulation is compatible with activation-associated remodelling of the ADAM17 axis and NK-cell surface phenotype in an inflammatory milieu where TNF-α and IL-6 accumulate over time. Indeed, the progressive increase in these cytokines may result in sustained TNFR engagement, continuous ADAM17 activation, and ongoing CD16/CD62L

shedding over the 1–7 day culture period [155,371,372,372]. This progressive engagement of ADAM17 allows dynamic regulation of NK-cell receptor availability in proportion to inflammatory intensity.

However, ADAM17 MFI alone does not uniquely report enzymatic activity or receptor shedding; thus, these findings should be interpreted as suggestive of dynamic immune tuning rather than definitive evidence of continuous ADAM17 activation and CD16/CD62L shedding. IL-6 provides an additional regulatory layer by amplifying inflammatory circuits and by acting through classical and trans-signalling pathways. In particular, ADAM17-mediated cleavage of the membrane-bound IL-6R generates sIL-6R, enabling IL-6/sIL-6R complexes to signal through gp130 on a broad range of cells and thereby extend IL-6 responsiveness. Prolonged IL-6 signalling can promote sustained STAT3 activation and contribute to a more activated transcriptional program; in parallel, inflammatory milieus in which both TNF-α and IL-6 are elevated may favour continued engagement of shedding pathways and consequent modulation of NK-cell surface receptors. Accordingly, earlier and sustained IL-6 production after CMV stimulation can be discussed as a marker of a more persistent inflammatory environment and immune cell cross-talk in that condition, whereas delayed IL-6 induction after SARS-CoV-2, HHV-8, and EBV stimulation is compatible with temporally postponed amplification dynamics [161,372,372,373].

7.3.7 Limitations of In Vitro model

In vitro stimulation of PBMCs with viral peptide pools is widely used because it is standardized, cost-effective, and ethically feasible; however, it has intrinsic limitations when modelling NK-cell regulation and ADAM17 dynamics during chronic viral infection. A key limitation is the absence of live viral replication and immune-evasion mechanisms, which in vivo generate persistent PAMPs that sustain PRR signalling, IFN-I production, and cytokine release such as IL-15 and IL-18, maintaining continuous immune activation [310,374].

Peptide stimulation instead provides a finite antigenic signal, producing an artificial temporal response. This limitation is particularly relevant for ADAM17 regulation: the decline in ADAM17 MFI observed after 3–7 days likely reflects feedback mechanisms such as auto-cleavage, internalization, or negative regulation, whereas *in vivo* persistent viral replication would be expected to maintain or periodically re-induce ADAM17 through cytokine-driven signalling [206,236,375]. The discrepancy is evident in CMV infection, where viral proteins

such as UL148 and UL148D can directly modulate ADAM17 activity and stabilize multiple cell-surface molecules normally subject to ADAM17-mediated shedding [329].

Another limitation is the absence of tissue microenvironmental signals. *In vivo*, NK cells are shaped by interactions with stromal, endothelial, and dendritic cells that provide cytokines, metabolic cues, and adhesion-mediated signals [376,377]. For example, IL-15 is commonly delivered through IL-15/IL-15Rα transpresentation by dendritic cells and monocytes/macrophages, a mechanism not fully reproduced in PBMC cultures. Tissue conditions such as hypoxia can also directly impair NK activation and cytotoxic function [378–380]. In addition, cell isolation and *ex vivo* culture can induce stress-related activation programs in myeloid cells, altering subset composition and cytokine production compared with physiological conditions, with potential consequences for ADAM17 regulation [381–383].

Finally, the model presents a temporal mismatch with chronic viral infections. PBMC stimulation captures a short activation phase (1–7 days), whereas persistent infections such as CMV or EBV evolve over months or years through cycles of viral reactivation, immune modulation, and compartment remodelling [206,236,329,375]. Consequently, although peptide stimulation is informative for early immune activation, it cannot fully reproduce the chronic, tissue-integrated regulation of ADAM17 characteristic of persistent viral infection.

8.CONCLUSION

This work provides an integrated perspective on NK-cell functional plasticity across both immunotherapy and viral infection contexts. A central aspect of this thesis is the use of liver perfusate–derived NK cells as the primary cellular source. Compared with peripheral blood NK cells, liver perfusate enables recovery of large numbers of viable immune cells that have already been conditioned by the hepatic microenvironment. These NK cells therefore represent not only circulating effectors but populations educated within a tolerogenic, metabolically complex, and chronically antigen-exposed organ, characteristics particularly relevant to the hepatic setting in which HCC develops. Importantly, the isolation procedure preserves viability and cytotoxic competence, allowing efficient *ex vivo* expansion and activation. These findings highlight how cell source selection represents a strategic parameter in adoptive immunotherapy, potentially influencing persistence, adaptability, and resistance to tumour-induced suppression.

Within this framework, short-term cytokine activation did not reveal relevant changes in receptor expression. NK cells stimulated with IFN-α or IL-12/IL-18 showed similar activating and inhibitory receptor profiles. These observations suggest that short-term cytokine stimulation preserves a largely stable receptor phenotype in hepatic NK cells.

The *in vivo proof-of-concept* experiments provided translational validation of these findings. Cytokine-activated NK cells significantly limited tumour progression in the orthotopic HCC model, with concordant reductions in BLI signal and serum AFP levels. IFN-α–activated NK cells showed the most pronounced antitumor activity. Rather than inducing tumour regression, NK therapy primarily delayed tumour growth, a biologically meaningful effect in solid tumours where hypoxia, metabolic stress, and microenvironmental suppression often restrict durable immune clearance. These results support the feasibility and biological relevance of NK-based strategies within the hepatic niche.

The generation of anti-GPC3 CAR-NK cells further strengthened the translational trajectory of this work. Efficient lentiviral production and transduction confirmed the feasibility of engineering perfusate-derived primary NK cells within a reproducible manufacturing framework. Both fourth-generation constructs showed stable surface expression and maintained functional cytotoxicity, demonstrating the structural and functional competence of anti-GPC3 CAR-NK cells derived from liver perfusate.

In parallel, the study of NK-cell regulation in viral contexts highlighted ADAM17 as a key modulatory axis. Across analyses of HHV-8–positive patients and peptide-based stimulation models, ADAM17 expression reflected immune calibration rather than simple activation or suppression. Cytokines such as TNF-α and IL-6 may sustain ADAM17 activity, linking inflammatory signalling to receptor shedding events that reshape the NK-cell surface landscape, including modulation of CD16 and other regulatory molecules. In chronic infection, where persistent antigen exposure risks NK dysfunction, this shedding-mediated regulation may represent an adaptive mechanism balancing antiviral defence with control of excessive inflammation.

The complexity of the biological processes examined in this thesis also underscores the value of Artificial Intelligence as a complementary analytical tool. By integrating flow-cytometry datasets, cytokine measurements, gene-expression profiles, and functional assays, AI-assisted approaches can support experimental prioritization and hypothesis generation. In the context of immunotherapy, such models may inform CAR design and cytokine-conditioning strategies, while in viral immunology they may help model inflammatory circuits and ADAM17-dependent regulatory dynamics.

Overall, this work integrates translational cellular engineering with mechanistic immune regulation, advancing both the therapeutic and biological understanding of NK cells. It provides *proof-of-concept* evidence supporting liver-derived NK cells as a viable platform for HCC immunotherapy and identifies ADAM17 as an important regulatory node controlling NK-cell responsiveness during viral challenge. Together, these findings support a rational framework for NK-based interventions in which cell source selection, cytokine conditioning, genetic engineering, and regulatory modulation are combined to advance next-generation NK-cell immunotherapy.

9. ACKNOWLEDGEMENTS

I would first like to express my deepest gratitude to Professor Pier Giulio Conaldi, former Scientific Director of IRCCS ISMETT, for giving me the opportunity to undertake this PhD program. His guidance, scientific rigor, and dedication to translational research have strongly influenced my professional and academic development. I am sincerely grateful for the trust he placed in me and for fostering an environment in which research and clinical application are closely integrated.

I am especially indebted to Dr. Ester Badami, Principal Investigator at Fondazione Ri.MED, and Dr. Rosalia Busà, researcher at IRCCS ISMETT, for their constant guidance throughout these years. Their scientific insight, constructive feedback, and daily support have been essential to the development of this work. Beyond their mentorship, their enthusiasm for research have been a continuous source of motivation.

I would also like to thank Professor Antonino Tuttolomondo, Director of the Doctoral Program, for his cordiality, availability, and institutional support throughout the course of my PhD.

A sincere thank you goes to Professor Domenico Di Raimondo for his generous support and constant availability. His professionalism, clarity, and readiness to help were truly valuable and sincerely appreciated throughout these years.

My deepest gratitude goes to my family, whose constant love, encouragement, and unwavering support have been the foundation of every achievement and the strength behind this journey.

To all those who contributed, directly or indirectly, to this journey, my heartfelt thanks.

10. REFERENCES

1. Medzhitov R, Janeway CA. Innate immunity: impact on the adaptive immune response. *Curr Opin Immunol*. 1997;9(1):4-9. doi:10.1016/s0952-7915(97)80152-5

2. Wang R, Lan C, Benlagha K, et al. The interaction of innate immune and adaptive immune system. *MedComm*. 2024;5(10):e714. doi:10.1002/mco2.714

3. Charles A Janeway J, Travers P, Walport M, Shlomchik MJ. Principles of innate and adaptive immunity. In: *Immunobiology: The Immune System in Health and Disease. 5th Edition*. Garland Science; 2001. Accessed February 15, 2026. https://www.ncbi.nlm.nih.gov/books/NBK27090/

4. Gonzalez VD. *Innate and Adaptive Cellular Immunity in Chronic HCV and HIV-1 Infection*. thesis. Karolinska Institutet; 2009. Accessed January 26, 2026. https://openarchive.ki.se/articles/thesis/Innate_and_adaptive_cellular_immunity_in_chronic_HCV_and_HIV-1_infection/26899549/1

5. Raulet DH. Interplay of natural killer cells and their receptors with the adaptive immune response. *Nat Immunol*. 2004;5(10):996-1002. doi:10.1038/ni1114

6. Nabekura T. Immunological memory in natural killer cells. *Int Immunol*. 2025;37(8):435-443. doi:10.1093/intimm/dxaf016

7. Jiang H, Jiang J. Balancing act: the complex role of NK cells in immune regulation. *Front Immunol*. 2023;14:1275028. doi:10.3389/fimmu.2023.1275028

8. Jordan SC. Innate and adaptive immune responses to SARS-CoV-2 in humans: relevance to acquired immunity and vaccine responses. *Clin Exp Immunol*. 2021;204(3):310-320. doi:10.1111/cei.13582

9. Goldman AS, Prabhakar BS. Immunology Overview. In: Baron S, ed. *Medical Microbiology*. 4th ed. University of Texas Medical Branch at Galveston; 1996. Accessed February 15, 2026. http://www.ncbi.nlm.nih.gov/books/NBK7795/

10. Whitmire JK, Eam B, Whitton JL. Tentative T cells: memory cells are quick to respond, but slow to divide. *PLoS Pathog*. 2008;4(4):e1000041. doi:10.1371/journal.ppat.1000041

11. Kaech SM, Cui W. Transcriptional control of effector and memory CD8+ T cell differentiation. *Nat Rev Immunol*. 2012;12(11):749-761. doi:10.1038/nri3307

12. Morandi F, Yazdanifar M, Cocco C, Bertaina A, Airoldi I. Engineering the Bridge between Innate and Adaptive Immunity for Cancer Immunotherapy: Focus on γδ T and NK Cells. *Cells*. 2020;9(8):1757. doi:10.3390/cells9081757

13. Xie G, Dong H, Liang Y, Ham JD, Rizwan R, Chen J. CAR-NK cells: A promising cellular immunotherapy for cancer. *EBioMedicine*. 2020;59:102975. doi:10.1016/j.ebiom.2020.102975

14. Gong JH, Maki G, Klingemann HG. Characterization of a human cell line (NK-92) with phenotypical and functional characteristics of activated natural killer cells. *Leukemia*. 1994;8(4):652-658.

15. Shimasaki N, Jain A, Campana D. NK cells for cancer immunotherapy. *Nat Rev Drug Discov*. 2020;19(3):200-218. doi:10.1038/s41573-019-0052-1

16. Sarvaria A, Jawdat D, Madrigal JA, Saudemont A. Umbilical Cord Blood Natural Killer Cells, Their Characteristics, and Potential Clinical Applications. *Front Immunol*. 2017;8:329. doi:10.3389/fimmu.2017.00329

17. Spanholtz J, Preijers F, Tordoir M, et al. Clinical-grade generation of active NK cells from cord blood hematopoietic progenitor cells for immunotherapy using a closed-system culture process. *PloS One*. 2011;6(6):e20740. doi:10.1371/journal.pone.0020740

18. Li Y, Hermanson DL, Moriarity BS, Kaufman DS. Human iPSC-Derived Natural Killer Cells Engineered with Chimeric Antigen Receptors Enhance Anti-tumor Activity. *Cell Stem Cell*. 2018;23(2):181-192.e5. doi:10.1016/j.stem.2018.06.002

19. Pagano D, Badami E, Conaldi PG, et al. Liver Perfusate Natural Killer Cells From Deceased Brain Donors and Association With Acute Cellular Rejection After Liver Transplantation: A Time-to-Rejection Analysis. *Transplantation*. 2019;103(2):371-380. doi:10.1097/TP.0000000000002322

20. Mace EM. Human natural killer cells: Form, function, and development. *J Allergy Clin Immunol*. 2023;151(2):371-385. doi:10.1016/j.jaci.2022.09.022

21. Freud AG, Mundy-Bosse BL, Yu J, Caligiuri MA. The Broad Spectrum of Human Natural Killer Cell Diversity. *Immunity*. 2017;47(5):820-833. doi:10.1016/j.immuni.2017.10.008

22. Del Zotto G, Marcenaro E, Vacca P, et al. Markers and function of human NK cells in normal and pathological conditions. *Cytometry B Clin Cytom*. 2017;92(2):100-114. doi:10.1002/cyto.b.21508

23. Wu Y, Tian Z, Wei H. Developmental and Functional Control of Natural Killer Cells by Cytokines. *Front Immunol*. 2017;8:930. doi:10.3389/fimmu.2017.00930

24. Rebuffet L, Melsen JE, Escalière B, et al. High-dimensional single-cell analysis of human natural killer cell heterogeneity. *Nat Immunol*. 2024;25(8):1474-1488. doi:10.1038/s41590-024-01883-0

25. Melsen JE, Lugthart G, Lankester AC, Schilham MW. Human Circulating and Tissue-Resident CD56(bright) Natural Killer Cell Populations. *Front Immunol*. 2016;7:262. doi:10.3389/fimmu.2016.00262

26. Cichocki F, Grzywacz B, Miller JS. Human NK Cell Development: One Road or Many? *Front Immunol*. 2019;10:2078. doi:10.3389/fimmu.2019.02078

27. Björkström NK, Ljunggren HG, Michaëlsson J. Emerging insights into natural killer cells in human peripheral tissues. *Nat Rev Immunol*. 2016;16(5):310-320. doi:10.1038/nri.2016.34

28. Quatrini L, Della Chiesa M, Sivori S, Mingari MC, Pende D, Moretta L. Human NK cells, their receptors and function. *Eur J Immunol*. 2021;51(7):1566-1579. doi:10.1002/eji.202049028

29. Bald T, Krummel MF, Smyth MJ, Barry KC. The NK cell-cancer cycle: advances and new challenges in NK cell-based immunotherapies. *Nat Immunol*. 2020;21(8):835-847. doi:10.1038/s41590-020-0728-z

30. Perera Molligoda Arachchige AS. Human NK cells: From development to effector functions. *Innate Immun*. 2021;27(3):212-229. doi:10.1177/17534259211001512

31. Sivori S, Vacca P, Del Zotto G, Munari E, Mingari MC, Moretta L. Human NK cells: surface receptors, inhibitory checkpoints, and translational applications. *Cell Mol Immunol*. 2019;16(5):430-441. doi:10.1038/s41423-019-0206-4

32. Schmidt D, Tirapelle MC, Ebrahimabadi S, et al. Engineered CAR-NK Cells for Cancer Immunotherapy: Lentiviral-Based CAR Transduction of NK-92 Cells. *Methods Mol Biol*. 2025;2930:267-275. doi:10.1007/978-1-0716-4558-1_19

33. Poznanski SM, Ashkar AA. What Defines NK Cell Functional Fate: Phenotype or Metabolism? *Front Immunol*. 2019;10:1414. doi:10.3389/fimmu.2019.01414

34. Lunemann S, Langeneckert AE, Martrus G, et al. Human liver-derived CXCR6+ NK cells are predominantly educated through NKG2A and show reduced cytokine production. *J Leukoc Biol*. 2019;105(6):1331-1340. doi:10.1002/JLB.1MA1118-428R

35. Gur C, Doron S, Kfir-Erenfeld S, et al. NKp46-mediated killing of human and mouse hepatic stellate cells attenuates liver fibrosis. *Gut*. 2012;61(6):885-893. doi:10.1136/gutjnl-2011-301400

36. Carreca AP, Gaetani M, Busà R, et al. Galectin-9 and Interferon-Gamma Are Released by Natural Killer Cells upon Activation with Interferon-Alpha and Orchestrate the Suppression of Hepatitis C Virus Infection. *Viruses*. 2022;14(7):1538. doi:10.3390/v14071538

37. Bänfer S, Jacob R. Galectins in Intra- and Extracellular Vesicles. *Biomolecules*. 2020;10(9):1232. doi:10.3390/biom10091232

38. Klibi J, Niki T, Riedel A, et al. Blood diffusion and Th1-suppressive effects of galectin-9-containing exosomes released by Epstein-Barr virus-infected nasopharyngeal carcinoma cells. *Blood*. 2009;113(9):1957-1966. doi:10.1182/blood-2008-02-142596

39. da Silva IP, Gallois A, Jimenez-Baranda S, et al. Reversal of NK-cell exhaustion in advanced melanoma by Tim-3 blockade. *Cancer Immunol Res*. 2014;2(5):410-422. doi:10.1158/2326-6066.CIR-13-0171

40. Motamedi M, Shahbaz S, Fu L, et al. Galectin-9 Expression Defines a Subpopulation of NK Cells with Impaired Cytotoxic Effector Molecules but Enhanced IFN-γ Production, Dichotomous to TIGIT, in HIV-1 Infection. *ImmunoHorizons*. 2019;3(11):531-546. doi:10.4049/immunohorizons.1900087

41. Okoye I, Xu L, Motamedi M, Parashar P, Walker JW, Elahi S. Galectin-9 expression defines exhausted T cells and impaired cytotoxic NK cells in patients with virus-associated solid tumors. *J Immunother Cancer*. 2020;8(2):e001849. doi:10.1136/jitc-2020-001849

42. Busà R, Bulati M, Badami E, et al. Tissue-Resident Innate Immune Cell-Based Therapy: A Cornerstone of Immunotherapy Strategies for Cancer Treatment. *Front Cell Dev Biol*. 2022;10:907572. doi:10.3389/fcell.2022.907572

43. Sun C, Xu J, Huang Q, et al. High NKG2A expression contributes to NK cell exhaustion and predicts a poor prognosis of patients with liver cancer. *Oncoimmunology*. 2017;6(1):e1264562. doi:10.1080/2162402X.2016.1264562

44. André P, Denis C, Soulas C, et al. Anti-NKG2A mAb Is a Checkpoint Inhibitor that Promotes Anti-tumor Immunity by Unleashing Both T and NK Cells. *Cell*. 2018;175(7):1731-1743.e13. doi:10.1016/j.cell.2018.10.014

45. Xie J, Liu M, Li Y, Nie Y, Mi Q, Zhao S. Ovarian tumor-associated microRNA-20a decreases natural killer cell cytotoxicity by downregulating MICA/B expression. *Cell Mol Immunol*. 2014;11(5):495-502. doi:10.1038/cmi.2014.30

46. Coudert JD, Zimmer J, Tomasello E, et al. Altered NKG2D function in NK cells induced by chronic exposure to NKG2D ligand-expressing tumor cells. *Blood*. 2005;106(5):1711-1717. doi:10.1182/blood-2005-03-0918

47. Lee JC, Lee KM, Kim DW, Heo DS. Elevated TGF-beta1 secretion and down-modulation of NKG2D underlies impaired NK cytotoxicity in cancer patients. *J Immunol*. 2004;172(12):7335-7340. doi:10.4049/jimmunol.172.12.7335

48. Mantovani S, Oliviero B, Lombardi A, et al. Deficient Natural Killer Cell NKp30-Mediated Function and Altered NCR3 Splice Variants in Hepatocellular Carcinoma. *Hepatology*. 2019;69(3):1165-1179. doi:10.1002/hep.30235

49. Zecca A, Barili V, Rizzo D, et al. Intratumor Regulatory Noncytotoxic NK Cells in Patients with Hepatocellular Carcinoma. *Cells*. 2021;10(3):614. doi:10.3390/cells10030614

50. Sun H, Liu L, Huang Q, et al. Accumulation of Tumor-Infiltrating CD49a+ NK Cells Correlates with Poor Prognosis for Human Hepatocellular Carcinoma. *Cancer Immunol Res*. 2019;7(9):1535-1546. doi:10.1158/2326-6066.CIR-18-0757

51. Zhang X, Zhu L, Zhang H, Chen S, Xiao Y. CAR-T Cell Therapy in Hematological Malignancies: Current Opportunities and Challenges. *Front Immunol*. 2022;13:927153. doi:10.3389/fimmu.2022.927153

52. Qian J, Liu Y. Recent advances in adoptive cell therapy for cancer immunotherapy. *Front Immunol*. 2025;16:1665488. doi:10.3389/fimmu.2025.1665488

53. Bhaskar ST, Dholaria B, Savani BN, Sengsayadeth S, Oluwole O. Overview of approved CAR-T products and utility in clinical practice. *Clin Hematol Int*. 2024;6(4):93-99. doi:10.46989/001c.124277

54. Cochran HC, Ghobadi KA, Ghobadi A. Chimeric antigen receptor natural killer (CAR-NK) cells: from preclinical promise to clinical reality in cancer immunotherapy. *Immunotherapy*. 2025;17(15):1115-1127. doi:10.1080/1750743X.2025.2582464

55. Li W, Wang X, Zhang X, Aziz AUR, Wang D. CAR-NK Cell Therapy: A Transformative Approach to Overcoming Oncological Challenges. *Biomolecules*. 2024;14(8):1035. doi:10.3390/biom14081035

56. Hu L, Fan C, Bross P, et al. FDA Approval Summary: Lifileucel for Unresectable or Metastatic Melanoma Previously Treated with an Anti-PD-1-Based Immunotherapy. *Clin Cancer Res Off J Am Assoc Cancer Res*. 2025;31(19):4004-4009. doi:10.1158/1078-0432.CCR-25-0880

57. Li Y, Abudureheman A, Xu J. Current progress in neoantigen-based dendritic cell vaccines for solid tumors. *Cancer Biol Med*. 2025;22(10):1143-1157. doi:10.20892/j.issn.2095-3941.2025.0267

58. Baulu E, Gardet C, Chuvin N, Depil S. TCR-engineered T cell therapy in solid tumors: State of the art and perspectives. *Sci Adv*. 2023;9(7):eadf3700. doi:10.1126/sciadv.adf3700

59. Rana S, Thomas L, Kirkham AM, et al. CAR-NK cells to treat patients with cancer: a systematic scoping review of published studies and registered clinical trials. *Cytotherapy*. 2025;27(10):1179-1189. doi:10.1016/j.jcyt.2025.06.006

60. Peng L, Sferruzza G, Yang L, Zhou L, Chen S. CAR-T and CAR-NK as cellular cancer immunotherapy for solid tumors. *Cell Mol Immunol*. 2024;21(10):1089-1108. doi:10.1038/s41423-024-01207-0

61. Zhang G, Bai M, Du H, et al. Current Advances and Challenges in CAR-T Therapy for Hematological and Solid Tumors. *ImmunoTargets Ther*. 2025;14:655-680. doi:10.2147/ITT.S519616

62. Arunachalam AK, Grégoire C, Coutinho de Oliveira B, Melenhorst JJ. Advancing CAR T-cell therapies: Preclinical insights and clinical translation for hematological malignancies. *Blood Rev*. 2024;68:101241. doi:10.1016/j.blre.2024.101241

63. Blüm P, Kayser S. Chimeric Antigen Receptor (CAR) T-Cell Therapy in Hematologic Malignancies: Clinical Implications and Limitations. *Cancers*. 2024;16(8):1599. doi:10.3390/cancers16081599

64. Jing J, Chen Y, Chi E, et al. New power in cancer immunotherapy: the rise of chimeric antigen receptor macrophage (CAR-M). *J Transl Med*. 2025;23(1):1182. doi:10.1186/s12967-025-07115-9

65. Alrehaili M, Couto PS, Khalife R, Rafiq QA. CAR-macrophages in solid tumors: promise, progress, and prospects. *NPJ Precis Oncol*. 2025;9(1):382. doi:10.1038/s41698-025-01170-7

66. Fang X, Yan S, He L, Deng C. CAR-γδ T cells: a new paradigm of programmable innate immune sentinels and their systemic applications in cancer and beyond. *Front Immunol*. 2025;16:1735763. doi:10.3389/fimmu.2025.1735763

67. White LG, Goy HE, Rose AJ, McLellan AD. Controlling Cell Trafficking: Addressing Failures in CAR T and NK Cell Therapy of Solid Tumours. *Cancers*. 2022;14(4):978. doi:10.3390/cancers14040978

68. Lam PY, Omer N, Wong JKM, et al. Enhancement of anti-sarcoma immunity by NK cells engineered with mRNA for expression of a EphA2-targeted CAR. *Clin Transl Med*. 2025;15(1):e70140. doi:10.1002/ctm2.70140

69. Chen Q, Xia M, Tang M, et al. DR5 CAR-NK cells demonstrate superior scalability and potent antitumor activity with favorable safety. *Mol Ther J Am Soc Gene Ther*. 2025;33(12):6063-6081. doi:10.1016/j.ymthe.2025.10.035

70. McErlean EM, McCarthy HO. Non-viral approaches in CAR-NK cell engineering: connecting natural killer cell biology and gene delivery. *J Nanobiotechnology*. 2024;22(1):552. doi:10.1186/s12951-024-02746-4

71. Colamartino ABL, Lemieux W, Bifsha P, et al. Efficient and Robust NK-Cell Transduction With Baboon Envelope Pseudotyped Lentivector. *Front Immunol*. 2019;10:2873. doi:10.3389/fimmu.2019.02873

72. Müller S, Bexte T, Gebel V, et al. High Cytotoxic Efficiency of Lentivirally and Alpharetrovirally Engineered CD19-Specific Chimeric Antigen Receptor Natural Killer Cells Against Acute Lymphoblastic Leukemia. *Front Immunol*. 2019;10:3123. doi:10.3389/fimmu.2019.03123

73. Finton KA, Strong RK. Structural insights into activation of antiviral NK cell responses. *Immunol Rev*. 2012;250(1):239-257. doi:10.1111/j.1600-065X.2012.01168.x

74. Allan DSJ, Chakraborty M, Waller GC, et al. Systematic improvements in lentiviral transduction of primary human natural killer cells undergoing ex vivo expansion. *Mol Ther Methods Clin Dev*. 2021;20:559-571. doi:10.1016/j.omtm.2021.01.008

75. Dan L, Kang-Zheng L. Optimizing viral transduction in immune cell therapy manufacturing: key process design considerations. *J Transl Med*. 2025;23(1):501. doi:10.1186/s12967-025-06524-0

76. Lan YJ, Nguyen QV, Chao TL, Yeh KL, Lin S. A robust platform for BaEVRless-lentiviral synthesis and primary natural killer cell transduction. *bioRxiv*. Preprint posted online April 4, 2024:2024.04.03.587896. doi:10.1101/2024.04.03.587896

77. Farley D, Stockdale S, Moore-Kelly C, Miskin J, Reiser J, Mitrophanous K. Risks of replication-competent retro/lentivirus from associated vector systems: Is it time for a roadmap toward reduced testing? *Mol Ther Methods Clin Dev*. 2025;33(4):101601. doi:10.1016/j.omtm.2025.101601

78. Jo DH, Kaczmarek S, Shin O, et al. Simultaneous engineering of natural killer cells for CAR transgenesis and CRISPR-Cas9 knockout using retroviral particles. *Mol Ther Methods Clin Dev*. 2023;29:173-184. doi:10.1016/j.omtm.2023.03.006

79. Izsvák Z, Hackett PB, Cooper LJN, Ivics Z. Translating Sleeping Beauty transposition into cellular therapies: victories and challenges. *BioEssays News Rev Mol Cell Dev Biol*. 2010;32(9):756-767. doi:10.1002/bies.201000027

80. Bexte T, Botezatu L, Miskey C, et al. Engineering of potent CAR NK cells using non-viral Sleeping Beauty transposition from minimalistic DNA vectors. *Mol Ther J Am Soc Gene Ther*. 2024;32(7):2357-2372. doi:10.1016/j.ymthe.2024.05.022

81. Ye L, Lam SZ, Yang L, et al. AAV-mediated delivery of a Sleeping Beauty transposon and an mRNA-encoded transposase for the engineering of therapeutic immune cells. *Nat Biomed Eng*. 2024;8(2):132-148. doi:10.1038/s41551-023-01058-6

82. Guo C, Ma X, Gao F, Guo Y. Off-target effects in CRISPR/Cas9 gene editing. *Front Bioeng Biotechnol*. 2023;11:1143157. doi:10.3389/fbioe.2023.1143157

83. Shankar K, Zingler-Hoslet I, Tabima DM, et al. Virus-free CRISPR knockin of a chimeric antigen receptor into KLRC1 generates potent GD2-specific natural killer cells. *Mol Ther J Am Soc Gene Ther*. 2025;33(3):1014-1030. doi:10.1016/j.ymthe.2025.01.024

84. Bexte T, Albinger N, Al Ajami A, et al. CRISPR/Cas9 editing of NKG2A improves the efficacy of primary CD33-directed chimeric antigen receptor natural killer cells. *Nat Commun*. 2024;15(1):8439. doi:10.1038/s41467-024-52388-1

85. Jiang N, Yu Y, Wu D, et al. HLA and tumour immunology: immune escape, immunotherapy and immune-related adverse events. *J Cancer Res Clin Oncol*. 2023;149(2):737-747. doi:10.1007/s00432-022-04493-1

86. Wu J, Mishra HK, Walcheck B. Role of ADAM17 as a regulatory checkpoint of CD16A in NK cells and as a potential target for cancer immunotherapy. *J Leukoc Biol*. 2019;105(6):1297-1303. doi:10.1002/JLB.2MR1218-501R

87. Wang M, Krueger JB, Gilkey AK, et al. Precision Enhancement of CAR-NK Cells through Non-Viral Engineering and Highly Multiplexed Base Editing. *BioRxiv Prepr Serv Biol*. Published online March 8, 2024:2024.03.05.582637. doi:10.1101/2024.03.05.582637

88. Felices M, Lenvik AJ, McElmurry R, et al. Continuous treatment with IL-15 exhausts human NK cells via a metabolic defect. *JCI Insight*. 2018;3(3):e96219, 96219. doi:10.1172/jci.insight.96219

89. Zhu H, Blum RH, Bernareggi D, et al. Metabolic Reprograming via Deletion of CISH in Human iPSC-Derived NK Cells Promotes In Vivo Persistence and Enhances Anti-tumor Activity. *Cell Stem Cell*. 2020;27(2):224-237.e6. doi:10.1016/j.stem.2020.05.008

90. Wang B, Bi J. TGF-β-mediated suppression of NK cell function and targeting strategies in tumor immunotherapy. *Crit Rev Oncol Hematol*. 2026;219:105141. doi:10.1016/j.critrevonc.2026.105141

91. Eyquem J, Mansilla-Soto J, Giavridis T, et al. Targeting a CAR to the TRAC locus with CRISPR/Cas9 enhances tumour rejection. *Nature*. 2017;543(7643):113-117. doi:10.1038/nature21405

92. Gargett T, Brown MP. The inducible caspase-9 suicide gene system as a "safety switch" to limit on-target, off-tumor toxicities of chimeric antigen receptor T cells. *Front Pharmacol*. 2014;5:235. doi:10.3389/fphar.2014.00235

93. Di Stasi A, Tey SK, Dotti G, et al. Inducible apoptosis as a safety switch for adoptive cell therapy. *N Engl J Med*. 2011;365(18):1673-1683. doi:10.1056/NEJMoa1106152

94. Oelsner S, Waldmann A, Billmeier A, et al. Genetically engineered CAR NK cells display selective cytotoxicity against FLT3-positive B-ALL and inhibit in vivo leukemia growth. *Int J Cancer*. 2019;145(7):1935-1945. doi:10.1002/ijc.32269

95. Kao RL, Truscott LC, Chiou TT, Tsai W, Wu AM, De Oliveira SN. A Cetuximab-Mediated Suicide System in Chimeric Antigen Receptor-Modified Hematopoietic Stem Cells for Cancer Therapy. *Hum Gene Ther*. 2019;30(4):413-428. doi:10.1089/hum.2018.180

96. Addressing graft-versus-host disease in allogeneic cell-based immunotherapy for cancer | Experimental Hematology & Oncology | Springer Nature Link. Accessed February 11, 2026. https://link.springer.com/article/10.1186/s40164-025-00654-3?utm_source=openai

97. Dos Reis FD, Saidani Y, Martín-Rubio P, Sanz-Pamplona R, Stojanovic A, Correia MP. CAR-NK cells: harnessing the power of natural killers for advanced cancer therapy. *Front Immunol*. 2025;16:1603757. doi:10.3389/fimmu.2025.1603757

98. Marin D, Li Y, Basar R, et al. Safety, efficacy and determinants of response of allogeneic CD19-specific CAR-NK cells in CD19+ B cell tumors: a phase 1/2 trial. *Nat Med*. 2024;30(3):772-784. doi:10.1038/s41591-023-02785-8

99. Vallera DA, Felices M, McElmurry R, et al. IL15 Trispecific Killer Engagers (TriKE) Make Natural Killer Cells Specific to CD33+ Targets While Also Inducing Persistence, In Vivo Expansion, and Enhanced Function. *Clin Cancer Res Off J Am Assoc Cancer Res*. 2016;22(14):3440-3450. doi:10.1158/1078-0432.CCR-15-2710

100. Shapiro RM, Romee R. iPSC-derived CD19 CAR NK cells for relapsed or refractory lymphoma. *Lancet*. 2025;405(10473):98-99. doi:10.1016/S0140-6736(24)02524-8

101. Goodridge JP, Mahmood S, Zhu H, et al. FT596: Translation of First-of-Kind Multi-Antigen Targeted Off-the-Shelf CAR-NK Cell with Engineered Persistence for the Treatment of B Cell Malignancies. *Blood*. 2019;134(Supplement_1):301. doi:10.1182/blood-2019-129319

102. Kong R, Liu B, Wang H, Lu T, Zhou X. CAR-NK cell therapy: latest updates from the 2024 ASH annual meeting. *J Hematol OncolJ Hematol Oncol*. 2025;18(1):22. doi:10.1186/s13045-025-01677-3

103. Development of glypican-3-specific chimeric antigen receptor-modified natural killer cells and optimization as a therapy for hepatocellular carcinoma | Journal of Leukocyte Biology | Oxford Academic. Accessed February 11, 2026. https://academic.oup.com/jleukbio/article-abstract/117/2/qiae144/7699666?redirectedFrom=fulltext&utm_source=openai

104. Li B, Zhu X, Ge J, et al. Intraperitoneal infusion of NKG2D CAR-NK cells induces endogenous CD8+ T cell activation in patients with advanced colorectal cancer. *Mol Ther J Am Soc Gene Ther*. 2025;33(9):4509-4528. doi:10.1016/j.ymthe.2025.05.026

105. https://link.springer.com/article/10.1186/s40164-025-00654-3?utm_source=openai Strassheimer F, Elleringmann P, Ludmirski G, et al. CAR-NK cell therapy combined with checkpoint inhibition induces an NKT cell response in glioblastoma. *Br J Cancer*. 2025;132(9):849-860. doi:10.1038/s41416-025-02977-8

106. Ghobadi A, Bachanova V, Patel K, et al. Induced pluripotent stem-cell-derived CD19-directed chimeric antigen receptor natural killer cells in B-cell lymphoma: a phase 1, first-in-human trial. *The Lancet*. 2025;405(10473):127-136. doi:10.1016/S0140-6736(24)02462-0

107. Frontiers | Genetic Engineering of Natural Killer Cells for Enhanced Antitumor Function. Accessed February 11, 2026. https://www.frontiersin.org/journals/immunology/articles/10.3389/fimmu.2020.607131/full?utm_source=openai

108. Ruella M, Xu J, Barrett DM, et al. Induction of resistance to chimeric antigen receptor T cell therapy by transduction of a single leukemic B cell. *Nat Med*. 2018;24(10):1499-1503. doi:10.1038/s41591-018-0201-9

109. Liu E, Marin D, Banerjee P, et al. Use of CAR-Transduced Natural Killer Cells in CD19-Positive Lymphoid Tumors. *N Engl J Med*. 2020;382(6):545-553. doi:10.1056/NEJMoa1910607

110. Pulè MA, Straathof KC, Dotti G, Heslop HE, Rooney CM, Brenner MK. A chimeric T cell antigen receptor that augments cytokine release and supports clonal expansion of primary human T cells. *Mol Ther J Am Soc Gene Ther*. 2005;12(5):933-941. doi:10.1016/j.ymthe.2005.04.016

111. Kokalaki E, Ma B, Ferrari M, et al. Dual targeting of CD19 and CD22 against B-ALL using a novel high-sensitivity aCD22 CAR. *Mol Ther*. 2023;31(7):2089-2104. doi:10.1016/j.ymthe.2023.03.020

112. Hosseinalizadeh H, Wang LS, Mirzaei H, Amoozgar Z, Tian L, Yu J. Emerging combined CAR-NK cell therapies in cancer treatment: Finding a dancing partner. *Mol Ther J Am Soc Gene Ther*. 2025;33(6):2406-2425. doi:10.1016/j.ymthe.2024.12.057

113. Chen X, Liu W, Wang Y, et al. Synergistic effects of radiotherapy and immunotherapy: improving oncological outcomes. *Front Immunol*. 2026;17. doi:10.3389/fimmu.2026.1771355

114. Xiang H, Chan AG, Ahene A, et al. Preclinical characterization of bemarituzumab, an anti-FGFR2b antibody for the treatment of cancer. *mAbs*. 2021;13(1):1981202. doi:10.1080/19420862.2021.1981202

115. Sabbah M, Jondreville L, Lacan C, et al. CAR-NK Cells: A Chimeric Hope or a Promising Therapy? *Cancers*. 2022;14(15):3839. doi:10.3390/cancers14153839

116. Dixon KJ, Wu J, Walcheck B. Engineering Anti-Tumor Monoclonal Antibodies and Fc Receptors to Enhance ADCC by Human NK Cells. *Cancers*. 2021;13(2):312. doi:10.3390/cancers13020312

117. Fabian KP, Padget MR, Donahue RN, et al. PD-L1 targeting high-affinity NK (t-haNK) cells induce direct antitumor effects and target suppressive MDSC populations. *J Immunother Cancer*. 2020;8(1):e000450. doi:10.1136/jitc-2019-000450

118. Elwood D, Segaran D, Thibault J, et al. Abstract 894: Generation of cytokine-induced memory-like PD-L1 t-haNK (NK-92®) cells. *Cancer Res*. 2025;85(8_Supplement_1):894. doi:10.1158/1538-7445.AM2025-894

119. Gutierrez E, Bigelow M, LaCroix C, et al. An optimized IL-12-Fc expands its therapeutic window, achieving strong activity against mouse tumors at tolerable drug doses. *Med*. 2023;4(5):326-340.e5. doi:10.1016/j.medj.2023.03.007

120. jhollister. ANKTIVA FDA Approval: First-in-Class IL-15 Agonist for NMIBC. ImmunityBio. April 22, 2024. Accessed February 15, 2026. https://immunitybio.com/immunitybio-announces-fda-approval-of-anktiva-first-in-class-il-15-receptor-agonist-for-bcg-unresponsive-non-muscle-invasive-bladder-cancer/

121. NK Cell Therapy Treatment Market Size, Drugs, Companies. Accessed February 15, 2026. https://www.delveinsight.com/report-store/nk-cell-therapy-market

122. Nikkhoi SK, Li G, Eleya S, Yang G, Vandavasi VG, Hatefi A. Bispecific killer cell engager with high affinity and specificity toward CD16a on NK cells for cancer immunotherapy. *Front Immunol*. 2023;13:1039969. doi:10.3389/fimmu.2022.1039969

123. Khoshtinat Nikkhoi S, Yang G, Owji H, et al. Bispecific immune cell engager enhances the anticancer activity of CD16+ NK cells and macrophages in vitro, and eliminates cancer metastasis in NK humanized NOG mice. *J Immunother Cancer*. 2024;12(3):e008295. doi:10.1136/jitc-2023-008295

124. Reusing SB, Vallera DA, Manser AR, et al. CD16xCD33 Bispecific Killer Cell Engager (BiKE) as potential immunotherapeutic in pediatric patients with AML and biphenotypic ALL. *Cancer Immunol Immunother CII*. 2021;70(12):3701-3708. doi:10.1007/s00262-021-03008-0

125. Cheng Y, Zheng X, Wang X, et al. Trispecific killer engager 161519 enhances natural killer cell function and provides anti-tumor activity against CD19-positive cancers. *Cancer Biol Med*. 2020;17(4):1026-1038. doi:10.20892/j.issn.2095-3941.2020.0399

126. Zhu A, Bai Y, Nan Y, Ju D. Natural killer cell engagers: From bi-specific to tri-specific and tetra-specific engagers for enhanced cancer immunotherapy. *Clin Transl Med*. 2024;14(11):e70046. doi:10.1002/ctm2.70046

127. Vallera DA, Oh F, Kodal B, et al. A HER2 Tri-Specific NK Cell Engager Mediates Efficient Targeting of Human Ovarian Cancer. *Cancers*. 2021;13(16):3994. doi:10.3390/cancers13163994

128. Myers JA, Miller JS. Exploring the NK cell platform for cancer immunotherapy. *Nat Rev Clin Oncol*. 2021;18(2):85-100. doi:10.1038/s41571-020-0426-7

129. Klein C, Brinkmann U, Reichert JM, Kontermann RE. The present and future of bispecific antibodies for cancer therapy. *Nat Rev Drug Discov*. 2024;23(4):301-319. doi:10.1038/s41573-024-00896-6

130. van Hall T, André P, Horowitz A, et al. Monalizumab: inhibiting the novel immune checkpoint NKG2A. *J Immunother Cancer*. 2019;7(1):263. doi:10.1186/s40425-019-0761-3

131. Patel SP, Alonso-Gordoa T, Banerjee S, et al. Phase 1/2 study of monalizumab plus durvalumab in patients with advanced solid tumors. *J Immunother Cancer*. 2024;12(2):e007340. doi:10.1136/jitc-2023-007340

132. Monalizumab data from NeoCOAST-2 Phase 2 study in early-stage NSCLC presented at the WCLC 2024 | Innate Pharma. Accessed February 15, 2026. https://www.innate-pharma.com/media/all-press-releases/monalizumab-data-neocoast-2-phase-2-study-early-stage-nsclc-presented-wclc-2024

133. Convergence of evolving artificial intelligence and machine learning techniques in precision oncology | npj Digital Medicine. Accessed February 16, 2026. https://www.nature.com/articles/s41746-025-01471-y

134. Chang TG, Park S, Schäffer AA, Jiang P, Ruppin E. Hallmarks of artificial intelligence contributions to precision oncology. *Nat Cancer*. 2025;6(3):417-431. doi:10.1038/s43018-025-00917-2

135. Bhalla S, Laganà A. Artificial Intelligence for Precision Oncology. *Adv Exp Med Biol*. 2022;1361:249-268. doi:10.1007/978-3-030-91836-1_14

136. Goda RY, Abdel-Aziz AK. Exploiting artificial intelligence in precision oncology: an updated comprehensive review. *J Transl Med*. 2025;23:1397. doi:10.1186/s12967-025-07308-2

137. Cai Z, Poulos RC, Liu J, Zhong Q. Machine learning for multi-omics data integration in cancer. *iScience*. 2022;25(2):103798. doi:10.1016/j.isci.2022.103798

138. Athaya T, Ripan RC, Li X, Hu H. Multimodal deep learning approaches for single-cell multi-omics data integration. *Brief Bioinform*. 2023;24(5):bbad313. doi:10.1093/bib/bbad313

139. Kang CY, Duarte SE, Kim HS, et al. Artificial Intelligence-based Radiomics in the Era of Immuno-oncology. *The Oncologist*. 2022;27(6):e471-e483. doi:10.1093/oncolo/oyac036

140. Naik AW, Kangas JD, Sullivan DP, Murphy RF. Active machine learning-driven experimentation to determine compound effects on protein patterns. *eLife*. 2016;5:e10047. doi:10.7554/eLife.10047

141. Grzesik P, Warth SC. One-Time Optimization of Advanced T Cell Culture Media Using a Machine Learning Pipeline. *Front Bioeng Biotechnol*. 2021;9:614324. doi:10.3389/fbioe.2021.614324

142. Narayanan H, Hinckley JA, Barry R, et al. Accelerating cell culture media development using Bayesian optimization-based iterative experimental design. *Nat Commun*. 2025;16(1):6055. doi:10.1038/s41467-025-61113-5

143. Azuaje F. Computational models for predicting drug responses in cancer research. *Brief Bioinform*. 2017;18(5):820-829. doi:10.1093/bib/bbw065

144. Ogilvie LA, Kovachev A, Wierling C, Lange BMH, Lehrach H. Models of Models: A Translational Route for Cancer Treatment and Drug Development. *Front Oncol*. 2017;7:219. doi:10.3389/fonc.2017.00219

145. Ahmad S, Xing K, Pereira MSF, et al. A framework integrating multiscale in silico modeling and experimental data predicts CAR-NK cell cytotoxicity across target cell types. *Proc Natl Acad Sci U S A*. 2026;123(5):e2500319123. doi:10.1073/pnas.2500319123

146. Chen S, Zhu H, Jounaidi Y. Comprehensive snapshots of natural killer cells functions, signaling, molecular mechanisms and clinical utilization. *Signal Transduct Target Ther*. 2024;9(1):302. doi:10.1038/s41392-024-02005-w

147. Cortés-Ríos J, Magee M, Sher A, Jusko WJ, Desikan R. A Step-by-Step Workflow for Performing In Silico Clinical Trials With Nonlinear Mixed Effects Models. *CPT Pharmacomet Syst Pharmacol*. 2025;14(12):1949-1964. doi:10.1002/psp4.70122

148. Wang B, Chen RQ, Li J, Roy K. Interfacing data science with cell therapy manufacturing: where we are and where we need to be. *Cytotherapy*. 2024;26(9):967-979. doi:10.1016/j.jcyt.2024.03.011

149. Scheller J, Chalaris A, Garbers C, Rose-John S. ADAM17: a molecular switch to control inflammation and tissue regeneration. *Trends Immunol*. 2011;32(8):380-387. doi:10.1016/j.it.2011.05.005

150. Björkström NK, Strunz B, Ljunggren HG. Natural killer cells in antiviral immunity. *Nat Rev Immunol*. 2022;22(2):112-123. doi:10.1038/s41577-021-00558-3

151. Wang K, Xuan Z, Liu X, Zheng M, Yang C, Wang H. Immunomodulatory role of metalloproteinase ADAM17 in tumor development. *Front Immunol*. 2022;13:1059376. doi:10.3389/fimmu.2022.1059376

152. Tsukerman P, Eisenstein EM, Chavkin M, et al. Cytokine secretion and NK cell activity in human ADAM17 deficiency. *Oncotarget*. 2015;6(42):44151-44160. doi:10.18632/oncotarget.6629

153. Menghini R, Fiorentino L, Casagrande V, Lauro R, Federici M. The role of ADAM17 in metabolic inflammation. *Atherosclerosis*. 2013;228(1):12-17. doi:10.1016/j.atherosclerosis.2013.01.024

154. Sisto M, Lisi S. Updates on Inflammatory Molecular Pathways Mediated by ADAM17 in Autoimmunity. *Cells*. 2024;13(24). doi:10.3390/cells13242092

155. de Queiroz TM, Lakkappa N, Lazartigues E. ADAM17-Mediated Shedding of Inflammatory Cytokines in Hypertension. *Front Pharmacol*. 2020;11:1154. doi:10.3389/fphar.2020.01154

156. Lorenzen I, Lokau J, Korpys Y, et al. Control of ADAM17 activity by regulation of its cellular localisation. *Sci Rep*. 2016;6:35067. doi:10.1038/srep35067

157. Lu F, Zhao H, Dai Y, Wang Y, Lee CH, Freeman M. Cryo-EM reveals that iRhom2 restrains ADAM17 protease activity to control the release of growth factor and inflammatory signals. *Mol Cell*. 2024;84(11):2152-2165.e5. doi:10.1016/j.molcel.2024.04.025

158. Maretzky T, McIlwain DR, Issuree PDA, et al. iRhom2 controls the substrate selectivity of stimulated ADAM17-dependent ectodomain shedding. *Proc Natl Acad Sci U S A*. 2013;110(28):11433-11438. doi:10.1073/pnas.1302553110

159. Maciag JJ, Slone CE, Alnajjar HF, et al. Structural insights into the activation and inhibition of the ADAM17-iRhom2 complex. *Proc Natl Acad Sci U S A*. 2025;122(24):e2500732122. doi:10.1073/pnas.2500732122

160. Li X, Maretzky T, Weskamp G, et al. iRhoms 1 and 2 are essential upstream regulators of ADAM17-dependent EGFR signaling. *Proc Natl Acad Sci U S A*. 2015;112(19):6080-6085. doi:10.1073/pnas.1505649112

161. Schumacher N, Rose-John S. ADAM17 orchestrates Interleukin-6, TNFα and EGF-R signaling in inflammation and cancer. *Biochim Biophys Acta Mol Cell Res*. 2022;1869(1):119141. doi:10.1016/j.bbamcr.2021.119141

162. Sun L, Jiao A, Liu H, et al. Targeting a disintegrin and metalloprotease (ADAM) 17-CD122 axis enhances CD8+ T cell effector differentiation and anti-tumor immunity. *Signal Transduct Target Ther*. 2024;9(1):152. doi:10.1038/s41392-024-01873-6

163. Anderko RR, Mailliard RB. Mapping the interplay between NK cells and HIV: therapeutic implications. *J Leukoc Biol*. 2023;113(2):109-138. doi:10.1093/jleuko/qiac007

164. Lajoie L, Congy-Jolivet N, Bolzec A, Thibault G. Gradual Increase of FcγRIIIa/CD16a Expression and Shift toward IFN-γ Secretion during Differentiation of CD56dim Natural Killer Cells. *Front Immunol*. 2017;8:1556. doi:10.3389/fimmu.2017.01556

165. Enhanced IL-15-mediated NK cell activation and proliferation by an ADAM17 function-blocking antibody involves CD16A, CD137, and accessory cells - PMC. Accessed February 16, 2026. https://pmc.ncbi.nlm.nih.gov/articles/PMC11284835/?utm_source=openai

166. Romee R, Foley B, Lenvik T, et al. NK cell CD16 surface expression and function is regulated by a disintegrin and metalloprotease-17 (ADAM17). *Blood*. 2013;121(18):3599-3608. doi:10.1182/blood-2012-04-425397

167. Althoff K, Reddy P, Voltz N, Rose-John S, Müllberg J. Shedding of interleukin-6 receptor and tumor necrosis factor alpha. Contribution of the stalk sequence to the cleavage pattern of transmembrane proteins. *Eur J Biochem*. 2000;267(9):2624-2631. doi:10.1046/j.1432-1327.2000.01278.x

168. Schumacher N, Meyer D, Mauermann A, et al. Shedding of Endogenous Interleukin-6 Receptor (IL-6R) Is Governed by A Disintegrin and Metalloproteinase (ADAM) Proteases while a Full-length IL-6R Isoform

Localizes to Circulating Microvesicles. *J Biol Chem*. 2015;290(43):26059-26071. doi:10.1074/jbc.M115.649509

169. Link MA, Lücke K, Schmid J, et al. The role of ADAM17 in the T-cell response against bacterial pathogens. *PloS One*. 2017;12(9):e0184320. doi:10.1371/journal.pone.0184320

170. Liu L, Tian E, Quan S, et al. ADAM17 as a promising therapeutic target: from structural basis to inhibitor discovery in human diseases. *Front Pharmacol*. 2025;16:1640090. doi:10.3389/fphar.2025.1640090

171. Lajoie L, Congy-Jolivet N, Bolzec A, et al. ADAM17-mediated shedding of FcγRIIIA on human NK cells: identification of the cleavage site and relationship with activation. *J Immunol*. 2014;192(2):741-751. doi:10.4049/jimmunol.1301024

172. Srpan K, Ambrose A, Karampatzakis A, et al. Shedding of CD16 disassembles the NK cell immune synapse and boosts serial engagement of target cells. *J Cell Biol*. 2018;217(9):3267-3283. doi:10.1083/jcb.201712085

173. Banerjee H, Kane LP. Immune regulation by Tim-3. *F1000Research*. 2018;7:316. doi:10.12688/f1000research.13446.1

174. Gleason MK, Lenvik TR, McCullar V, et al. Tim-3 is an inducible human natural killer cell receptor that enhances interferon gamma production in response to galectin-9. *Blood*. 2012;119(13):3064-3072. doi:10.1182/blood-2011-06-360321

175. Yu L, Liu X, Wang X, et al. TIGIT+ TIM-3+ NK cells are correlated with NK cell exhaustion and disease progression in patients with hepatitis B virus-related hepatocellular carcinoma. *Oncoimmunology*. 2021;10(1):1942673. doi:10.1080/2162402X.2021.1942673

176. Möller-Hackbarth K, Dewitz C, Schweigert O, et al. A Disintegrin and Metalloprotease (ADAM) 10 and ADAM17 Are Major Sheddases of T Cell Immunoglobulin and Mucin Domain 3 (Tim-3). *J Biol Chem*. 2013;288(48):34529-34544. doi:10.1074/jbc.M113.488478

177. Sahin U, Weskamp G, Kelly K, et al. Distinct roles for ADAM10 and ADAM17 in ectodomain shedding of six EGFR ligands. *J Cell Biol*. 2004;164(5):769-779. doi:10.1083/jcb.200307137

178. Hojyo S, Uchida M, Tanaka K, et al. How COVID-19 induces cytokine storm with high mortality. *Inflamm Regen*. 2020;40:37. doi:10.1186/s41232-020-00146-3

179. Riethmueller S, Ehlers JC, Lokau J, et al. Cleavage Site Localization Differentially Controls Interleukin-6 Receptor Proteolysis by ADAM10 and ADAM17. *Sci Rep*. 2016;6:25550. doi:10.1038/srep25550

180. Minimal Interleukin 6 (IL-6) Receptor Stalk Composition for IL-6 Receptor Shedding and IL-6 Classic Signaling - PMC. Accessed February 16, 2026. https://pmc.ncbi.nlm.nih.gov/articles/PMC3663500/?utm_source=openai

181. Serum interleukin-6 is an indicator for severity in 901 patients with SARS-CoV-2 infection: a cohort study | Journal of Translational Medicine | Springer Nature Link. Accessed February 16, 2026. https://link.springer.com/article/10.1186/s12967-020-02571-x?utm_source=openai

182. Schumertl T, Lokau J, Garbers C. IL-6 Signaling in Immunopathology: From Basic Biology to Selective Therapeutic Intervention. *ImmunoTargets Ther*. 2025;14:681-695. doi:10.2147/ITT.S485684

183. Apoptosis is a natural stimulus of IL6R shedding and contributes to the proinflammatory trans-signaling function of neutrophils | Blood | American Society of Hematology. Accessed February 16, 2026. https://ashpublications.org/blood/article/110/6/1748/24184/Apoptosis-is-a-natural-stimulus-of-IL6R-shedding?utm_source=openai

184. TNFR2 unlocks a RIPK1 kinase activity-dependent mode of proinflammatory TNFR1 signaling | Cell Death & Disease. Accessed February 16, 2026. https://www.nature.com/articles/s41419-018-0973-3?utm_source=openai

185. Fang M. Natural Killer Cells in Viral Infection: Special Issue Editorial. *Viruses*. 2025;17(3):391. doi:10.3390/v17030391

186. Becker-Pauly C, Rose-John S. TNFα cleavage beyond TACE/ADAM17: matrix metalloproteinase 13 is a potential therapeutic target in sepsis and colitis. *EMBO Mol Med*. 2013;5(7):EMMM201302899. doi:10.1002/emmm.201302899

187. Palacios Y, Ruiz A, Ramón-Luing LA, et al. Severe COVID-19 Patients Show an Increase in Soluble TNFR1 and ADAM17, with a Relationship to Mortality. *Int J Mol Sci*. 2021;22(16):8423. doi:10.3390/ijms22168423

188. Romee R, Lenvik T, Wang Y, Walcheck B, Verneris MR, Miller JS. ADAM17, a Novel Metalloproteinase, Mediates CD16 and CD62L Shedding in Human NK Cells and Modulates IFNγ Responses. *Blood*. 2011;118(21):2184. doi:10.1182/blood.V118.21.2184.2184

189. ADAM17 expression in normal tissues. (A) The summary of ADAM17 mRNA and... ResearchGate. Accessed February 15, 2026. https://www.researchgate.net/figure/ADAM17-expression-in-normal-tissues-A-The-summary-of-ADAM17-mRNA-and-protein_fig2_361060908

190. Khan H, Patel S, Majumdar A. Role of NRF2 and Sirtuin activators in COVID-19. *Clin Immunol Orlando Fla*. 2021;233:108879. doi:10.1016/j.clim.2021.108879

191. Parihar R, Dierksheide J, Hu Y, Carson WE. IL-12 enhances the natural killer cell cytokine response to Ab-coated tumor cells. *J Clin Invest*. 2002;110(7):983-992. doi:10.1172/JCI15950

192. Shoucair PE, Bowman A, DePuyt AE, Bilben HA, Anderko RR, Mailliard RB. ADAM17 regulates NK cell production of IL-10 and drives of NK cell "helper" function through the activation of TNFa 4631. *J Immunol*. 2025;214(Supplement_1):vkaf283.2286. doi:10.1093/jimmun/vkaf283.2286

193. Alomair BM, Al-Kuraishy HM, Al-Gareeb AI, et al. Mixed storm in SARS-CoV-2 infection: A narrative review and new term in the Covid-19 era. *Immun Inflamm Dis*. 2023;11(4):e838. doi:10.1002/iid3.838

194. Cardresearch. *A Multicenter, Prospective, Adaptive, Double-Blind, Randomized, Placebo-Controlled Study to Evaluate the Effect of Fluvoxamine Plus Budesonide, Fluoxetine Plus Budesonide and Spirulin Platensis, in High Risk Patients With Mild COVID-19*. clinicaltrials.gov; 2024. Accessed February 16, 2026. https://clinicaltrials.gov/study/NCT04727424

195. Zanza C, Romenskaya T, Manetti AC, et al. Cytokine Storm in COVID-19: Immunopathogenesis and Therapy. *Medicina (Mex)*. 2022;58(2):144. doi:10.3390/medicina58020144

196. Xu J, Sriramula S, Xia H, et al. Clinical Relevance and Role of Neuronal AT1 Receptors in ADAM17-Mediated ACE2 Shedding in Neurogenic Hypertension. *Circ Res*. 2017;121(1):43-55. doi:10.1161/CIRCRESAHA.116.310509

197. Adamalysins in COVID-19 – Potential mechanisms behind exacerbating the disease - PMC. Accessed February 16, 2026. https://pmc.ncbi.nlm.nih.gov/articles/PMC9010236/?utm_source=openai

198. Iwasaki M, Saito J, Zhao H, Sakamoto A, Hirota K, Ma D. Inflammation Triggered by SARS-CoV-2 and ACE2 Augment Drives Multiple Organ Failure of Severe COVID-19: Molecular Mechanisms and Implications. *Inflammation*. 2021;44(1):13-34. doi:10.1007/s10753-020-01337-3

199. Gómez-Rial J, Currás-Tuala MJ, Rivero-Calle I, et al. Increased Serum Levels of sCD14 and sCD163 Indicate a Preponderant Role for Monocytes in COVID-19 Immunopathology. *Front Immunol*. 2020;11:560381. doi:10.3389/fimmu.2020.560381

200. Zingaropoli MA, Nijhawan P, Carraro A, et al. Increased sCD163 and sCD14 Plasmatic Levels and Depletion of Peripheral Blood Pro-Inflammatory Monocytes, Myeloid and Plasmacytoid Dendritic Cells in Patients With Severe COVID-19 Pneumonia. *Front Immunol*. 2021;12:627548. doi:10.3389/fimmu.2021.627548

201. Guo L, Niu J, Yu H, et al. Modulation of CD163 Expression by Metalloprotease ADAM17 Regulates Porcine Reproductive and Respiratory Syndrome Virus Entry. *J Virol*. 2014;88(18):10448-10458. doi:10.1128/JVI.01117-14

202. Wang K, Deng H, Song B, et al. The Correlation Between Immune Invasion and SARS-COV-2 Entry Protein ADAM17 in Cancer Patients by Bioinformatic Analysis. *Front Immunol*. 2022;13:923516. doi:10.3389/fimmu.2022.923516

203. Sun J, Edsfeldt A, Svensson J, Ruge T, Goncalves I, Swärd P. ADAM-17 Activity and Its Relation to ACE2: Implications for Severe COVID-19. *Int J Mol Sci*. 2024;25(11):5911. doi:10.3390/ijms25115911

204. Xu J, Xu X, Jiang L, Dua K, Hansbro PM, Liu G. SARS-CoV-2 induces transcriptional signatures in human lung epithelial cells that promote lung fibrosis. *Respir Res*. 2020;21:182. doi:10.1186/s12931-020-01445-6

205. Ozgun O, Ozturk SD, Vural C, et al. Exploring the association of ADAM17 expression with survival in patients with non-small cell lung cancer. *J Investig Med Off Publ Am Fed Clin Res*. 2024;72(8):848-856. doi:10.1177/10815589241270543

206. Rubina A, Patel M, Nightingale K, et al. ADAM17 targeting by human cytomegalovirus remodels the cell surface proteome to simultaneously regulate multiple immune pathways. *Proc Natl Acad Sci U S A*. 2023;120(33):e2303155120. doi:10.1073/pnas.2303155120

207. Geary CD, Sun JC. Memory responses of natural killer cells. *Semin Immunol*. 2017;31:11-19. doi:10.1016/j.smim.2017.08.012

208. JCI Insight - Glycolytic requirement for NK cell cytotoxicity and cytomegalovirus control. Accessed February 16, 2026. https://insight.jci.org/articles/view/95128?utm_source=openai

209. JCI - Chronic stimulation drives human NK cell dysfunction and epigenetic reprograming. Accessed February 16, 2026. https://www.jci.org/articles/view/125916?utm_source=openai

210. Rölle A, Pollmann J, Ewen EM, et al. IL-12–producing monocytes and HLA-E control HCMV-driven NKG2C^{+} NK cell expansion. *J Clin Invest*. 2014;124(12):5305-5316. doi:10.1172/JCI77440

211. Desimio MG, Covino DA, Cancrini C, Doria M. Entry into the lytic cycle exposes EBV-infected cells to NK cell killing via upregulation of the MICB ligand for NKG2D and activation of the CD56bright and NKG2A+KIR+CD56dim subsets. *Front Immunol*. 2024;15:1467304. doi:10.3389/fimmu.2024.1467304

212. Dunn LEM, Lu F, Su C, Lieberman PM, Baines JD. Reactivation of Epstein-Barr Virus from Latency Involves Increased RNA Polymerase Activity at CTCF Binding Sites on the Viral Genome. *J Virol*. 2023;97(2):e0189422. doi:10.1128/jvi.01894-22

213. Chijioke O, Landtwing V, Münz C. NK Cell Influence on the Outcome of Primary Epstein–Barr Virus Infection. *Front Immunol*. 2016;7:323. doi:10.3389/fimmu.2016.00323

214. Png YT, Yang AZY, Lee MY, Chua MJM, Lim CM. The Role of NK Cells in EBV Infection and EBV-Associated NPC. *Viruses*. 2021;13(2):300. doi:10.3390/v13020300

215. Della Chiesa M, De Maria A, Muccio L, Bozzano F, Sivori S, Moretta L. Human NK Cells and Herpesviruses: Mechanisms of Recognition, Response and Adaptation. *Front Microbiol*. 2019;10. doi:10.3389/fmicb.2019.02297

216. Williams LR, Quinn LL, Rowe M, Zuo J. Induction of the Lytic Cycle Sensitizes Epstein-Barr Virus-Infected B Cells to NK Cell Killing That Is Counteracted by Virus-Mediated NK Cell Evasion Mechanisms in the Late Lytic Cycle. *J Virol*. 2015;90(2):947-958. doi:10.1128/JVI.01932-15

217. Sausen DG, Poirier MC, Spiers LM, Smith EN. Mechanisms of T cell evasion by Epstein-Barr virus and implications for tumor survival. *Front Immunol*. 2023;14:1289313. doi:10.3389/fimmu.2023.1289313

218. Romee R, Foley B, Lenvik T, et al. NK cell CD16 surface expression and function is regulated by a disintegrin and metalloprotease-17 (ADAM17). *Blood*. 2013;121(18):3599-3608. doi:10.1182/blood-2012-04-425397

219. Shin HJ, DeCotiis J, Giron M, Palmeri D, Lukac DM. Histone deacetylase classes I and II regulate Kaposi's sarcoma-associated herpesvirus reactivation. *J Virol*. 2014;88(2):1281-1292. doi:10.1128/JVI.02665-13

220. Zhang X, Wang JF, Kunos G, Groopman JE. Cannabinoid modulation of Kaposi's sarcoma-associated herpesvirus infection and transformation. *Cancer Res*. 2007;67(15):7230-7237. doi:10.1158/0008-5472.CAN-07-0960

221. Down-regulation of NKG2D and NKp80 ligands by Kaposi's sarcoma-associated herpesvirus K5 protects against NK cell cytotoxicity - PMC. Accessed February 16, 2026. https://pmc.ncbi.nlm.nih.gov/articles/PMC2234200/?utm_source=openai

222. Human Herpesviridae Methods of Natural Killer Cell Evasion - PMC. Accessed February 16, 2026. https://pmc.ncbi.nlm.nih.gov/articles/PMC3399383/?utm_source=openai

223. Busà R, Timoneri F, Miele M, et al. Immune profiling in solid organ transplant recipients with HHV-8 infection: Identification of immunological biomarkers for KICS and Kaposi's sarcoma. *Clin Immunol*. 2025;280:110562. doi:10.1016/j.clim.2025.110562

224. Le-Trilling VTK, Maaßen F, Katschinski B, Hengel H, Trilling M. Deletion of the non-adjacent genes UL148 and UL148D impairs human cytomegalovirus-mediated TNF receptor 2 surface upregulation. *Front Immunol*. 2023;14:1170300. doi:10.3389/fimmu.2023.1170300

225. Rubina A, Patel M, Nightingale K, et al. ADAM17 targeting by human cytomegalovirus remodels the cell surface proteome to simultaneously regulate multiple immune pathways. *Proc Natl Acad Sci U S A*. 120(33):e2303155120. doi:10.1073/pnas.2303155120

226. The iRhom homology domain is indispensable for ADAM17-mediated TNFα and EGF receptor ligand release - PMC. Accessed February 16, 2026. https://pmc.ncbi.nlm.nih.gov/articles/PMC8233286/?utm_source=openai

227. Cavadas M, Oikonomidi I, Gaspar CJ, et al. Phosphorylation of iRhom2 Controls Stimulated Proteolytic Shedding by the Metalloprotease ADAM17/TACE. *Cell Rep*. 2017;21(3):745-757. doi:10.1016/j.celrep.2017.09.074

228. Hepatitis C viral infection is associated with activated cytolytic natural killer cells expressing high levels of T cell immunoglobulin- and mucin-domain-containing molecule-3. - ScienceDirect. Accessed February 16, 2026. https://www.sciencedirect.com/science/article/abs/pii/S1521661615000984?utm_source=openai

229. Role of Tim-3 in hepatitis B virus infection: An overview - PMC. Accessed February 16, 2026. https://pmc.ncbi.nlm.nih.gov/articles/PMC4735003/?utm_source=openai

230. Wijaya RS, Read SA, Schibeci S, et al. Expansion of dysfunctional CD56-CD16+ NK cells in chronic hepatitis B patients. *Liver Int Off J Int Assoc Study Liver*. 2021;41(5):969-981. doi:10.1111/liv.14784

231. Badami E. NK-Mediated Immunotherapy and Uses Thereof. Published online June 7, 2018:2018/099988.

232. Jonsson JR, Hogan PG, Balderson GA, et al. Human liver transplant perfusate: an abundant source of donor liver-associated leukocytes. *Hepatology*. 1997;26(5):1111-1114. doi:10.1002/hep.510260504

233. Busà R, Iannolo G, Douradinha B, et al. Glypican-3-Specific CAR NK Cells Co-Secreting IL-15 and IFN-α Have Increased Anti-Tumor Function Versus Hepatocellular Carcinoma In Vitro. *Int J Mol Sci*. 2025;26(24):11892. doi:10.3390/ijms262411892

234. De Rham C, Ferrari-Lacraz S, Jendly S, Schneiter G, Dayer JM, Villard J. The proinflammatory cytokines IL-2, IL-15 and IL-21 modulate the repertoire of mature human natural killer cell receptors. *Arthritis Res Ther*. 2007;9(6):R125. doi:10.1186/ar2336

235. Wagner J, Pfannenstiel V, Waldmann A, et al. A Two-Phase Expansion Protocol Combining Interleukin (IL)-15 and IL-21 Improves Natural Killer Cell Proliferation and Cytotoxicity against Rhabdomyosarcoma. *Front Immunol*. 2017;8:676. doi:10.3389/fimmu.2017.00676

236. Mishra HK, Dixon KJ, Pore N, Felices M, Miller JS, Walcheck B. Activation of ADAM17 by IL-15 Limits Human NK Cell Proliferation. *Front Immunol*. 2021;12:711621. doi:10.3389/fimmu.2021.711621

237. Poli A, Michel T, Thérésine M, Andrès E, Hentges F, Zimmer J. CD56bright natural killer (NK) cells: an important NK cell subset. *Immunology*. 2009;126(4):458-465. doi:10.1111/j.1365-2567.2008.03027.x

239. Lopez-Vergès S, Milush JM, Pandey S, et al. CD57 defines a functionally distinct population of mature NK cells in the human CD56dimCD16+ NK-cell subset. *Blood*. 2010;116(19):3865-3874. doi:10.1182/blood-2010-04-282301

240. Nielsen N, Ødum N, Ursø B, Lanier LL, Spee P. Cytotoxicity of CD56(bright) NK cells towards autologous activated CD4+ T cells is mediated through NKG2D, LFA-1 and TRAIL and dampened via CD94/NKG2A. *PloS One*. 2012;7(2):e31959. doi:10.1371/journal.pone.0031959

241. Etxeberria I, Glez-Vaz J, Teijeira Á, Melero I. New emerging targets in cancer immunotherapy: CD137/4-1BB costimulatory axis. *ESMO Open*. 2020;4(Suppl 3):e000733. doi:10.1136/esmoopen-2020-000733

242. Sanchez-Paulete AR, Labiano S, Rodriguez-Ruiz ME, et al. Deciphering CD137 (4-1BB) signaling in T-cell costimulation for translation into successful cancer immunotherapy. *Eur J Immunol*. 2016;46(3):513-522. doi:10.1002/eji.201445388

243. Matson AW, Hullsiek RH, Dixon KJ, et al. Enhanced IL-15-mediated NK cell activation and proliferation by an ADAM17 function-blocking antibody involves CD16A, CD137, and accessory cells. *BioRxiv Prepr Serv Biol*. Published online May 14, 2024:2024.05.09.593347. doi:10.1101/2024.05.09.593347

244. Quatrini L, Molfetta R, Zitti B, et al. Ubiquitin-dependent endocytosis of NKG2D-DAP10 receptor complexes activates signaling and functions in human NK cells. *Sci Signal*. 2015;8(400):ra108. doi:10.1126/scisignal.aab2724

245. Gallois A, Silva I, Osman I, Bhardwaj N. Reversal of natural killer cell exhaustion by TIM-3 blockade. *Oncoimmunology*. 2014;3(12):e946365. doi:10.4161/21624011.2014.946365

246. Dao TN, Utturkar S, Atallah Lanman N, Matosevic S. TIM-3 Expression Is Downregulated on Human NK Cells in Response to Cancer Targets in Synergy with Activation. *Cancers*. 2020;12(9):2417. doi:10.3390/cancers12092417

247. Liang S, Wei H, Sun R, Tian Z. IFNα regulates NK cell cytotoxicity through STAT1 pathway. *Cytokine*. 2003;23(6):190-199. doi:10.1016/S1043-4666(03)00226-6

248. Barnes SA, Audsley KM, Newnes HV, et al. Type I interferon subtypes differentially activate the anti-leukaemic function of natural killer cells. *Front Immunol*. 2022;13:1050718. doi:10.3389/fimmu.2022.1050718

249. Platanias LC. Mechanisms of type-I- and type-II-interferon-mediated signalling. *Nat Rev Immunol*. 2005;5(5):375-386. doi:10.1038/nri1604

250. Nguyen KB, Salazar-Mather TP, Dalod MY, et al. Coordinated and distinct roles for IFN-alpha beta, IL-12, and IL-15 regulation of NK cell responses to viral infection. *J Immunol*. 2002;169(8):4279-4287. doi:10.4049/jimmunol.169.8.4279

251. Oh JH, Kim MJ, Choi SJ, et al. Sustained Type I Interferon Reinforces NK Cell-Mediated Cancer Immunosurveillance during Chronic Virus Infection. *Cancer Immunol Res*. 2019;7(4):584-599. doi:10.1158/2326-6066.CIR-18-0403

252. Poznanski SM, Lee AJ, Nham T, et al. Combined Stimulation with Interleukin-18 and Interleukin-12 Potently Induces Interleukin-8 Production by Natural Killer Cells. *J Innate Immun*. 2017;9(5):511-525. doi:10.1159/000477172

253. Lusty E, Poznanski SM, Kwofie K, et al. IL-18/IL-15/IL-12 synergy induces elevated and prolonged IFN-γ production by ex vivo expanded NK cells which is not due to enhanced STAT4 activation. *Mol Immunol*. 2017;88:138-147. doi:10.1016/j.molimm.2017.06.025

254. Vivier E, Raulet DH, Moretta A, et al. Innate or adaptive immunity? The example of natural killer cells. *Science*. 2011;331(6013):44-49. doi:10.1126/science.1198687

255. Bhat R, Watzl C. Serial killing of tumor cells by human natural killer cells--enhancement by therapeutic antibodies. *PloS One*. 2007;2(3):e326. doi:10.1371/journal.pone.0000326

256. Prager I, Liesche C, van Ooijen H, et al. NK cells switch from granzyme B to death receptor-mediated cytotoxicity during serial killing. *J Exp Med*. 2019;216(9):2113-2127. doi:10.1084/jem.20181454

257. Lasfar A, de laTorre A, Abushahba W, et al. Concerted action of IFN-α and IFN-λ induces local NK cell immunity and halts cancer growth. *Oncotarget*. 2016;7(31):49259-49267. doi:10.18632/oncotarget.10272

258. Sun C, Sun H yu, Xiao W hua, Zhang C, Tian Z gang. Natural killer cell dysfunction in hepatocellular carcinoma and NK cell-based immunotherapy. *Acta Pharmacol Sin*. 2015;36(10):1191-1199. doi:10.1038/aps.2015.41

259. Sajid M, Liu L, Sun C. The Dynamic Role of NK Cells in Liver Cancers: Role in HCC and HBV Associated HCC and Its Therapeutic Implications. *Front Immunol*. 2022;13:887186. doi:10.3389/fimmu.2022.887186

260. Smyth MJ, Cretney E, Takeda K, et al. Tumor necrosis factor-related apoptosis-inducing ligand (TRAIL) contributes to interferon gamma-dependent natural killer cell protection from tumor metastasis. *J Exp Med*. 2001;193(6):661-670. doi:10.1084/jem.193.6.661

261. Sato K, Hida S, Takayanagi H, et al. Antiviral response by natural killer cells through TRAIL gene induction by IFN-alpha/beta. *Eur J Immunol*. 2001;31(11):3138-3146. doi:10.1002/1521-4141(200111)31:11<3138::aid-immu3138>3.0.co;2-b

262. Cardoso Alves L, Berger MD, Koutsandreas T, et al. Non-apoptotic TRAIL function modulates NK cell activity during viral infection. *EMBO Rep*. 2020;21(1):e48789. doi:10.15252/embr.201948789

263. Galle PR, Foerster F, Kudo M, et al. Biology and significance of alpha-fetoprotein in hepatocellular carcinoma. *Liver Int Off J Int Assoc Study Liver*. 2019;39(12):2214-2229. doi:10.1111/liv.14223

264. Rusie D, Mercan Stanciu A, Toma L, Iliescu EL. Correlation Between Serum Alpha-Fetoprotein and Tumour Size in Patients With Hepatocellular Carcinoma Treated With Direct-Acting Antivirals. *Cureus*. 2022;14(4):e24506. doi:10.7759/cureus.24506

265. Kärre K, Ljunggren HG, Piontek G, Kiessling R. Selective rejection of H-2-deficient lymphoma variants suggests alternative immune defence strategy. *Nature*. 1986;319(6055):675-678. doi:10.1038/319675a0

266. Vivier E, Artis D, Colonna M, et al. Innate Lymphoid Cells: 10 Years On. *Cell*. 2018;174(5):1054-1066. doi:10.1016/j.cell.2018.07.017

267. Waldhauer I, Steinle A. NK cells and cancer immunosurveillance. *Oncogene*. 2008;27(45):5932-5943. doi:10.1038/onc.2008.267

268. Ito M, Hiramatsu H, Kobayashi K, et al. NOD/SCID/gamma(c)(null) mouse: an excellent recipient mouse model for engraftment of human cells. *Blood*. 2002;100(9):3175-3182. doi:10.1182/blood-2001-12-0207

269. Müller L, Aigner P, Stoiber D. Type I Interferons and Natural Killer Cell Regulation in Cancer. *Front Immunol*. 2017;8:304. doi:10.3389/fimmu.2017.00304

270. Yu R, Zhu B, Chen D. Type I interferon-mediated tumor immunity and its role in immunotherapy. *Cell Mol Life Sci CMLS*. 2022;79(3):191. doi:10.1007/s00018-022-04219-z

271. Ramasawmy R, Johnson SP, Roberts TA, et al. Monitoring the Growth of an Orthotopic Tumour Xenograft Model: Multi-Modal Imaging Assessment with Benchtop MRI (1T), High-Field MRI (9.4T), Ultrasound and Bioluminescence. *PLoS ONE*. 2016;11(5):e0156162. doi:10.1371/journal.pone.0156162

272. Lee TK, Na KS, Kim J, Jeong HJ. Establishment of animal models with orthotopic hepatocellular carcinoma. *Nucl Med Mol Imaging*. 2014;48(3):173-179. doi:10.1007/s13139-014-0288-y

273. Rozemuller H, van der Spek E, Bogers-Boer LH, et al. A bioluminescence imaging based in vivo model for preclinical testing of novel cellular immunotherapy strategies to improve the graft-versus-myeloma effect. *Haematologica*. 2008;93(7):1049-1057. doi:10.3324/haematol.12349

274. Lu Y, Lin B, Li M. The role of alpha-fetoprotein in the tumor microenvironment of hepatocellular carcinoma. *Front Oncol*. 2024;14:1363695. doi:10.3389/fonc.2024.1363695

275. Poznanski SM, Singh K, Ritchie TM, et al. Metabolic flexibility determines human NK cell functional fate in the tumor microenvironment. *Cell Metab*. 2021;33(6):1205-1220.e5. doi:10.1016/j.cmet.2021.03.023

276. Kennedy PR, Arvindam US, Phung SK, et al. Metabolic programs drive function of therapeutic NK cells in hypoxic tumor environments. *Sci Adv*. 2024;10(44):eadn1849. doi:10.1126/sciadv.adn1849

277. Christodoulou I, Ho WJ, Marple A, et al. Engineering CAR-NK cells to secrete IL-15 sustains their anti-AML functionality but is associated with systemic toxicities. *J Immunother Cancer*. 2021;9(12):e003894. doi:10.1136/jitc-2021-003894

278. Baughan SL, Folsom T, Johnson M, Kreuger J, Webber BR, Moriarity BS. Perspective: IL-15 cytokine-armored NK cells as ready-to-use immunotherapy for diverse malignancies: therapeutic potential and toxicity risks. *Front Immunol*. 16:1704404. doi:10.3389/fimmu.2025.1704404

279. Feng D, Sun L, Hu D, et al. Expression of membrane-bound Interleukin-15 sustains the growth and survival of CAR-NK cells. *Int Immunopharmacol*. 2025;166:115577. doi:10.1016/j.intimp.2025.115577

280. Silvestre RN, Eitler J, de Azevedo JTC, et al. Engineering NK-CAR.19 cells with the IL-15/IL-15Rα complex improved proliferation and anti-tumor effect in vivo. *Front Immunol*. 2023;14:1226518. doi:10.3389/fimmu.2023.1226518

281. Marçais A, Cherfils-Vicini J, Viant C, et al. The metabolic checkpoint kinase mTOR is essential for IL-15 signaling during the development and activation of NK cells. *Nat Immunol*. 2014;15(8):749-757. doi:10.1038/ni.2936

282. Mazewski C, Perez RE, Fish EN, Platanias LC. Type I Interferon (IFN)-Regulated Activation of Canonical and Non-Canonical Signaling Pathways. *Front Immunol*. 2020;11:606456. doi:10.3389/fimmu.2020.606456

283. Ma H, Yang W, Zhang L, et al. Interferon-alpha promotes immunosuppression through IFNAR1/STAT1 signalling in head and neck squamous cell carcinoma. *Br J Cancer*. 2019;120(3):317-330. doi:10.1038/s41416-018-0352-y

284. Holicek P, Guilbaud E, Klapp V, et al. Type I interferon and cancer. *Immunol Rev*. 2024;321(1):115-127. doi:10.1111/imr.13272

285. Ruppel KE, Fricke S, Köhl U, Schmiedel D. Taking Lessons from CAR-T Cells and Going Beyond: Tailoring Design and Signaling for CAR-NK Cells in Cancer Therapy. *Front Immunol*. 2022;13:822298. doi:10.3389/fimmu.2022.822298

286. Chalaris A, Gewiese J, Paliga K, et al. ADAM17-mediated shedding of the IL6R induces cleavage of the membrane stub by gamma-secretase. *Biochim Biophys Acta*. 2010;1803(2):234-245. doi:10.1016/j.bbamcr.2009.12.001

287. Briso EM, Dienz O, Rincon M. Cutting edge: soluble IL-6R is produced by IL-6R ectodomain shedding in activated CD4 T cells. *J Immunol*. 2008;180(11):7102-7106. doi:10.4049/jimmunol.180.11.7102

288. Lee HR, Brulois K, Wong L, Jung JU. Modulation of Immune System by Kaposi's Sarcoma-Associated Herpesvirus: Lessons from Viral Evasion Strategies. *Front Microbiol*. 2012;3:44. doi:10.3389/fmicb.2012.00044

289. Yang S, Liu F, Wang QJ, Rosenberg SA, Morgan RA. The shedding of CD62L (L-selectin) regulates the acquisition of lytic activity in human tumor reactive T lymphocytes. *PloS One*. 2011;6(7):e22560. doi:10.1371/journal.pone.0022560

290. Bell JH, Herrera AH, Li Y, Walcheck B. Role of ADAM17 in the ectodomain shedding of TNF-alpha and its receptors by neutrophils and macrophages. *J Leukoc Biol*. 2007;82(1):173-176. doi:10.1189/jlb.0307193

291. Wong JP, Damania B. Modulation of oncogenic signaling networks by Kaposi's sarcoma-associated herpesvirus. *Biol Chem*. 2017;398(8):911-918. doi:10.1515/hsz-2017-0101

292. Sugawara S, Hueber B, Woolley G, et al. Multiplex interrogation of the NK cell signalome reveals global downregulation of CD16 signaling during lentivirus infection through an IL-18/ADAM17-dependent mechanism. *PLoS Pathog*. 2023;19(9):e1011629. doi:10.1371/journal.ppat.1011629

293. Lenart M, Kluczewska A, Szaflarska A, et al. Selective downregulation of natural killer activating receptors on NK cells and upregulation of PD-1 expression on T cells in children with severe and/or recurrent Herpes simplex virus infections. *Immunobiology*. 2021;226(3):152097. doi:10.1016/j.imbio.2021.152097

294. Veenhuis RT, Astemborski J, Chattergoon MA, et al. Systemic Elevation of Proinflammatory Interleukin-18 in Human Immunodeficiency Virus (HIV)/Hepatitis C Virus (HCV) Coinfection Versus HIV or HCV Monoinfection. *Clin Infect Dis Off Publ Infect Dis Soc Am*. 2017;64(5):589-596. doi:10.1093/cid/ciw771

295. Romee R, Schneider SE, Leong JW, et al. Cytokine activation induces human memory-like NK cells. *Blood*. 2012;120(24):4751-4760. doi:10.1182/blood-2012-04-419283

296. Razonable RR. Human herpesviruses 6, 7 and 8 in solid organ transplant recipients. *Am J Transplant Off J Am Soc Transplant Am Soc Transpl Surg*. 2013;13 Suppl 3:67-77; quiz 77-78. doi:10.1111/ajt.12008

297. Letafati A, Ardekani OS, Naderisemiromi M, et al. Unraveling the dynamic mechanisms of natural killer cells in viral infections: insights and implications. *Virol J*. 2024;21(1):18. doi:10.1186/s12985-024-02287-0

298. Künzel U, Grieve AG, Meng Y, Sieber B, Cowley SA, Freeman M. FRMD8 promotes inflammatory and growth factor signalling by stabilising the iRhom/ADAM17 sheddase complex. *eLife*. 2018;7:e35012. doi:10.7554/eLife.35012

299. Ishido S, Wang C, Lee BS, Cohen GB, Jung JU. Downregulation of major histocompatibility complex class I molecules by Kaposi's sarcoma-associated herpesvirus K3 and K5 proteins. *J Virol*. 2000;74(11):5300-5309. doi:10.1128/jvi.74.11.5300-5309.2000

300. Coscoy L, Ganem D. A viral protein that selectively downregulates ICAM-1 and B7-2 and modulates T cell costimulation. *J Clin Invest*. 2001;107(12):1599-1606. doi:10.1172/JCI12432

301. Ishido S, Choi JK, Lee BS, et al. Inhibition of natural killer cell-mediated cytotoxicity by Kaposi's sarcoma-associated herpesvirus K5 protein. *Immunity*. 2000;13(3):365-374. doi:10.1016/s1074-7613(00)00036-4

302. Thomas M, Boname JM, Field S, et al. Down-regulation of NKG2D and NKp80 ligands by Kaposi's sarcoma-associated herpesvirus K5 protects against NK cell cytotoxicity. *Proc Natl Acad Sci U S A*. 2008;105(5):1656-1661. doi:10.1073/pnas.0707883105

303. Kared H, Martelli S, Tan SW, et al. Adaptive NKG2C+CD57+ Natural Killer Cell and Tim-3 Expression During Viral Infections. *Front Immunol*. 2018;9:686. doi:10.3389/fimmu.2018.00686

304. Hassen K, Martelli S, Ng T, Pender S, Larbi A. CD57 in human natural killer cells and T-lymphocytes. *Cancer Immunol Immunother*. 2016;65. doi:10.1007/s00262-016-1803-z

305. Al-Salihi MA, Lang PA. iRhom2: An Emerging Adaptor Regulating Immunity and Disease. *Int J Mol Sci*. 2020;21(18):6570. doi:10.3390/ijms21186570

306. Dupuy S, Lambert M, Zucman D, et al. Human Herpesvirus 8 (HHV8) sequentially shapes the NK cell repertoire during the course of asymptomatic infection and Kaposi sarcoma. *PLoS Pathog*. 2012;8(1):e1002486. doi:10.1371/journal.ppat.1002486

307. Atamna A, Yahav D, Hirzel C. Prevention of Oncogenic Gammaherpesvirinae (EBV and HHV8) Associated Disease in Solid Organ Transplant Recipients. *Transpl Int Off J Eur Soc Organ Transplant*. 2023;36:11856. doi:10.3389/ti.2023.11856

308. Damani-Yokota P, Khanna KM. Innate immune memory: The evolving role of macrophages in therapy. *eLife*. 2025;14:e108276. doi:10.7554/eLife.108276

309. Uyangaa E, Choi JY, Park SO, et al. TLR3/TRIF pathway confers protection against herpes simplex encephalitis through NK cell activation mediated by a loop of type I IFN and IL-15 from epithelial and dendritic cells. *Immunology*. 2023;170(1):83-104. doi:10.1111/imm.13664

310. McNab F, Mayer-Barber K, Sher A, Wack A, O'Garra A. Type I interferons in infectious disease. *Nat Rev Immunol*. 2015;15(2):87-103. doi:10.1038/nri3787

311. O'Connor CM, Sen GC. Innate Immune Responses to Herpesvirus Infection. *Cells*. 2021;10(8):2122. doi:10.3390/cells10082122

312. Xu Y, Lee MKS, de Weerd NA, et al. Type I interferon signaling controls the early hematopoietic expansion in response to β-glucan. *iScience*. 2025;28(5):112347. doi:10.1016/j.isci.2025.112347

313. Chiba Y, Mizoguchi I, Hasegawa H, et al. Regulation of myelopoiesis by proinflammatory cytokines in infectious diseases. *Cell Mol Life Sci CMLS*. 2018;75(8):1363-1376. doi:10.1007/s00018-017-2724-5

314. Buechler MB, Teal TH, Elkon KB, Hamerman JA. Type I IFN drives emergency myelopoiesis and peripheral myeloid expansion during chronic Toll-like receptor 7 signaling. *J Immunol Baltim Md 1950*. 2013;190(3):886-891. doi:10.4049/jimmunol.1202739

315. Nicholas J, Ruvolo VR, Burns WH, et al. Kaposi's sarcoma-associated human herpesvirus-8 encodes homologues of macrophage inflammatory protein-1 and interleukin-6. *Nat Med*. 1997;3(3):287-292. doi:10.1038/nm0397-287

316. Polizzotto MN, Uldrick TS, Wang V, et al. Human and viral interleukin-6 and other cytokines in Kaposi sarcoma herpesvirus-associated multicentric Castleman disease. *Blood*. 2013;122(26):4189-4198. doi:10.1182/blood-2013-08-519959

317. Münz C. Natural killer cell responses to human oncogenic γ-herpesvirus infections. *Semin Immunol*. 2022;60:101652. doi:10.1016/j.smim.2022.101652

318. Liang C, Lee JS, Jung JU. Immune evasion in Kaposi's sarcoma-associated herpes virus associated oncogenesis. *Semin Cancer Biol*. 2008;18(6):423-436. doi:10.1016/j.semcancer.2008.09.003

319. Razonable RR, Humar A. Cytomegalovirus in solid organ transplant recipients-Guidelines of the American Society of Transplantation Infectious Diseases Community of Practice. *Clin Transplant*. 2019;33(9):e13512. doi:10.1111/ctr.13512

320. Giese AA, Babendreyer A, Krappen P, et al. Inflammatory activation of surface molecule shedding by upregulation of the pseudoprotease iRhom2 in colon epithelial cells. *Sci Rep*. 2021;11(1):24230. doi:10.1038/s41598-021-03522-2

321. Naranbhai V, Bartman P, Ndlovu D, et al. Impact of blood processing variations on Natural Killer cell frequency, activation, chemokine receptor expression and function. *J Immunol Methods*. 2011;366(1-2):28-35. doi:10.1016/j.jim.2011.01.001

322. Kutscher S, Dembek CJ, Deckert S, et al. Overnight Resting of PBMC Changes Functional Signatures of Antigen Specific T- Cell Responses: Impact for Immune Monitoring within Clinical Trials. *PLoS ONE*. 2013;8(10):e76215. doi:10.1371/journal.pone.0076215

323. Kallemeijn MJ, Boots AMH, van der Klift MY, et al. Ageing and latent CMV infection impact on maturation, differentiation and exhaustion profiles of T-cell receptor gammadelta T-cells. *Sci Rep*. 2017;7(1):5509. doi:10.1038/s41598-017-05849-1

324. Schönrich G, Raftery MJ. CD1-Restricted T Cells During Persistent Virus Infections: "Sympathy for the Devil." *Front Immunol*. 2018;9:545. doi:10.3389/fimmu.2018.00545

325. Kumar A, Suryadevara N, Hill TM, Bezbradica JS, Van Kaer L, Joyce S. Natural Killer T Cells: An Ecological Evolutionary Developmental Biology Perspective. *Front Immunol*. 2017;8:1858. doi:10.3389/fimmu.2017.01858

326. Cohen NR, Garg S, Brenner MB. Antigen Presentation by CD1 Lipids, T Cells, and NKT Cells in Microbial Immunity. *Adv Immunol*. 2009;102:1-94. doi:10.1016/S0065-2776(09)01201-2

327. Chung BK, Priatel JJ, Tan R. CD1d Expression and Invariant NKT Cell Responses in Herpesvirus Infections. *Front Immunol*. 2015;6:312. doi:10.3389/fimmu.2015.00312

328. Meckiff BJ, Ladell K, McLaren JE, et al. Primary EBV Infection Induces an Acute Wave of Activated Antigen-Specific Cytotoxic CD4+ T Cells. *J Immunol*. 2019;203(5):1276-1287. doi:10.4049/jimmunol.1900377

329. Jackson SE, Noor M, Lim E, Wills M. The immune response to human cytomegalovirus: impact of age, co-morbidities and the significance of anti-viral activity assessment. *Philos Trans R Soc B Biol Sci*. 380(1938):20240408. doi:10.1098/rstb.2024.0408

330. Abel AM, Yang C, Thakar MS, Malarkannan S. Natural Killer Cells: Development, Maturation, and Clinical Utilization. *Front Immunol*. 2018;9:1869. doi:10.3389/fimmu.2018.01869

331. Khan MA, Khan A. Role of NKT Cells during Viral Infection and the Development of NKT Cell-Based Nanovaccines. *Vaccines*. 2021;9(9):949. doi:10.3390/vaccines9090949

332. Lugli E, Marcenaro E, Mavilio D. NK Cell Subset Redistribution during the Course of Viral Infections. *Front Immunol*. 2014;5:390. doi:10.3389/fimmu.2014.00390

333. Tessmer MS, Fatima A, Paget C, Trottein F, Brossay L. NKT cell immune responses to viral infection. *Expert Opin Ther Targets*. 2009;13(2):153-162. doi:10.1517/14712590802653601

334. Durante-Mangoni E, Wang R, Shaulov A, et al. Hepatic CD1d Expression in Hepatitis C Virus Infection and Recognition by Resident Proinflammatory CD1d-Reactive T Cells1. *J Immunol*. 2004;173(3):2159-2166. doi:10.4049/jimmunol.173.3.2159

335. Leite-de-Moraes MC, Herbelin A, Gouarin C, Koezuka Y, Schneider E, Dy M. Fas/Fas ligand interactions promote activation-induced cell death of NK T lymphocytes. *J Immunol*. 2000;165(8):4367-4371. doi:10.4049/jimmunol.165.8.4367

336. Webster KE, Kim HO, Kyparissoudis K, et al. IL-17-producing NKT cells depend exclusively on IL-7 for homeostasis and survival. *Mucosal Immunol*. 2014;7(5):1058-1067. doi:10.1038/mi.2013.122

337. Schubert K, Collins LE, Green P, Nagase H, Troeberg L. LRP1 Controls TNF Release via the TIMP-3/ADAM17 Axis in Endotoxin-Activated Macrophages. *J Immunol*. 2019;202(5):1501-1509. doi:10.4049/jimmunol.1800834

338. Waller K, James C, de Jong A, et al. ADAM17-Mediated Reduction in CD14++CD16+ Monocytes ex vivo and Reduction in Intermediate Monocytes With Immune Paresis in Acute Pancreatitis and Acute Alcoholic Hepatitis. *Front Immunol*. 2019;10:1902. doi:10.3389/fimmu.2019.01902

339. Ebsen H, Lettau M, Kabelitz D, Janssen O. Subcellular localization and activation of ADAM proteases in the context of FasL shedding in T lymphocytes. *Mol Immunol*. 2015;65(2):416-428. doi:10.1016/j.molimm.2015.02.008

340. Smulski CR, Kury P, Seidel LM, et al. BAFF- and TACI-Dependent Processing of BAFFR by ADAM Proteases Regulates the Survival of B Cells. *Cell Rep*. 2017;18(9):2189-2202. doi:10.1016/j.celrep.2017.02.005

341. Lownik JC, Wimberly JL, Takahashi-Ruiz L, Martin RK. B cell ADAM17 controls T cell independent humoral immune responses through regulation of TACI and CD138. *Biochem Biophys Res Commun*. 2020;522(2):442-447. doi:10.1016/j.bbrc.2019.11.124

342. Mohammed RN, Wehenkel SC, Galkina EV, et al. ADAM17-dependent proteolysis of L-selectin promotes early clonal expansion of cytotoxic T cells. *Sci Rep*. 2019;9(1):5487. doi:10.1038/s41598-019-41811-z

343. Hou W, Gibbs JS, Lu X, et al. Viral infection triggers rapid differentiation of human blood monocytes into dendritic cells. *Blood*. 2012;119(13):3128-3131. doi:10.1182/blood-2011-09-379479

344. Dong MB, Rahman MJ, Tarbell KV. Flow cytometric gating for spleen monocyte and DC subsets: differences in autoimmune NOD mice and with acute inflammation. *J Immunol Methods*. 2016;432:4-12. doi:10.1016/j.jim.2015.08.015

345. Cao W, Taylor AK, Biber RE, et al. Rapid differentiation of monocytes into type I IFN-producing myeloid dendritic cells as an antiviral strategy against influenza virus infection. *J Immunol*. 2012;189(5):2257-2265. doi:10.4049/jimmunol.1200168

346. Thomas IJ, Petrich de Marquesini LG, Ravanan R, et al. CD86 has sustained costimulatory effects on CD8 T cells. *J Immunol*. 2007;179(9):5936-5946. doi:10.4049/jimmunol.179.9.5936

347. Grewal IS, Flavell RA. The role of CD40 ligand in costimulation and T-cell activation. *Immunol Rev*. 1996;153:85-106. doi:10.1111/j.1600-065x.1996.tb00921.x

348. Faassen AE, Dalke DP, Berton MT, Warren WD, Pierce SK. CD40-CD40 ligand interactions stimulate B cell antigen processing. *Eur J Immunol*. 1995;25(12):3249-3255. doi:10.1002/eji.1830251208

349. Nakanishi K, Matsui K, Kashiwamura S, et al. IL-4 and anti-CD40 protect against Fas-mediated B cell apoptosis and induce B cell growth and differentiation. *Int Immunol*. 1996;8(5):791-798. doi:10.1093/intimm/8.5.791

350. Charles A Janeway J, Travers P, Walport M, Shlomchik MJ. B-cell activation by armed helper T cells. In: *Immunobiology: The Immune System in Health and Disease. 5th Edition*. Garland Science; 2001. Accessed February 14, 2026. https://www.ncbi.nlm.nih.gov/books/NBK27142/

351. Rush JS, Hodgkin PD. B cells activated via CD40 and IL-4 undergo a division burst but require continued stimulation to maintain division, survival and differentiation. *Eur J Immunol*. 2001;31(4):1150-1159. doi:10.1002/1521-4141(200104)31:4<1150::aid-immu1150>3.0.co;2-v

352. Nie J, Zhou L, Tian W, et al. Deep insight into cytokine storm: from pathogenesis to treatment. *Signal Transduct Target Ther*. 2025;10(1):112. doi:10.1038/s41392-025-02178-y

353. Ramasamy S, Subbian S. Critical Determinants of Cytokine Storm and Type I Interferon Response in COVID-19 Pathogenesis. *Clin Microbiol Rev*. 2021;34(3):e00299-20. doi:10.1128/CMR.00299-20

354. Cabrera-Rivera GL, Madera-Sandoval RL, León-Pedroza JI, et al. Increased TNF-α production in response to IL-6 in patients with systemic inflammation without infection. *Clin Exp Immunol*. 2022;209(2):225-235. doi:10.1093/cei/uxac055

355. Sabio G, Davis RJ. TNF and MAP kinase signalling pathways. *Semin Immunol*. 2014;26(3):237-245. doi:10.1016/j.smim.2014.02.009

356. Preedy MK, White MRH, Tergaonkar V. Cellular heterogeneity in TNF/TNFR1 signalling: live cell imaging of cell fate decisions in single cells. *Cell Death Dis*. 2024;15(3):202. doi:10.1038/s41419-024-06559-z

357. Costela-Ruiz VJ, Illescas-Montes R, Puerta-Puerta JM, Ruiz C, Melguizo-Rodríguez L. SARS-CoV-2 infection: The role of cytokines in COVID-19 disease. *Cytokine Growth Factor Rev*. 2020;54:62-75. doi:10.1016/j.cytogfr.2020.06.001

358. Eberhardt MK, Deshpande A, Fike J, et al. Exploitation of Interleukin-10 (IL-10) Signaling Pathways: Alternate Roles of Viral and Cellular IL-10 in Rhesus Cytomegalovirus Infection. *J Virol*. 2016;90(21):9920-9930. doi:10.1128/JVI.00635-16

359. Humphreys IR, de Trez C, Kinkade A, Benedict CA, Croft M, Ware CF. Cytomegalovirus exploits IL-10-mediated immune regulation in the salivary glands. *J Exp Med*. 2007;204(5):1217-1225. doi:10.1084/jem.20062424

360. Wilson EB, Brooks DG. The role of IL-10 in regulating immunity to persistent viral infections. *Curr Top Microbiol Immunol*. 2011;350:39-65. doi:10.1007/82_2010_96

361. Brooks DG, Ha SJ, Elsaesser H, Sharpe AH, Freeman GJ, Oldstone MBA. IL-10 and PD-L1 operate through distinct pathways to suppress T-cell activity during persistent viral infection. *Proc Natl Acad Sci U S A*. 2008;105(51):20428-20433. doi:10.1073/pnas.0811139106

362. Chijioke O, Azzi T, Nadal D, Münz C. Innate immune responses against Epstein Barr virus infection. *J Leukoc Biol*. 2013;94(6):1185-1190. doi:10.1189/jlb.0313173

363. Farina A, Rosato E, York M, Gewurz BE, Trojanowska M, Farina GA. Innate Immune Modulation Induced by EBV Lytic Infection Promotes Endothelial Cell Inflammation and Vascular Injury in Scleroderma. *Front Immunol*. 2021;12:651013. doi:10.3389/fimmu.2021.651013

364. Palianina D, Mietz J, Stühler C, et al. Stem cell memory EBV-specific T cells control EBV tumor growth and persist in vivo. *Sci Adv*. 2024;10(34):eado2048. doi:10.1126/sciadv.ado2048

365. Fettelschoss A, Kistowska M, LeibundGut-Landmann S, et al. Inflammasome activation and IL-1β target IL-1α for secretion as opposed to surface expression. *Proc Natl Acad Sci U S A*. 2011;108(44):18055-18060. doi:10.1073/pnas.1109176108

366. Netea MG, Nold-Petry CA, Nold MF, et al. Differential requirement for the activation of the inflammasome for processing and release of IL-1beta in monocytes and macrophages. *Blood*. 2009;113(10):2324-2335. doi:10.1182/blood-2008-03-146720

367. Shi W, Jin M, Chen H, et al. Inflammasome activation by viral infection: mechanisms of activation and regulation. *Front Microbiol*. 2023;14:1247377. doi:10.3389/fmicb.2023.1247377

368. Baricza E, Marton N, Királyhidi P, et al. Distinct In Vitro T-Helper 17 Differentiation Capacity of Peripheral Naive T Cells in Rheumatoid and Psoriatic Arthritis. *Front Immunol*. 2018;9:606. doi:10.3389/fimmu.2018.00606

369. Crawford MP, Sinha S, Renavikar PS, Borcherding N, Karandikar NJ. CD4 T cell-intrinsic role for the T helper 17 signature cytokine IL-17: Effector resistance to immune suppression. *Proc Natl Acad Sci U S A*. 2020;117(32):19408-19414. doi:10.1073/pnas.2005010117

370. Kumar P, Kolls JK. Lymphocyte Isolation, Th17 Cell Differentiation, Activation, and Staining. *Bio-Protoc*. 2016;6(23):e2047. doi:10.21769/BioProtoc.2047

371. Kanzaki H, Shinohara F, Suzuki M, et al. A-Disintegrin and Metalloproteinase (ADAM) 17 Enzymatically Degrades Interferon-gamma. *Sci Rep*. 2016;6(1):32259. doi:10.1038/srep32259

372. Schumacher N, Rose-John S. ADAM17 Activity and IL-6 Trans-Signaling in Inflammation and Cancer. *Cancers*. 2019;11(11):1736. doi:10.3390/cancers11111736

373. Rose-John S, Scheller J, Elson G, Jones SA. Interleukin-6 biology is coordinated by membrane-bound and soluble receptors: role in inflammation and cancer. *J Leukoc Biol*. 2006;80(2):227-236. doi:10.1189/jlb.1105674

374. Snell LM, Brooks DG. New insights into type I interferon and the immunopathogenesis of persistent viral infections. *Curr Opin Immunol*. 2015;34:91-98. doi:10.1016/j.coi.2015.03.002

375. Paust S, Blish CA, Reeves RK. Redefining Memory: Building the Case for Adaptive NK Cells. *J Virol*. 2017;91(20):e00169-17. doi:10.1128/JVI.00169-17

376. O'Neill A, Zakaria N, Bull C, et al. Stromal cells modulate innate immune cell phenotype and function in colorectal cancer via the Sialic acid/Siglec axis. *J Immunother Cancer*. 2025;13(10):e012491. doi:10.1136/jitc-2025-012491

377. Hildreth AD, O'Sullivan TE. Tissue-Resident Innate and Innate-Like Lymphocyte Responses to Viral Infection. *Viruses*. 2019;11(3):272. doi:10.3390/v11030272

378. Lucas M, Schachterle W, Oberle K, Aichele P, Diefenbach A. Dendritic cells prime natural killer cells by trans-presenting interleukin 15. *Immunity*. 2007;26(4):503-517. doi:10.1016/j.immuni.2007.03.006

379. Castillo EF, Stonier SW, Frasca L, Schluns KS. Dendritic cells support the in vivo development and maintenance of NK cells via IL-15 trans-presentation. *J Immunol*. 2009;183(8):4948-4956. doi:10.4049/jimmunol.0900719

380. Balsamo M, Manzini C, Pietra G, et al. Hypoxia downregulates the expression of activating receptors involved in NK-cell-mediated target cell killing without affecting ADCC. *Eur J Immunol*. 2013;43(10):2756-2764. doi:10.1002/eji.201343448

381. Higdon LE, Scheiding S, Kus AM, et al. Impact on in-depth immunophenotyping of delay to peripheral blood processing. *Clin Exp Immunol*. 2024;217(2):119-132. doi:10.1093/cei/uxae041

382. Navas A, Giraldo-Parra L, Prieto MD, Cabrera J, Gómez MA. Phenotypic and functional stability of leukocytes from human peripheral blood samples: considerations for the design of immunological studies. *BMC Immunol*. 2019;20(1):5. doi:10.1186/s12865-019-0286-z

383. Johnston L, Harding SA, La Flamme AC. Comparing methods for ex vivo characterization of human monocyte phenotypes and in vitro responses. *Immunobiology*. 2015;220(12):1305-1310. doi:10.1016/j.imbio.2015.07.014